www.wsgs.uwyo.edu

Geology — Interpreting the past – providing for the future

ISBN 978-1-884589-56-0

Velocity Trends in Cretaceous Rocks In Wyoming Laramide Basins

Yuriy Ganshin

Report of Investigation No. 62 • 2012

WYOMING STATE GEOLOGICAL SURVEY
Thomas A. Drean, Director and State Geologist

Director and State Geologist Thomas A. Drean

Edited by:
David A. Copeland

Design & Layout by:
Brendon B. Orr

View toward the west from Bliss Ranch, near the northeast edge of a small portion of the vast Powder River Basin, Wyoming. 44°59′45.33″ N. 105°11′27.10″ W. 6/15/2011, 05:47hrs, EL: 3932′, Fort Union formation, Paleocene, 55.8-65.50 MA, Lance formation, Cretaceous, 65.50-99.60 MA. Photograph #WSGS.WLU.2884 by Wallace Ulrich.

Velocity Trends in Cretaceous Rocks In Wyoming Laramide Basins

Wyoming State Geological Survey (WSGS) Report of Investigations No. 62, 2012.
ISBN 978-1-884589-56-0

Velocity Trends in Cretaceous Rocks In Wyoming Laramide Basins

Wyoming State Geological Survey
Report of Investigations No. 62
2012

Yuriy Ganshin

TABLE OF CONTENTS

ABSTRACT

Models based on anomalously slow rock velocity have been proposed to characterize various low-porosity and low-permeability (tight) rock-fluid systems within the Cretaceous rocks of Wyoming sedimentary basins. The anomalously slow velocity domain is routinely associated with continuous gas accumulations trapped below a relatively uniform, enigmatic pressure seal defined by a given thermal-maturation depth or regional velocity inversion surface. In the current models, this regional velocity inversion surface separates normally pressured, water-dominated rocks above the surface from under- or overpressured, gas-charged compartments below it. However, there is scant empirical evidence for velocity dependence on degree of gas saturation in low-porosity rock-fluid systems that exist at depth within old sedimentary basins. This velocity-based approach to delineating tight-gas plays may overestimate drilling success rates and lead to overstated determinations of gas reserves.

The goal of this study is to investigate the data contained in suites of well logs and to suggest a synergistic interpretation of these data for detecting the presence of gas-bearing layers in the Cretaceous strata in Wyoming sedimentary basins. Sonic velocity variation with depth is analyzed with care and is calibrated with other geophysical logs. This study also attempts to find common features in geophysical logs acquired in basins throughout Wyoming.

Wide scatter within a broad range in measured sonic P-wave velocity is the most common feature of the well logs observed in this study. For the data sets presented, velocities are nearly independent of depth and density porosity but show pronounced inverse dependence on neutron porosity. Evidence from the wireline logs suggests that variable clay content introduces wide scatter into the velocity-porosity relationship. Clay affects velocity not only by changing the rock matrix but also by introducing the crack-like pores associated with clays. Only such microcracks produce pronounced velocity variation with very small porosity change.

Velocity measurements within low-porosity gas-saturated rocks do not differ much from the mean velocity values of associated non-reservoir rocks. In many cases, natural gas present in pores does not seem to slow rock velocity as much as does elevated clay content and associated microcracks. Rock velocity plotted versus depth (vertical velocity profiles) could not be used as a valid diagnostic tool for gas exploration in the low-porosity rocks described in eight case studies. As is shown in a ninth case study, gas-charged compartments within a "tight gas sand" reservoir are best delineated by means of horizon-based analysis in map view.

INTRODUCTION

Let us call the velocity of compressional (or P) waves (sonic, sound, or seismic) propagating through a volume of rock the rock velocity. My intention here is to investigate the present state of knowledge of the rock velocities measured in Wyoming Cretaceous-age strata. The approach will be to present suites of geophysical borewell log data that illustrate specific aspects of rock velocity and to show how the crossplots (scatterplots) can help us understand the relationships between the constituent logs within a suite. This study does not aim at a rigorous geophysical description of individual gas-bearing formations within the Cretaceous section. The goal is rather to seek out the statistically meaningful general trends in rock velocity behavior that are characteristic of the source and reservoir rocks that compose Wyoming Cretaceous strata. For this purpose the crossplotting technique was chosen because it shows the best results as applied to numerous log measurements acquired over a broad depth interval.

Rock velocity depends on many factors; in particular, we distinguish porosity, lithology, pore structure, clay content, cementation type, fluid saturation, and fluid composition. Of these, only porosity may have an ordered depth distribution through the whole sedimentary section, since porosity depends directly on overburden pressure and hence on depth. The other major factors affecting rock velocity have no clear expression in relation to depth and may produce highly fluctuating velocity functions of depth.

During several years of research (e.g. Surdam, Jiao, and Ganshin, 2005), I accepted the concept that the presence of gas-charged rock/fluid systems can be deduced from a reversal in the velocity-depth curve that indicates an anomalously slow domain. Reversal here means an abrupt decrease in rock velocity. Use of the velocity-versus-depth functional relationship is well-established in modeling processes such as rock porosity calculation (e.g.,Wyllie, Gregory, and Gardner, 1956), basin erosion analysis (e.g., Issler, 1992), subsurface pressure profiles calculation (e.g. Magara, 1976), and anomalous velocity calculation (e.g., Surdam, Jiao, and Heasler, 1997; Surdam et al., 2001; Surdam, Jiao, and Ganshin, 2005). To calculate the anomalous velocity profile, the observed velocities are "removed" (subtracted) from the ideal regional velocity-depth trend (Surdam, Jiao, and Ganshin, 2005). To estimate such a velocity depth trend, three requirements should be considered (Magara, 1976). First, the direct dependence of sonic velocity on porosity should be established. Second, a trend calculation should cover a depth interval having uniform lithology (e.g., shale). Finally, this depth interval should be relatively shallow to satisfy an exponential or any other non-linear velocity-depth model (e.g., Bell, 2002). In many case studies some—or all—of these requirements are not satisfied.

Multiple analyses of sonic logs from various sedimentary basins in Wyoming now make me believe that the ideal velocity/depth trend is an artificial construct that cannot be reliably achieved because of the natural entropy of the sedimentation process. Due to rock heterogeneity at all scales, it is even invalid to assign a single velocity to a volume in the subsurface. Well data demonstrate that rock properties, including velocity, can vary appreciably between two points just one foot apart. Thus, the general impossibility of defining any reliable trend in velocity/depth measurements makes the methodology of establishing ideal velocity-depth trends highly subjective. The wide scatter in sonic data and the contraction effect of a logarithmically transformed plot commonly allow an acceptable visual fit, especially if undesirable data (outliers) are "edited," "deselected," or "normalized." However, for any given set of velocity/depth data, there exist an infinite number of equally valid solutions. There is no such thing as a "true" or "ideal" solution in the case of analytic velocity-versus-depth functions (Al-Chalabi, 1997). Thus, the approach of an artificial trend determination may lead to the erroneous interpretation of geologic data.

To overcome the nonuniqueness of analytic velocity-versus-depth functions, we need to find a quantitative alternative to the velocity/depth relationship, a quantity that is not dependent on depth. Herein, I suggest that a trend between two or more rock properties measured at the same depth can be this quantity. For example, velocity-porosity crossplots presented in this study demonstrate trends that can readily be interpreted in terms of rock/fluid composition, rock texture, and pore geometry.

This presentation of ongoing research shows, first of all, the measurements plotted as they were acquired (logged) over their depth domain. Crossplots of the velocity/density domains are then presented as another way to visualize the log data. I have made certain observations about these presentations, but I have tried not to overwhelm the plots with my own interpretation, to allow for alternative conclusions.

GEOLOGICAL SETTING

Wyoming basins are of the most prolific natural gas producers on the North American continent. Most Wyoming gas reserves occur in the low-permeability Cretaceous

sedimentary strata. The most common, most widespread of these Cretaceous stratigraphic units, youngest to oldest, are the Lance Formation, the Lewis Shale, the Mesaverde Group (including the Almond Formation), the Cody (Baxter, Hilliard, or Steele) Shale, the Frontier Formation, the Mowry Shale, and the Cloverly (Dakota) Formation. The succession of Cretaceous strata, as much as 10,000 ft thick, is composed mostly of thick marine shaly intervals and multiple thin clastic layers such as interbedded sandstones and shales. All these formations have the potential to generate and store hydrocarbons. The generally low porosity and low permeability of the Cretaceous rocks greatly influence estimates of the reserves and producibility of Wyoming gas fields.

From among the hundreds of wells that penetrate the Cretaceous strata within Wyoming basins, eight high-quality suites of well logs were used in this study to analyze gamma-ray intensity, P-wave velocity, caliper, density and neutron porosity, and deep resistivity in eight case studies. Figure 1 shows the distribution of the chosen wells in the major Wyoming sedimentary basins. The Public Land Survey System coordinates and API numbers for the eight wells are given in Table 1. In a ninth case study, methods discussed in this paper are applied to data from many wells in an area of gas fields, designated the Wamsutter Field (Figure 1), to compare rock velocity variation with the surface distribution of gas-producing wells. Although the examples chosen for

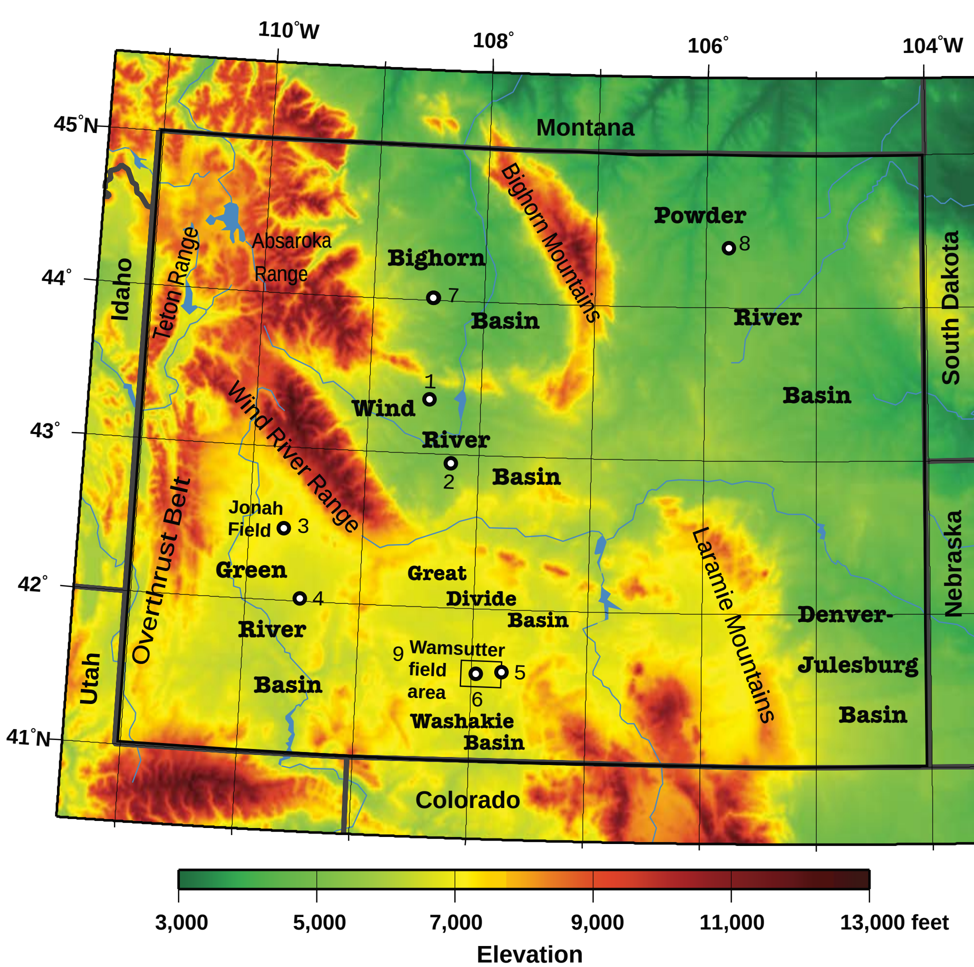

Figure 1. Map of Wyoming showing elevation, some major structural features, and Case Study 1–9 locations: Well-1 through Well-8 and Wamsutter field area.

Table 1. Case Studies

[BHB, Bighorn Basin; GGRB, Greater Green River Basin; GRB, Green River Basin; PRB, Powder River Basin; WRB, Wind River Basin]

Case study	Text same	Well name	API no.	Sec.-T.-R.	Location
1	Well-1	Owl Creek Tribal 1	1321077	26-5N-3E[1]	WRB
2	Well-2	Riverton Tribal 52	1321875	24-1S-4E[1]	WRB
3	Well-3	SHB 14-34	3522343	34-29N-108W	GRB
4	Well-4	Stagecoach Draw 16A	3724246	32-23N-107W	GRB
5	Well-5	Fillmore Creek 9-1	722568	9-19N-91W	GGRB[2]
6	Well-6	Echo Springs 17-5	722877	17-19N-93W	GGRB[2]
7	Well-7	Tenneco-Federal 1-29	1720413	29-47N-97W	BHB
8	Well-8	Echeta Federal 11-13	548180	13-51N-75W	PRB
9	Wamsutter Field				GGRB[2]

[1] Wind River Indian Reservation land divisions.

[2] On the Wamsutter arch dividing the Washakie and Great Divide Basins-see Figure 37.

interpretation are few, there is no impediment to extending these analytical techniques and conclusions to other areas in Wyoming and to other sedimentary basins of the Rocky Mountain region.

WELL-LOG ANALYSIS

Well log descriptions in this study were completed using two techniques: a general comparative display of a suite of logs presented in bar graph mode and color-coded crossplots. The crossplotting technique was found to be especially useful in identifying velocity distribution trends. The general log analysis and the crossplotting were done in an attempt to determine if any log values – P-wave velocity in particular correlated with the occurrence of gas. The detection of natural gas with wireline logs is tied primarily to the use of porosity logs. These are the only logs generally run in open hole that are truly influenced by the presence of gas versus the presence of oil or water. Geological formations with high shale (or clay) content are known to be much less likely to produce accumulated

hydrocarbons. Therefore, zones with a high volume of shale should be identified and eliminated from analysis. Traditionally, this task is accomplished through the use of gamma-ray measurements.

The logging-tool response physics must be understood to fully appreciate the results of log analysis. The following section refers to a basic, cursory approach to scanning a suite of geophysical log measurements, and to distinguishing clean gas-saturated zones from water-saturated shales. The basic principles of well-log analysis and interpretation provided below are adopted from Asquith and Krygowski (2004), Ellis and Singer (2007), Dewan (1983), and Whittaker (1991).

Gamma Ray Log (GR)

The natural gamma-ray (GR) logging tool consists of a Geiger counter that responds to the concentration of natural gamma-ray emitters in rocks. The gamma ray signal generally increases in magnitude with increase in shale content, thus enabling lithologic identification. Shale-free ("clean") sandstones and carbonates have low concentrations of radioactive material and give low gamma-ray readings. As shale content increases, the gamma ray log response increases because of the higher concentration of radioactive material (mostly potassium) in shales.

Neutron porosity log

The key to definitive gas detection, the neutron porosity log, is not directly related to porosity but rather responds to all sources of hydrogen. The neutron porosity tool measures porosity only when it operates in an environment similar to that of a corresponding calibration standard (water-filled sandstone, limestone, or dolomite tank). In reality, a neutron porosity reading should be considered an apparent porosity that is perturbed by the mineral composition of the rock fabric, the presence of clay minerals in the matrix, and the presence of gas in the pore spaces. Thus, shale-rich intervals are characterized by relatively large values of apparent porosity due to the hydroxyls in clay minerals. On the other hand, the apparent neutron porosity will become very small (occasionally negative) in intervals in which normally expected pore water is replaced by lower density gas.

Density porosity

A tool composed of a gamma-ray energy source and two gamma-ray detectors that compensate for borehole conditions records a density log. The transmission of gamma rays through a formation is directly related to its density, called the bulk density (combined solid and fluid parts of the formation). Bulk density ρ_b can be used for the calculation of density porosity ϕ, provided known matrix density ρ_{ma} and pore fluid density ρ_f:

$$\phi = (\rho_{ma} - \rho_b) \; / \; (\rho_{ma} - \rho_f)$$

The use of this equation assumes that lithology and fluid density are constant parameters that do not vary with depth. However, this condition is never fulfilled, and this creates several problems for determination of porosity. Calculated negative porosity values is one of them. For this study, the sandstone matrix density, with ρ_{ma} = 2.65 g/cm^3, was chosen to match the neutron porosity logs. The fluid density was chosen to be ρ_f = 1.0 g/cm^3.

Combined neutron porosity and density-derived porosity logs

When plotted together (using the same scale and the same porosity units) the neutron porosity and density porosity logs might be used to establish the presence of gas-saturated layers. Partial replacement of the water component by gas in the pore space of rocks reduces both bulk density and hydrogen content. As a result, the log over a depth interval containing a gas-bearing layer will show higher density porosity and a lower neutron porosity. Within that interval the two plotted porosity curves will cross each other (density porosity will exceed or nearly exceed neutron porosity); this is the so-called "gas effect." The gas effect also shows up as negative values on crossplots with one axis defined as the difference between neutron porosity and density porosity (ϕ_N-ϕ_D). However, the magnitude of the crossover (the difference between the two porosity logs) is rather qualitatively than quantitatively related to the gas saturation, due to uncertainties inherent in the porosity calculation methods discussed above. Thus, in the simplest of cases, gas is associated with any zone in which the neutron porosity is less than the density porosity.

Shale produces the opposite effect; the neutron porosity may far exceed the density porosity. Some log analysts report a so-called "clay effect" estimated from the difference between neutron porosity and density porosity. Katahara (2008) considers this difference to be a better measure of clay content than the GR. Anyway, well log crossplots with the ϕ_N-ϕ_D quantity being one of the axes may be very useful in determining petrophysical trends characteristic of different lithological units (Katahara, 2008). All of these statements are true only if the principle lithology within the measured depth interval corresponds to the matrix setting on the log, as explained under Neutron porosity log, above.

Caliper log

A caliper log measures changes in the diameter of a borehole caused by casing as well as by such environmental effects as mud cakes, cavities in the borehole wall, washed-out zones, and fractures. The information provided by the caliper log should be used to validate other wireline logs by checking and evaluating suspect log values. The caliper log can be used as a lithology control tool, since shale sections are more likely to "wash out," increasing the borehole size, than are the cleaner sand sections that retain their structural integrity. Experience has shown that Cretaceous shales in Wyoming are normally significantly softer than the associated sandstones.

Resistivity log

Resistivity is an inherent electrical property of the formation and may be defined as a measure of the ease of electric conduction. The contrast in resistivity between relatively insulating hydrocarbons and conductive formation brines is the basis for hydrocarbon detection. Basically, if the porous formation contains conductive brine, its resistivity is low, whereas if it contains some amount of nonconducting hydrocarbon, the formation resistivity is relatively high. However, high resistivity readings may characterize purely water-saturated formations due to their extremely low porosity. The presence of clay minerals usually decreases overall resistivity, due to additional conduction through exchange of cations on the clay mineral particles.

Mud log

Traditionally, this type of log has several different functions, but only the formation gas monitor will be considered in this study. Standard total gas (TG) monitoring involves gas measurement and analysis on samples that have been transported several thousand feet from their original location. The gaseous hydrocarbons present at depth undergo enormous expansion and change in composition during transport to the surface. As a result the quantitative TG evaluations are rarely repeatable from well to well. The mud log analyses are accurate and reliable in themselves; the difficulty lies in relating their results to the properties of the formation as it was at depth and prior to the disintegrating action of the drill bit and drilling-fluid circulation. The inconsistency in surface gas measurement results largely from the way the gas is extracted from the drilling fluid in analysis. Therefore, TG curves should be considered rather qualitatively as an aid in identifying the presence of petroleum reservoirs.

Sonic log

The acoustic tool measures compressional wave slowness or interval transit time Dt (reported in μs/ft). The travel time varies between 40 μs/ft in hard formations and 140 μs/ft in soft ones. The corresponding rock velocities, the inverse of transit times, are 25,000 and 7,140 ft/sec. The velocity of drilling

mud (or water) is less than 6,000 ft/sec. A logging tool will occasionally read these low values in large drill-hole washouts where the direct mud wave is recorded first. The vertical resolution of a sonic tool is defined as the span between receivers—2 feet for the standard Schlumberger sonic tools used mostly in the twentieth century in Wyoming. Depth of penetration is not well defined and is controlled by the basic sonic wavelength. At 25 kHz frequency, sonic wavelengths are 4 to 10 inches in most sedimentary rocks. Consequently, the propagating sonic waves do not "sense" individual rock grains or pores but rather are affected by the overall formation rigidity and density. Therefore, the effect of porosity on rock velocity is through its influence on these physical rock properties.

VELOCITY-POROSITY RELATIONS

The sonic log is one of the three porosity estimators used in formation evaluation. Its relative importance follows from the link that it provides between surface seismic measurements and the subsurface "geological truth" observed in wells. The sensitivity of rock velocities to such important reservoir parameters as porosity, lithofacies, pore fluid type, saturation, and pore pressure has been recognized for many years. The wave propagation theory provides the fundamental link between compressional (P-wave) velocity V_p and rock properties with the classical equation

$$V_p = \sqrt{(K+(4/3\mu)/\rho)},$$

where K is the bulk modulus, μ is the shear modulus, and ρ is the rock density.

This equation assumes a homogeneous, elastic, and isotropic medium. However, real sedimentary rocks rarely satisfy these criteria. The situation is even more complicated because the bulk modulus and density are interrelated, both dependent on the material and structure of the rock, the lithology, porosity, pore fluids, pressure, cementation, and so on. That is why it is common practice in industry to use simplistic and sometimes inappropriate velocity/porosity relations for detecting hydrocarbon-saturated intervals. Such are the empirical trends of Wyllie, Gregory, and Gardner (1956), Raymer, Hunt, and Gardner (1980), and Han, Nur, and Morgan (1986). "Sonic porosity," derived from sonic logs using the time average of Wyllie, Gregory, and Gardner, is perhaps the worst example. As with any empirical relation, these velocity/porosity trends are most meaningful for the data from which they were derived and can never produce a satisfactory well-log data interpretation over a broad depth interval. However, the simplistic, linear velocity/porosity relation is still widely used in a variety of geophysical applications.

Indeed, porosity does have a significant influence on rock velocity in sedimentary strata. So too does the content of fines in the strata (clays, muds, or shales), which in this study is referred to as the clay content. Clays normally have pores with a much smaller aspect ratio than that within sands (about ten times smaller). Variations in both clay content and pore aspect ratio produce bias in measurements and should be considered in making predictions (modeling) from velocity/porosity relations. Examples of such an approach are found in Marion et al. (1992) and Xu and White (1995). In an experimental study with sand-clay mixture samples, Marion et al. observed two different trends in the velocity-porosity relations, one for *shaly sand* and the other for *sandy shale* (Figure 2). The load-bearing minerals define the difference between these two lithologic types. Figure 2a, modified from Marion et al., illustrates schematically what happens as clay content increases from clean sandstone on the left to clay-rich shale on the right. In the sandstone on the left, rigid quartz grains and grain contacts support stress. Moving to the right in Figure 2a, small amounts of clay are incorporated in the inter-granular spaces but do not support external stress. With increasing clay content, the sand-grain contacts are disrupted. Finally, the sand grains float in a clay-mineral matrix

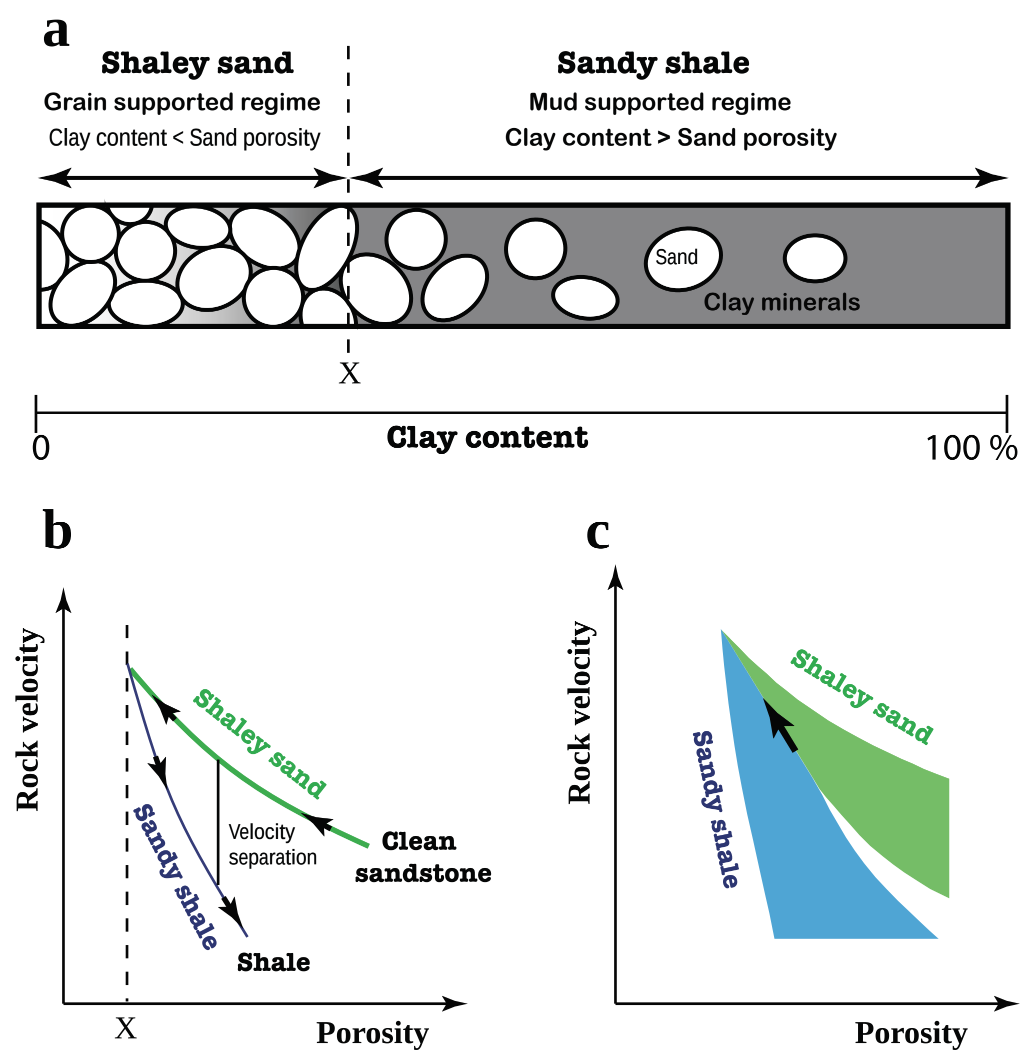

Figure 2. (**a**) Sand-shale transition diagram with clay-mineral content increasing from zero in clean sandstone on the left to 100% in clay-rich shales on the right. X indicates point on clay-content axis where clay content (%) equals clean sand porosity (%). (**b**) Schematic velocity/porosity trends observed for shaley sand and sandy shale at constant confining pressure. X Indicates point on porosity axis where clay content equals sand porosity. Arrows indicate increasing clay content. (**c**) Velocity/porosity trends computed for different confining pressures using the sand-shale transition model. Pressure variation creates data scatter shown as color-filled shapes on the velocity/porosity plot. The arrow indicates direction of pressure increase. All figures modified from Marion et al. (1992).

that is load bearing. There is a threshold clay content separating shaley sand from sandy shale (X on Figure 2a) at which clay particles exactly fill the pure sand pore space.

Unlike the widely used *linear* velocity-porosity relations, the model of Marion et al. (1992) predicts *nonlinear*, inverted-V-shaped trends for clastic sediments with bimodal grain size distributions. Figure 2b shows two separate trends in the porosity-velocity relationship, one for shaley sands and the other for sandy shales. Marion et al. conclude that each trend at constant confining pressure is due primarily to clay content, but that the influence of clay content on velocity is opposite for the two lithologies: velocity in shaley sand increases with increase in clay content, while velocity in sandy shale decreases with increase in clay content. The two trends intersect at a singular point at which clay content is equal to pure sand porosity (Figure 2b). Pressure variation with depth creates additional

data scattering that shows up as a smeared V-shape on the velocity porosity plot (Figure 2c). Increase in confining pressure decreases velocity separation between the two trends.

The model of Marion et al. (1992) was based on laboratory measurements. Unlike laboratory measurements, well logging measurements are taken in real geological conditions that are difficult to duplicate in the laboratory. Besides, well logging provides us with the vast amount of data necessary for studying velocity/porosity dependency accurately. On the basis of several well-log studies, Xu and White (1995) explain most of the scatter in the velocity porosity relationship as due to pore geometry (pore aspect ratio). They state that the relationship for sands is fundamentally different from that for shales and propose a relationship between the effect of clay content and that of aspect ratio. They also agree qualitatively with the laboratory measurements of Marion et al. (1992) and explain the two distinct trends, one for shaley sand and the other for sandy shale, by the notably different mean aspect ratios of clay-related and sand-related pores. Basically, for a given porosity, rounded pores make the velocity faster, and elongate (crack-like), pores (as well as fractures) make it slower. The Xu and White model may be used to predict velocities from well-log data in sand-clay mixtures. Figure 3 shows computed compressional velocities in brine-saturated rocks with different porosities and pore aspect ratios. As shown in Figure 3, the greatest velocity separation due to different aspect ratios occurs in rocks with low porosity. That observed well-log sonic velocities closely match those computed with the Xu-White method has led to the method's wide recognition and successful application (e.g. Keys and Xu, 2002).

INFLUENCE OF CLAY CONTENT ON LOG RESPONSE

Until recently, the author regarded shales as a unique type of lithology in log data analysis and did not pay much attention to possible variation in mineralogy, texture, and porosity within shaley sequences. This was because of a paucity of publications on this subject due to difficulties of laboratory measurement on shale samples, and also because the petroleum industry gives low priority to log data and core-sample acquisition in shale sequences. However, with increased attention to unconventional plays such as shale gas, geoscientists are accumulating more petrophysical information about shales (e.g., Katahara, 2008). Since shales are the most abundant Cretaceous sedimentary rocks in Wyoming and clays are present in abundance in shales, knowledge of the clastic properties of clays is of importance for comprehensive log data analysis. An understanding of in-situ shale properties is essential for the interpretation and modeling of their seismic response. Among these properties, the bulk modulus of shales remains unclear. This is largely because shales are composites of many minerals, some of whose properties change with burial due to diagenetic reactions. Modeling sequences even in the few cases where the shale mineralogy is known is difficult because literature values of clay mineral properties are various and uncertain.

The following case studies show that clay in rocks affects all the log readings that have been considered. For example, the presence of hydrogen associated with the clay in a formation can increase apparent neutron porosity by as much as 40 porosity units (percent in this report). For the same reason, clays alter the electric conductivity of the formation, and the affected readings may result in elevated water-saturation estimates. The presence of clay is seen to decrease the overall resistivity of rocks if the assocated gamma-ray (GR) log response is used as a measure of clay content. In clay-rich shales, the sand and silt grains appear to be suspended in a clay-mineral matrix that is characterized by lower bulk modulus, K. Thus, in the case of the compressional wave velocity measurements (sonic log), higher clay content generally results in slower velocity (Figure 3).

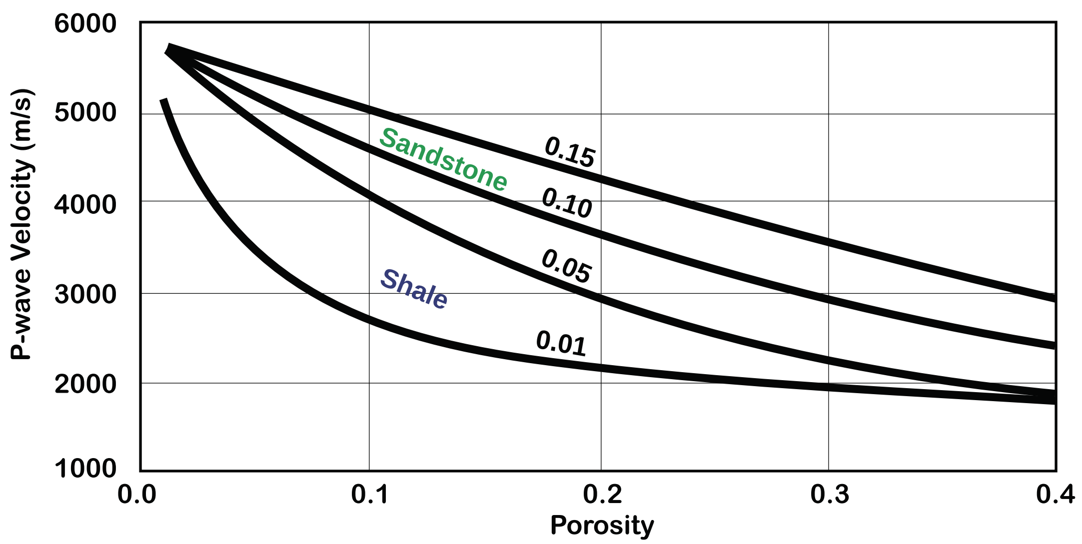

Figure 3. Velocity/porosity trends computed for brine-saturated rocks with different porosities and pore aspect ratios using the Xu-White method (Xu and White, 1995). Assumed rock matrix compressional wave velocity, 5850 m/s; rock matrix density, 2.65 gm/cm^3. Pore aspect ratios given as numbers above curves. Modified from Keys and Xu (2002).

It is not the only elemental composition of clay minerals that affects log response, but also their platy nature. These thin, sheet-like particles have high ratios of surface area to volume (specific surface area). The specific surface area is different for different clay minerals. Correspondingly, the amount of bound water surrounding the clay minerals is different, which affects neutron porosity and resistivity log readings. Thus, shale composed of minerals with greater specific surface area is characterized by greater apparent porosity and lesser resistivity values. Also in contrast to sandstones, shales are anisotropic rocks because of the preferred orientation of clay minerals and the low aspect ratio of their pores (crack-like pores).

CASE STUDIES

Case study 1: Owl Creek Tribal 1 well, Wind River Basin

The Owl Creek Tribal 1 well (herein Well-1) is located in the northern Wind River Basin (Figure 1). The Cretaceous rock sequence penetrated by this well is one of the thickest in Wyoming. It starts with the Lance Formation at a depth of about 12,700 feet and ends in the Dakota Sandstone at 23,790 feet depth. The available digital log data cover almost the entire Upper Cretaceous section. Figure 4 shows the gamma ray, P-wave velocity, density, caliper, density and neutron porosity (blue and orange, respectively), and resistivity logs, as well as a corresponding stratigraphic column, for the 12,700-ft to 23,00-ft depth interval. The black solid line in velocity panel (Figure 4) represents the velocity trend line obtained by smoothing the sonic velocities with a 250-foot Gaussian operator. This well is known to have significant and multiple gas shows and gas flares starting in the lower Meeteetse interval and continuing into the upper Cody Shale interval (lithology log on the WOGCC Web site). High deep-resistivity values (100+ ohmm) also indicate increased gas saturation within the whole Mesaverde section (Figure 4). However, the well has never been completed as a gas well.

Broad scatter within the Lance, Meeteetse, and Mesaverde Formations characterizes the sonic rock velocities. The smoothed sonic velocities for the same depth interval do not show any pronounced trend and fluctuate around 15,000 ft/s (Figure 4). Figure 5 is an expanded section of the Well-1 log data

for the Mesaverde gas interval between 16,200 ft and 16,900 ft deep in the well. The gamma-ray log is color-coded and plotted as deviations from a value of 50 gAPI, because gamma-ray readings below 50 gAPI (orange) are more representative of sandy lithologies, while those above 50gAPI (brown) generally represent shales. The gas-reservoir rocks (depth interval 16,400 to 16,620 feet in Figure 5) are mostly sandstones characterized by high resistivity values and by density porosity (blue) crossing over neutron porosity (orange). However, the sonic velocity values within this depth interval cannot be called anomalously low since they fluctuate around the mean velocity value of 15,000 ft/s (Figure 4). Rather, the slowest rock velocities were measured within the washed-out intervals characterized by an abrupt increase of caliper values and an abrupt decrease of density values (Figure 5). The Cody Shale interval is characterized by a pronounced decrease in rock velocities from the top to the base of the interval and an increase in neutron porosity values over the same depth interval. Thus, there is an apparent inverse correlation of rock velocities with neutron porosity values for the shale interval (Figure 4). Density porosity and deep-resistivity have relatively small values and do not vary much within the Cody Shale strata. On the basis of the log-analysis principles discussed above, the log behavior within the Cody Shale interval indicates a water-saturated shale lithology with progressively increasing clay content toward the deeper parts of the Cody Shale section.

Crossplots allow us to better discern possible rock velocity dependencies and trends. Here we consider crossplots of rock velocity vs. neutron porosity (Figure 6), rock velocity vs. density porosity (Figure 7), and rock velocity vs. difference between neutron porosity and density porosity (Figure 8). Figure 6 shows the rock velocity versus neutron-porosity crossplot for Well-1. The logged depth interval, 12,700 to 23,000 feet, is the same as that of Figure 4 and corresponds to the Upper Cretaceous stratigraphic section. The crossplot in Figure 6 is color-coded. Green dots indicate measurements within the rocks that have relatively low natural gamma-ray intensity. In this case study the natural radioactivity level of 50 gAPI was chosen as the threshold separating shaley sandstones (labeled "sands" in all figures) from sandy shales (labeled "shales") – see Figure 2a. Based on this nomenclature, blue dots indicate measurements within the "shales" (natural gamma-ray intensity above 50 gAPI). Red dots indicate measurements within the rocks showing high resistivity readings (above 150 ohmm in this case). This color-coding is used in all the crossplots in this report.

Broad scatter of data is the most common feature for all measured rock velocity values within the Cretaceous strata intersected by Well-1. What causes this scatter? The majority of data points in Figure 6 are blue; they correspond to shaley rocks. With this color-coding it is apparent on Figure 6 that measurements within shaley rocks show a pronounced inverse trend in distribution: velocity decreases with increasing neutron porosity. As explained above, the neutron-porosity tool primarily senses hydrogen and therefore gives high readings in clay-rich rocks. It follows that clay content is the major source of velocity scatter in the Well-1 measurements. The linear trend in measurements within shaly rocks ranges in rock velocity from ~13,000 to ~18,000 ft/s (Figure 6). The slowest velocity values within this trend, ~13,000 ft/s, were measured at the base of the Cody Shale, the part of the Cody characterized by the highest neutron-porosity values and the lowest resistivity– and that is gas free.

Rock velocities measured within the "sands" (green dots) have a range, ~14,000 to ~18,000 ft/s, similar to that of the "shales," but are more randomly distributed (Figure 6). Presumed gas-saturated rocks with high resistivity readings (red dots) do not have extreme velocity values and tend to have small neutron-porosity values; i.e., they have relatively poor clay content (Figure 6). Most extremely slow velocities (less than 13,000 ft/s) correspond to caliper-log readings

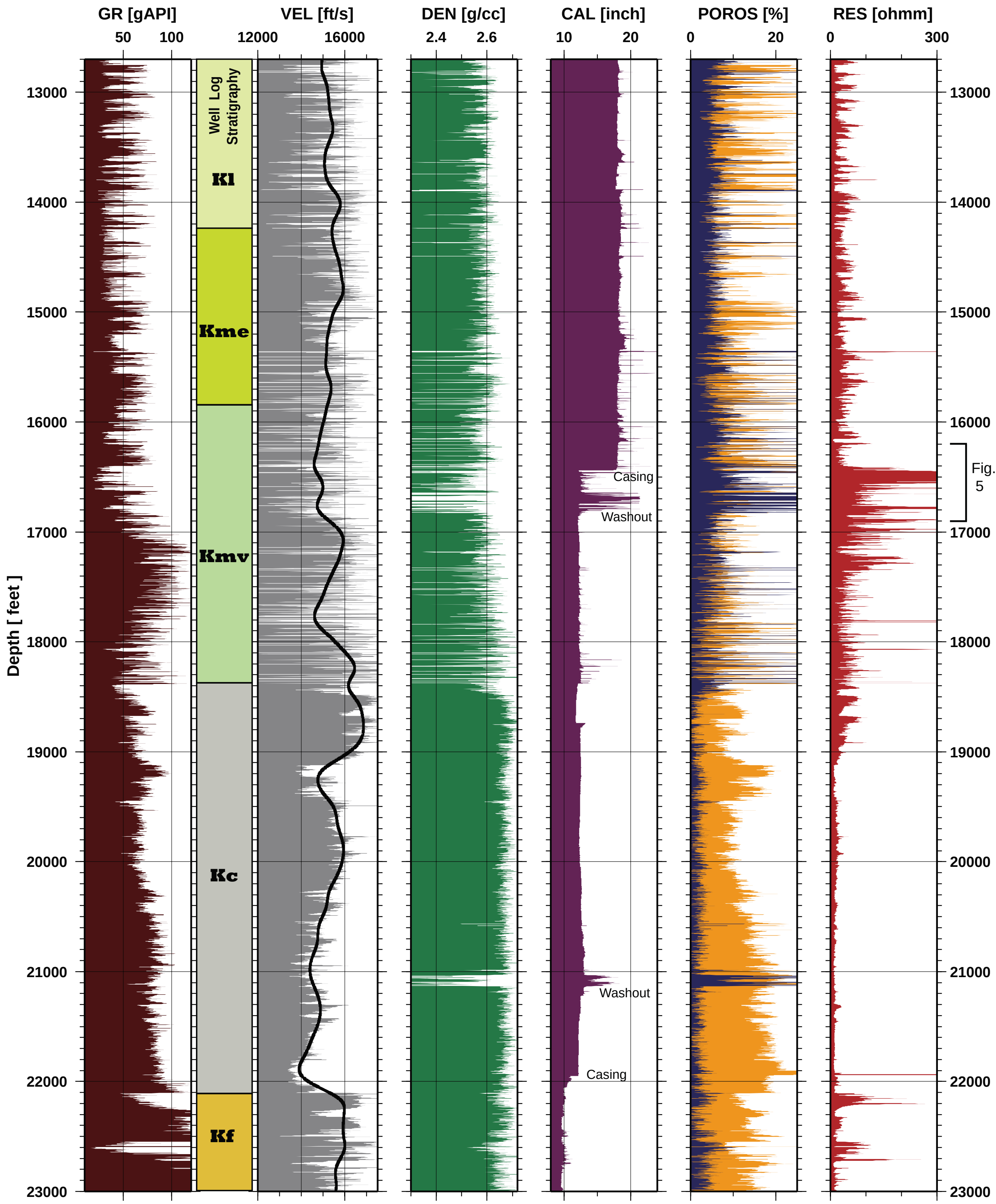

Figure 4. Well-1 composite wireline logs (Owl Creek Tribal 1 well, Wind River Basin): GR, gamma-ray; VEL, sonic p-wave velocity; DEN, bulk density; CAL, caliper; POROS, density (blue) and neutron (orange) porosity; RES, resistivity. Solid black line in VEL panel, velocity smoothed with 250-ft Gaussian operator. Stratigraphy based on WOGCC geologic markers and wire line log characteristics: Kl, Lance Fm.; Kme, Meeteetse Fm.; Kmv, Mesaverde Fm.; Kc, Cody Sh.; Kf, Frontier Fm.

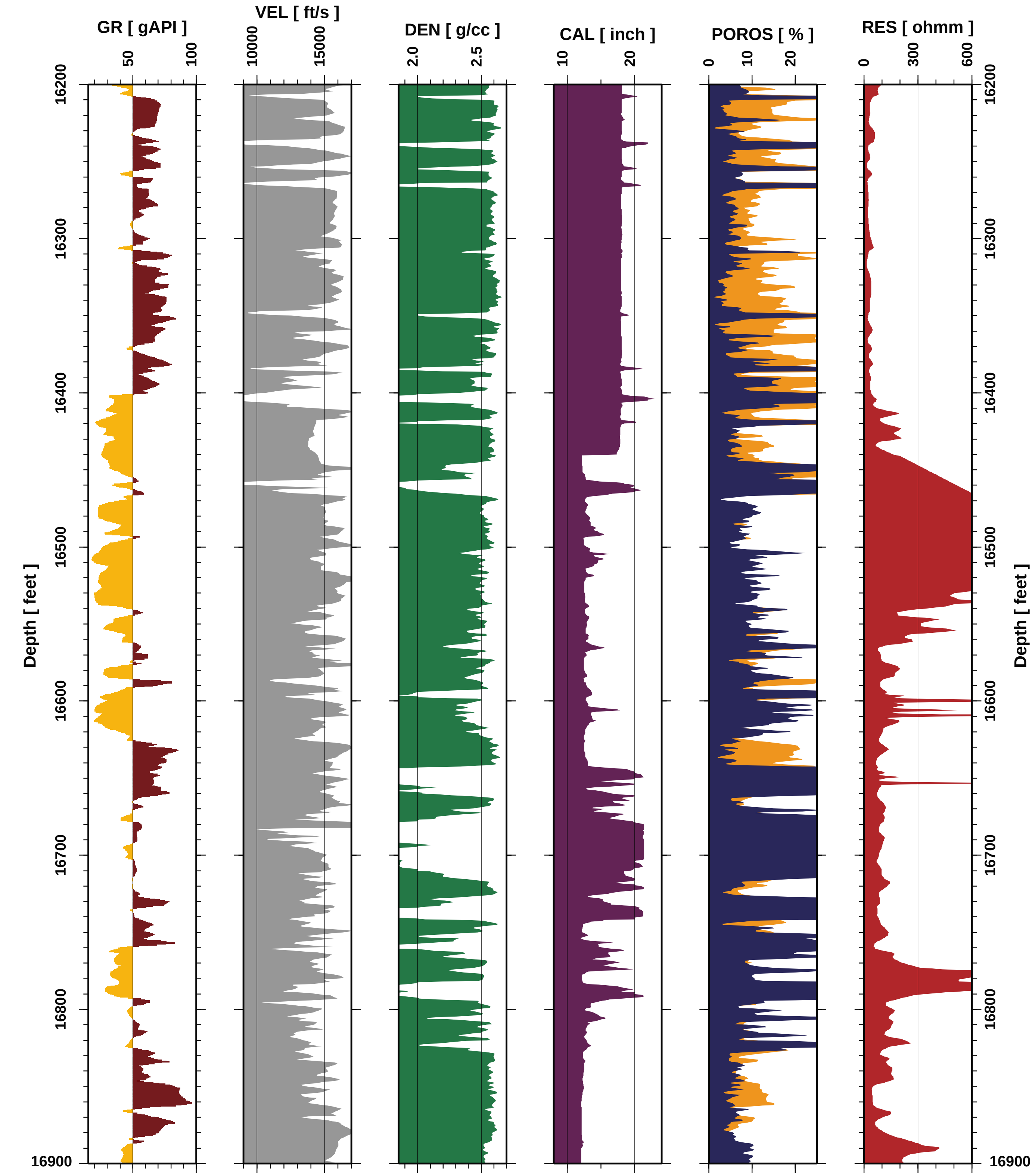

Figure 5. Expanded Well-1 composite wireline logs, depth interval 16,200 to 16,900 ft: GR, gamma-ray; VEL, sonic P-wave velocity; DEN, bulk density; CAL, caliper; POROS, density (blue) and neutron (orange) porosity; RES, resistivity. Gamma-ray log color-coded by intensity: yellow, shaley sand; brown, sandy shale. Washed-out intervals recorded as increased caliper correlate with low readings of density and velocity.

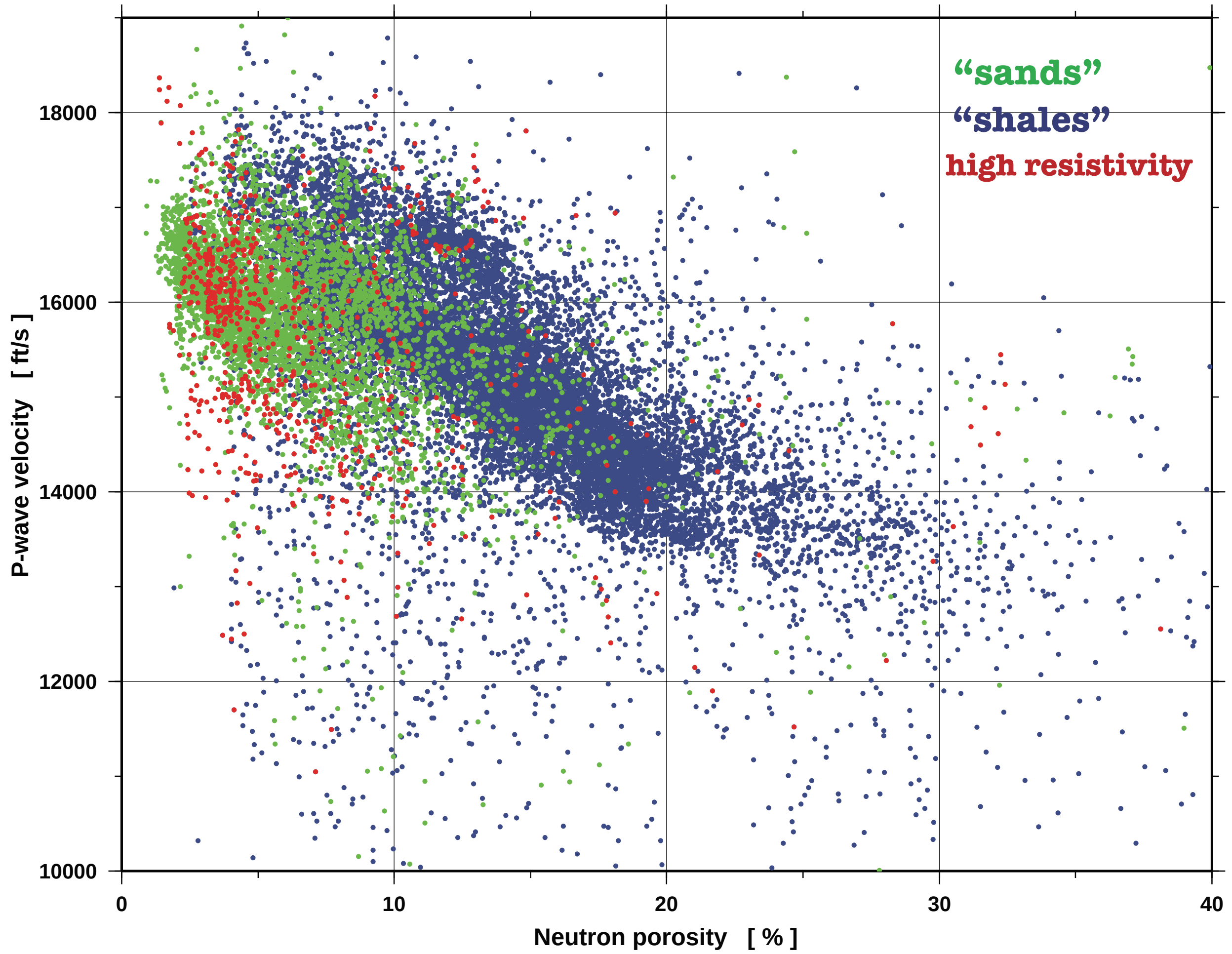

Figure 6. Well-1 velocity versus neutron-prosity crossplot, depth interval 12,700 to 23,00 ft (Upper Cretaceous stratigraphic section down to Mowry Shale). Green dots, "sands," rocks having natural gamma-ray intensity below 50 gAPI; blue dots, "shales," rocks having gamma-ray intensity above 50 gAPI; red dots, rocks showing resistivity above 150 ohmm. "Shales" show a pronounced inverse trend in distribution: velocity decreases with increasing neutron porosity. Presumed gas-saturated rocks (high resistivity, red dots) are not characterized by extreme velocity and are quite scattered.

that indicate washed-out zones and are not considered in our velocity trend analysis.

Figure 7 is the Well-1 rock velocity versus density-porosity crossplot. The measured depth interval, 12,700 to 23,000 feet, corresponds to deeply buried Upper Cretaceous strata. Velocity measurements within this depth interval show broad scatter. During a conventional petrophysical analysis, it is often assumed that this velocity variation is due to variation in porosity. However, Figure 7 shows that there is only poor correlation of velocity with porosity in "sands" (green dots). Velocity measurements within "shales" (blue dots) are widely scattered and do not appear to correlate with porosity. Velocities in the "sand" also show significant scatter. However, the seemingly disordered velocity distribution in Figure 7 can be interpreted using the sand-shale transition model of Marion et al. (1992). Color-coding with the gamma-ray threshold (50 gAPI) allows identification of two different trends in Figure 7, a relatively gentle slope for sands and a steep slope for shales. Overall, the color-coded distribution for Well-1 measurements matches the V-shape distribution in Figure 2c. Thus, the broad scatter of data points in Figure 7 can be

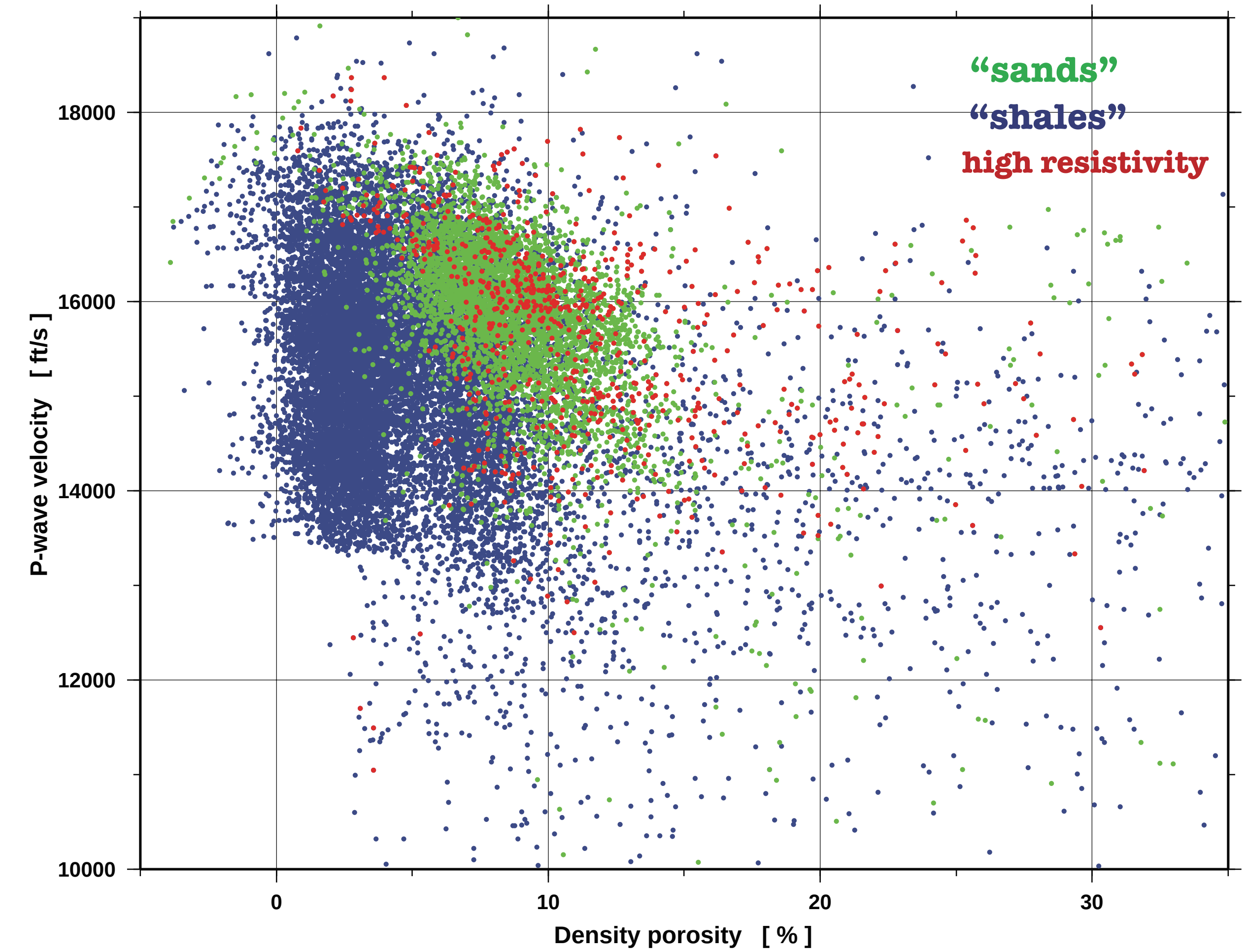

Figure 7. Well-1 velocity versus density-porosity crossplot, depth interval 12,700 to 23,00 ft (Upper Cretaceous stratigraphic section down to Mowry Shale). Green dots, "sands," rocks having natural gamma-ray intensity below 50 gAPI; blue dots, "shales," rocks having gamma-ray intensity above 50 gAPI; red dots, rocks showing resistivity above 150 ohmm. Note (1) absence of overall correlation between velocity and porosity; (2) wide range of measured P-wave velocities; (3) apparent presence of two groups of data ("sands" and "shales"). Presumed gas-saturated rocks with high resistivity values (red dots) are not characterized by extreme (anomalous?) velocity.

attributed to variations both in clay content and in confining pressure. However, some of the measurements shown in Figure 7 may in fact be related to laminated shaly sands, interlayered sands and shales that do not conform to the concept in Figure 2. This create additional data scatter due to anisotropy produced by interlayering rocks with different physical properties.

Figure 8 shows the Well-1 rock velocity versus difference between neutron-porosity and density-porosity (ϕ_N-ϕ_D) crossplot. The purpose of this plot is twofold, (1) to isolate measurements within the gas-charged rocks using a well-known porosity crossover and (2) to investigate the possible influence of clay content on rock velocity measurements within the Upper Cretaceous rocks. As mentioned above, the GR log is used in this report to separate shaley and sandy lithologies. The GR log often works well for this purpose but not always, because not all clay minerals are significantly radioactive. From this point of view, the difference between the two porosities, ϕ_N-ϕ_D, may be a better measure of clay content than the GR. In my experience, the ϕ_N-ϕ_D measure has its own shortcoming, the uncertainty inherent in both types of porosity measurement. That is why, in this report, both types of lithology discriminators (GR and ϕ_N-ϕ_D) were used in order to increase the reliability of the crossplot interpretations. As for the Well-1 measurements, the GR and the difference between the two porosities show good agreement and separate "sands" from "shales" both in color and in space (Figure 8). The measurements within "sands" are characterized by low GR readings, and mostly negative differences between neutron porosity and density porosity. No significant trend in "sand" velocities can be observed in Figure 8. However, the "sands" with relatively high resistivity readings (above 150 ohmm – in this case) do tend to demonstrate the gas effect, greater negative separation between the neutron-porosity and density-porosity values. Rock velocities of presumably gas-saturated rocks (red dots) range mostly from 14,000 to 17,000 ft/s and cluster around 16,000 ft/s (Figure 8). Hence, it is not possible to conclude that gas saturated rocks penetrated by Well-1 are characterized by anomalously slow rock velocities. On the contrary, the slow rock velocities in this interval are in "shales" that demonstrate a pronounced inverse trend in velocity distribution with clay content (Figure 8). A relatively large number of velocity measurements within "shales" have values of

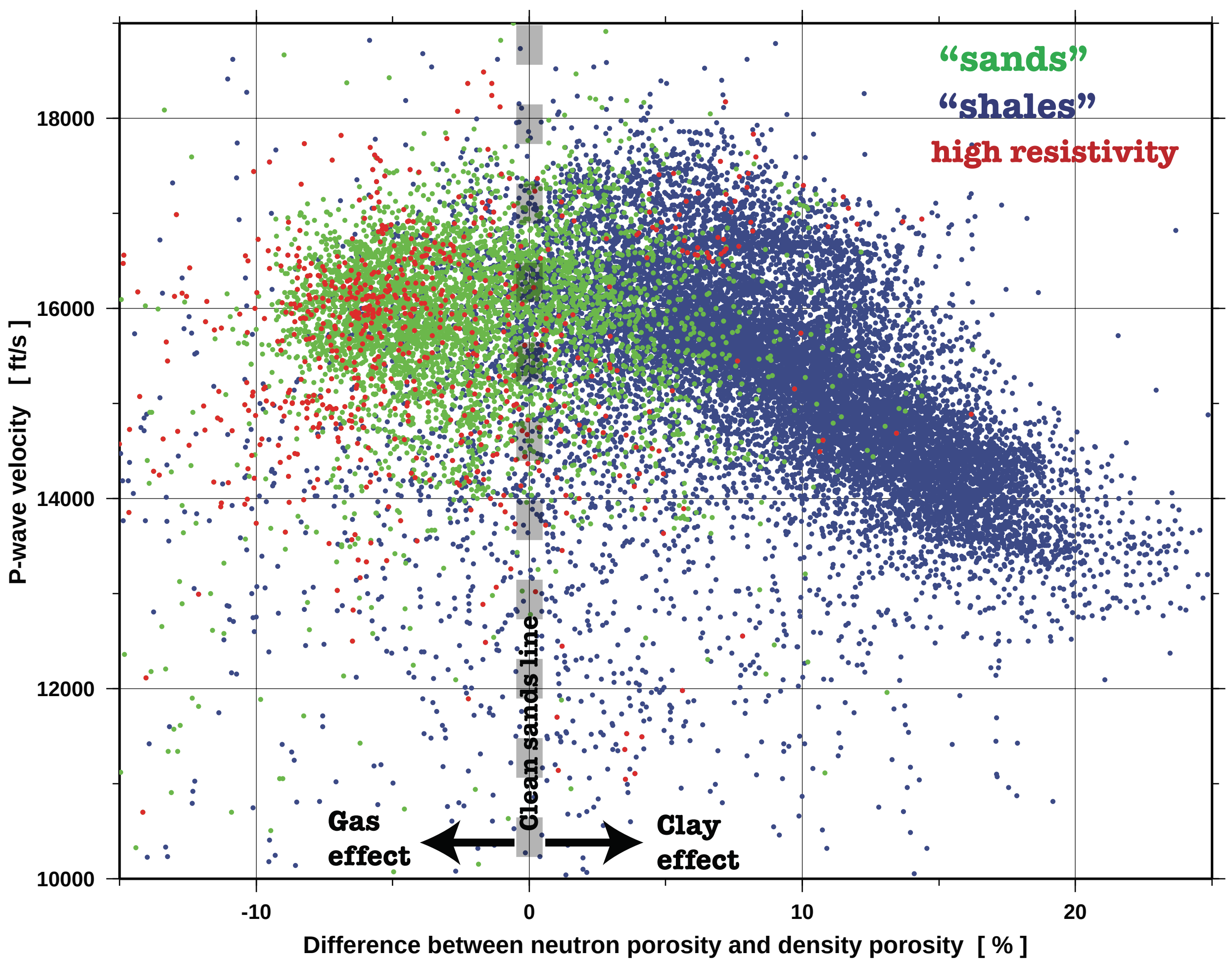

Figure 8. Well-1 velocity versus difference between neutron-porosity and density-porosity crossplot, with interpretive lithology estimation, depth interval 12,700 to 23,00 ft (Upper Cretaceous stratigraphic section down to Mowry shale). Green dots, "sands," rocks having natural gamma-ray intensity below 50 gAPI; blue dots, "shales," rocks having gamma-ray intensity above 50 gAPI; red dots, rocks showing resistivity above 150 ohmm. "Shales" show pronounce diverse trend in distribution: velocity decreases with increasing difference between neutron and density porosities.

14,000 ft/s and lower. The increased clay effect (increased neutron porosity relative to density porosity) is manifest in greatly decreased rock velocities (Figure 8).

The wide range in rock velocity observed in Figures 6–8, along with the very poor correlation with porosity, is interpreted to be the result of highly varied clay content and pore geometry within the rocks. Even a small volume of crack-like pores within the rock matrix can significantly weaken the rock and lower velocity.

Case study 2: Riverton Tribal 52 well, Wind River Basin

The Riverton Tribal 52 well (herein Well-2) is located in the southern Wind River Basin (Figure 1). It was drilled in 1998 as a gas well within the mature Riverton Dome Field, discovered in 1949. Historically, the Riverton Dome Field yielded commercial oil production from the Tensleep and Phosphoria Formations. Around 1960, commercial gas production was established from the Frontier and Muddy Formations. Well-2 is one of the most gas-prolific wells in the field, with initial production of more than 1 million ft^3/d from the Muddy Sandstone, 10 ft thick. The Cretaceous rock sequence penetrated by Well starts with the Lance Formation at a depth of about 1,710 feet and ends with the "Dakota Sandstone" at 9,778 feet. The available high-quality digital log data span almost the entire Upper Cretaceous section. Figure 9 shows the gamma-ray, P-wave velocity, density, density and neutron porosity (blue and orange, respectively), and resistivity logs, as well as a corresponding stratigraphic column, for the 1,710-to-9,778-foot depth interval. The black solid line in the velocity panel (Figure 9) represents the velocity trend obtained by smoothing the sonic velocities with a 250-foot Gaussian operator.

Broad scatter of values within the whole Upper Cretaceous section characterizes the sonic rock velocities. The smoothed sonic velocities gradually increase from the top of the logged interval to a depth of about 3,200 ft and fluctuate between 12,000 and 15,000 ft/s over the rest of the section (Figure 9). Figure 10 is an expanded section of the Well-2 log data for the gas production interval, between 9,400 and 9,750 feet deep in the well. The gas-reservoir rocks, quartzitic sands at depth interval from 9,690 to 9,700 feet (red star in the strat column, Figure 10), are characterized by anomalously low density and velocity values. Gas is indicated by a significant density-neutron porosity crossover.

Figure 11 is the Well-2 rock velocity versus neutron-porosity crossplot. The measured depth interval, 4,750 to 9,750 feet, corresponds to the Cretaceous Cody Shale through Thermopolis Shale stratigraphic section. Differently than in Case Study 1, red dots in Figure 11 indicate measurements within the gas production interval (Muddy Sandstone, 9,690–9,700 ft – star in strat column, Figure 10). The crossplot demonstrates a wide range in velocity values (10,500 to ~17,000 ft/s) and a pronounced inverse trend in the distribution of both "sands" and "shales." As was noted in Case Study 1, velocities decrease linearly with increasing neutron-porosity readings. However, there is a distinct shift in velocities measured within the gas-charged interval. These velocities (red dots) are about 4,000 ft/s slower than those on the major trend line with the same neutron-porosity values (Figure 11). This is an example of really *anomalous* velocity due to gas in reservoir rocks, as compared with the velocity in non-reservoir rocks (blue dots) and brine-saturated sands (green dots).

Figure 12 is the Well-2 rock velocity versus density-porosity crossplot for the 4,750-to-9,750 foot depth interval. Velocity measurements within "shales" (blue dots) are widely scattered and do not correlate with porosity. Velocities in the "sands" are also characterized by significant scatter but seem to be more organized in the velocity-density-porosity domain. The measurements within the "sands" can be fitted to a straight line in the least-squares sense with a correlation coefficient r = –0.79. Velocity measurements within the gas-saturated sands (red dots in Figure 12) are characterized by both greater porosity values (15%–25%) and slowest

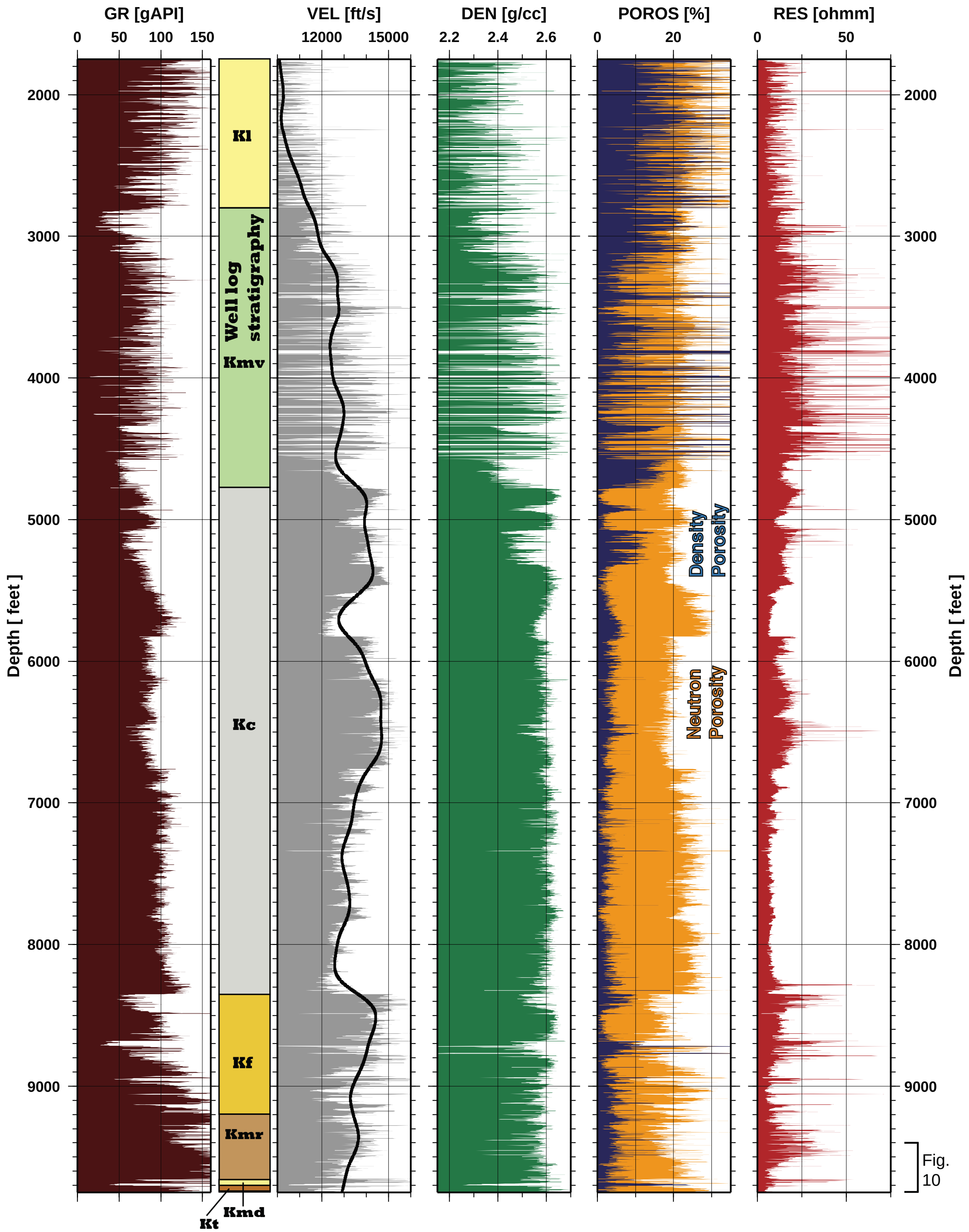

Figure 9, facing page. Well-2 composite wireline logs (Riverton Tribal 52, Riveton Dome, Wind River Basin): GR, gamma-ray; VEL, sonic P-wave velocity; DEN, bulk density; POROS, density (blue) and neutron (orange) porosity; RES, resistivity. Black solid line in VEL panel, velocity smoothed with 250-ft Gaussian operator. Stratigraphic interpretation based on WOGCC geologic markers and wireline log characteristics: Kl, Lance Fm; Kmv, Mesaverde Fm; Kc, Cody Sh; Kf, Fontier Fm; Kmr, Mowry Sh; Kmd, Muddy Ss; Kt, Thermopolis Sh. Production interval, 9,690–9,700 ft.

velocities (10,500–12,000 ft/s). However, the velocity separation caused by the presence of gas is not as obvious in the velocity-density-porosity domain as it is in the velocity-neutron-porosity domain (Figure 11). This separation, which marks an actual anomalous velocity difference, is on the order of 2,000 ft/s (Figure 12).

An abrupt change in the correlation of velocity with density measurements in the Upper Cretaceous section penetrated by Well-2 is shown in Figure 13. The boundary between relatively strong (negative) correlation ($r < -0.75$) and apparently uncorrelatable measurements matches the stratigraphic boundary between the Mesaverde Formation and the Cody Shale. The lack of velocity-density-porosity correlation in the Upper Cretaceous rocks below the Mesaverde calls into question the use of any empirical trends, such as Wyllie's time average equation (Wyllie et al., 1956), within this section. "Sonic porosity," in this case, fails to produce a satisfactory well-log data interpretation over a broad depth interval. Moreover, velocity modeling based on the "normal" exponential shale compaction trend (Athy, 1930) is also inappropriate for the depth interval that lacks velocity-porosity correlation. Jiao and Surdam (1997) displayed several sonic logs from various Wyoming basins with "anomalously" low sonic velocities. They assumed that sonic velocity normally increases exponentially with burial, and they derived their anomalous velocity profiles by taking the difference between the observed sonic velocity and their calculated trend representing normal compaction. There was no consideration of velocity-porosity correlation in this work. However, the displayed depth intervals for their typical sonic logs (Jiao and Surdam, 1997, Figures 2–5) range from 2,500 to 5,000 meters (8,200 to 16,400 feet), and there is no evidence for consistent velocity-porosity correlation within these wide depth intervals. This makes interpretation of the "anomalous" velocity profiles of Jiao and Surdam equivocal. Velocity trend estimation as a function of depth should be accompanied by a velocity-porosity correlation analysis similar to the one shown in Figure 13. Intervals with poor velocity-porosity correlation cannot be considered "anomalous" on the basis of "trend" subtraction because no trend is defined for these intervals. On the other hand, the correlation coefficient calculated for velocity and neutron porosity logs indicates strong and consistent interrelation between the two properties (Figure 13). Considering this, the 4,000-ft/s velocity shift from the velocity-neutron porosity trend-line in Figure 11 can be considered really anomalous. As described above, this anomaly is caused by gas saturation.

Case study 3: Stud Horse Butte 14-34 well, Jonah Field, Green River Basin

The Stud Horse Butte 14-34 well (herein Well-3) is located in the northwestern corner of the Greater Green River Basin in the south-central Jonah Field (Figure 1). The Jonah Field produces gas from overpressured, discontinuous sandstone reservoirs in the Upper Cretaceous Lance Formation. The reservoir rocks are stacked within an interval that spans hundreds of feet in thickness. The sandstone reservoir rocks are intercalated with thin layers of low-permeability shales and mudstones. Well-3 is perforated within the depth interval 7,891 to 10,842 feet; the greatest perforation density is below a depth of 8,972 feet. Figure 14 shows the gamma-ray, P-wave velocity, TG mud (total-gas mud), caliper, density and neutron porosity (blue and orange, respectively), and resistivity logs, as well as a corresponding stratigraphic column,

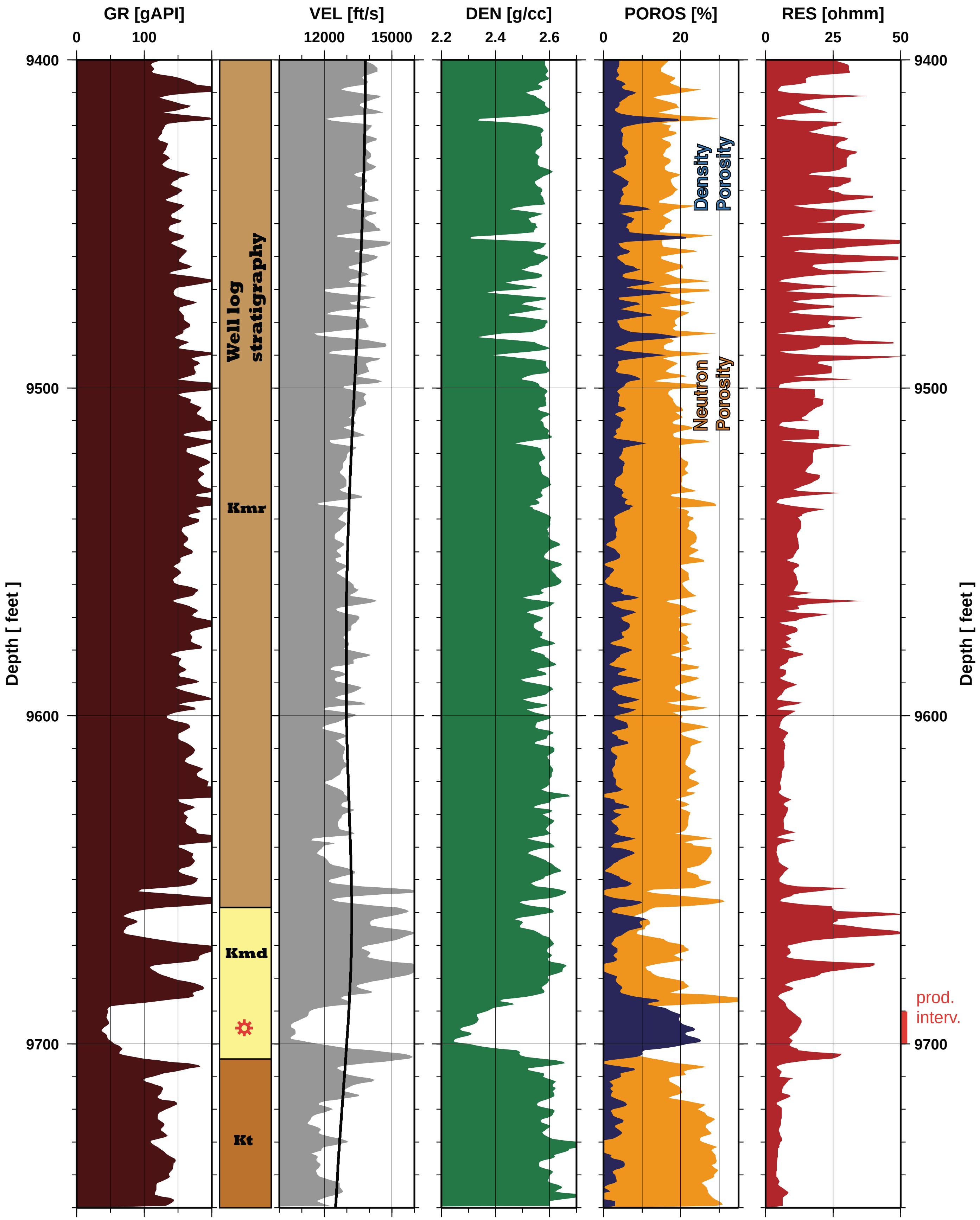

Figure 10, facing page. Expanded Well-2 composite wireline logs, depth interval 9,400–9,750 ft, including production interval 9,690–9,700 ft: GR, gamma-ray; VEL, sonic P-wave velocity; DEN, bulk density; POROS, density (blue) and neutron (orange) porosity; RES, resistivity. Black solid line in velocity panel, velocity smoothed with 250-ft Gaussian operator. Kmr, Mowry Sh; Kmd, Muddy Ss; Kt, Thermopolis Sh.

for the 6,500-to-11,000-foot depth interval. The mud log indicates the top of true overpressure at a depth of about 8,350 feet. At same depth there is a velocity reversal clearly identifiable on the smoothed sonic curve (Figure 14). The mud log continues with high gas shows all the way down to the second overpressure zone at about 10,500 feet depth. Over the same depth interval, sonic velocity values are characterized by great fluctuation, while the smoothed velocity function generally increases with depth (Figure 14). The porosity and resistivity logs also show great fluctuation within the pay zone that is likely consistent with sand-shale intercalations. Figure 15 is an expanded section of the Well-3 log data, between 8,250 and 8,900 feet deep in the well, that includes the first overpressured depth interval. The lithology log data available for this interval enables one to correlate lithologic variations with wireline log data. The sandy intervals (yellow bars in the lithology column, Figure 15) appear to be mechanically stronger (have smaller caliper values), higher in rock velocity, and less porous than the shales and mudstones. The deep-resistivity measure increases abruptly within the sandy intervals, which indicate elevated gas saturation (Figure 15).

Figure 16 shows the Well-3 rock velocity versus neutron-porosity crossplot. The measured depth interval, 6,500 to 11,000 feet, is the same as in Figure 14, and corresponds to the Lower Tertiary – Upper Cretaceous stratigraphic section. The color-coding scheme in Figure 16 is consistent with that of Figures 6 through 8 for Case study 1, with the exception that the resistivity threshold is 50 ohmm in this case (red dots). The crossplot demonstrates a wide range of velocity values (~9,000 to ~17,000 ft/s) and a pronounced inverse trend in distribution that is characteristic of shaley lithologies (blue dots). Velocity clearly decreases with neutron-porosity readings.

Figure 17 shows the Well-3 rock velocity versus density-porosity crossplot. The rock velocities measured within the mostly gas-saturated section at Jonah Field match the V-shape distribution (Figure 2c) predicted by Marion et al. (1992) for the sand-shale transition model with variable clay content. Again, as in Case Study 2, the wide scatter of data points in Figure 17 can be largely attributed to the variation in clay content within sandy shales and shaley sands.

Figure 18 shows the Well-3 rock velocity versus difference between neutron-porosity and density-porosity (ϕ_N-ϕ_D) crossplot. The "clean sands" line, in this case, is shifted from the zero value due to uncertainties in the matrix porosity estimates. Nevertheless, the crossplot allows separating "sands" from "shales" both in color and in space. Extreme scatter characterizes velocity measurements within the "shales" around a general trend of velocity decrease with increasing ϕ_N-ϕ_D. The rock velocities measured in highly gas-saturated rocks (red dots) cluster around 14,000 ft/s, which cannot be regarded as anomalously slow. A relatively great number of velocity measurements in the "shales" have values that are much lower than 14,000 ft/s. The increased clay effect (increased neutron porosity relative to density porosity) here again is manifest in decreased rock velocities (Figure 18).

Case study 4: Stagecoach Draw 16A well, Sandy Bend arch, Green River Basin

The Stagecoach Draw 16A well (herein Well-4) is located in the relatively underexplored central Green River Basin between the Moxa Arch and the Rock Springs Uplift. The recently discovered (1993) Stagecoach Draw field produces gas from the Upper Cretaceous marine influenced sandstones of the Almond Formation. Well-4 is perforated within the narrow depth interval from 7,990 to 7,993 feet. Figure 19 shows the gamma-ray, P-wave velocity, bulk density, caliper, density

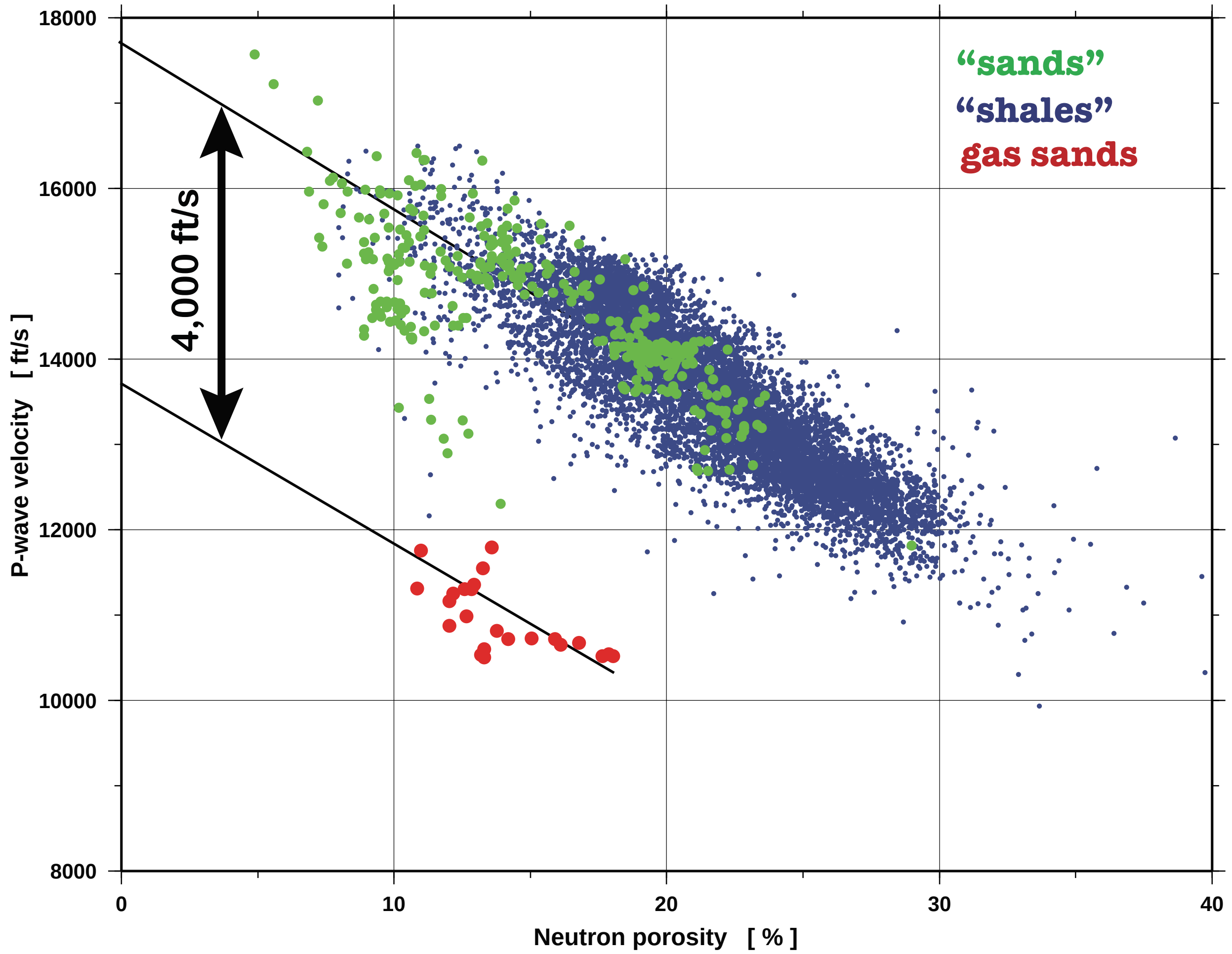

Figure 11. Well-2 velocity versus neutron-porosity crossplot, depth interval 4,750 to 9,750 ft (Cretaceous Cody Shale through Thermoplis Shale). Green dots, "sands," rocks having natural gamma-ray intensity below 60 gAPI; blue dots, "shales," rocks having gamma-ray intensity above 60 gAPI; red dots, measurements within the gas production interval, 9,690–9,700 ft, in the Muddy Sandstone. Measurements in the "shales" show a pronounced inverse trend in distribution: velocity decreases with increasing neutron porosity. Measurements in the presumed brine sands (green dots) follow approximately the "shale" trend while the gas-saturated sands (red dots) have velocity values ~4,000 ft/s slower than the shale-trend velocities at the same porosity values.

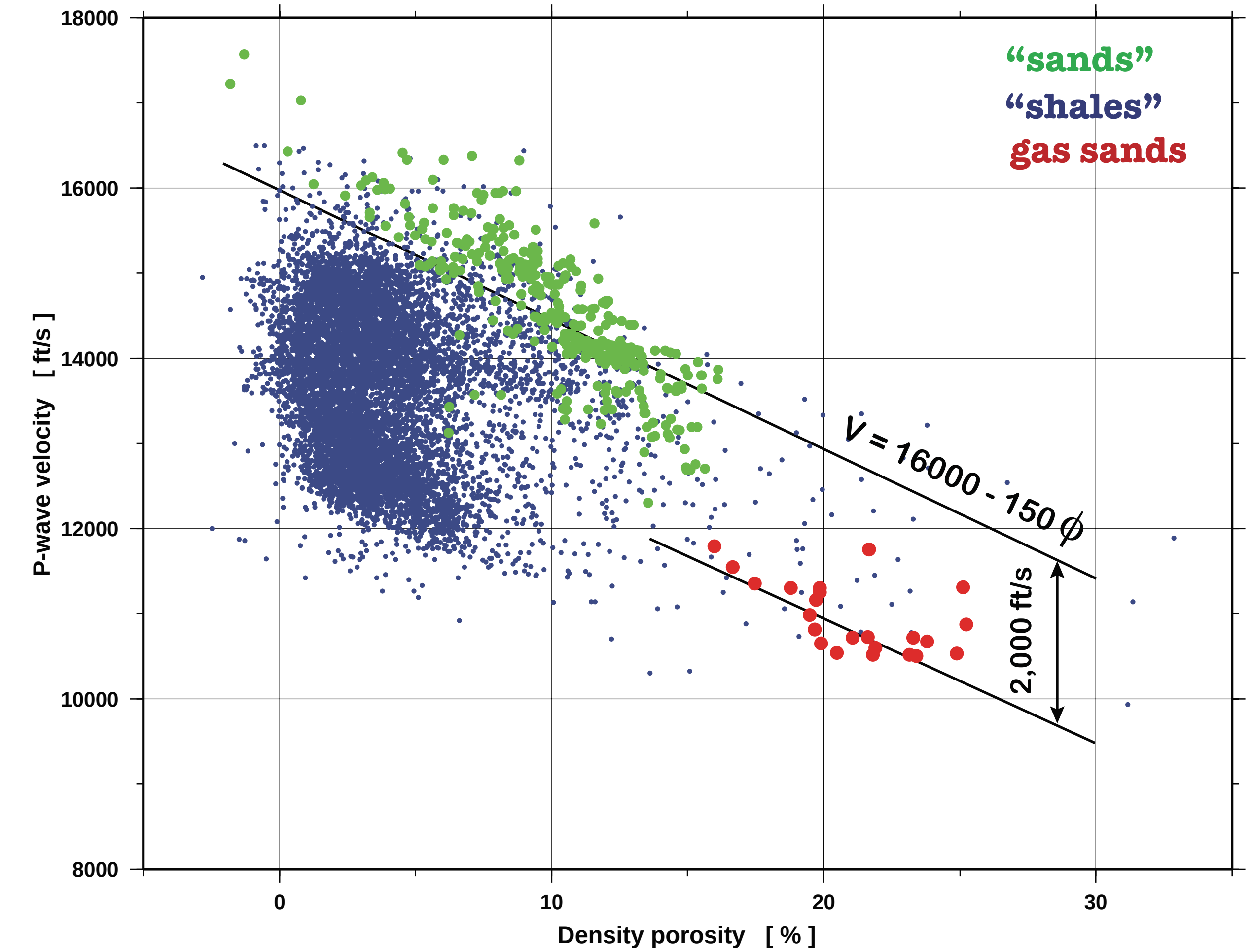

Figure 12. Well-2 velocity versus density-porosity crossplot, depth interval 4,750 to 9,750 ft (Cretaceous Cody Shale through Thermoplis Shale). Green dots, "sands," rocks having natural gamma-ray intensity below 60g API; blue dots, "shales," rocks having gamma-ray intensity above 60 gAPI; red dots, measurements within the gas production interval, 9,690–9,700 ft, in the Muddy Sandstone. Note (1) the absence of correlation between velocity and porosity for shales; (2) presumed brine sands characterized by moderate correlation (black solid line $V = 16{,}000 - 150\phi$ with $r = -0.79$ and $dV = \pm 800$ ft/s); (3) gas sands characterized by increased porosity values (15%–25%) and anomalously slow velocities relative to the velocity trend line established for the brine sands: the general velocity separation of brine sands from gas sands of ~2,000 ft/s as against the significantly smaller variation of velocity about the regression lines. V, velocity; ϕ, density porosity as decimal fraction; r, correlation coefficient; dV, general variation about the regression line.

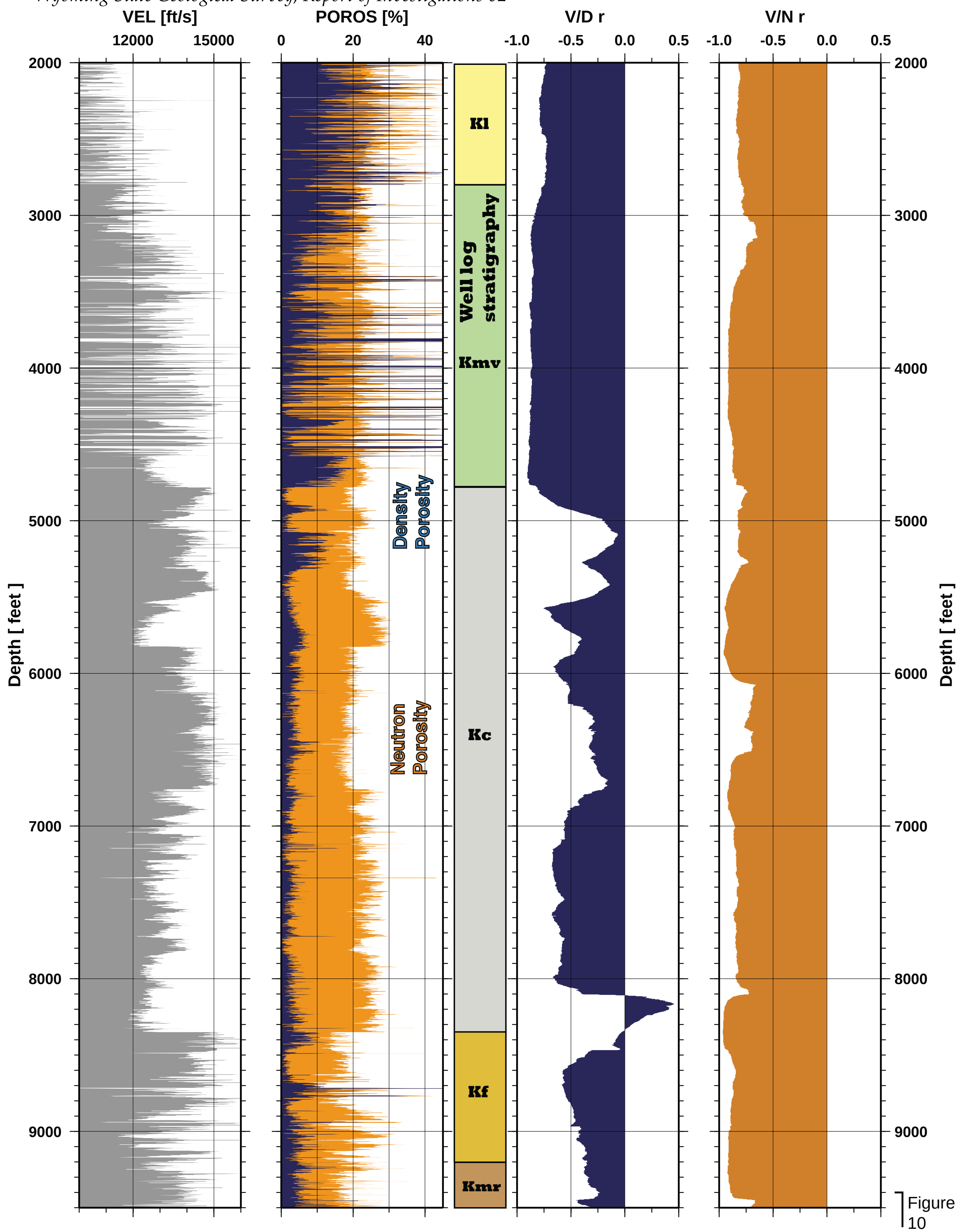

Figure 13, facing page. Well-2 velocity and porosity logs with interpreted stratigraphy and calculated correlation coefficients: VEL, sonic P-wave velocity; POROS, density (blue) and neutron (orange) porosity; V/Dr, correlation coefficient for velocity vs. density porosity; V/Nr, correlation coefficient for velocity vs. neutron porosity. Continuous correlation coefficients calculated with a 500-ft running window, and thus truncated 250 ft top and bottom with respect to Figure 9. Kl, Lance Fm; Kmv, Mesaverde Fm; Kc, Cody Sh; Kf, Frontier Fm; Kmr, Mowry Sh.

and neutron porosity (blue and orange, respectively), and resistivity logs, as well as a corresponding stratigraphic column, for the 5,000–8,080-foot depth interval.

As in the case studies above, sonic velocity shows significant fluctuation within the measured depth interval. The smoothed velocity function demonstrates several low-magnitude velocity reversals while generally increasing with depth. One of these reversals, where the smoothed velocity drops to ~13,000 ft/s from 14,000 ft/s, correlates with top of the Almond Formation (Figure 19). Increasing gas saturation with depth is manifested by the relative increase in deep-resistivity readings with depth toward and into the Upper Cretaceous (Lance) strata. There are also several high-resistivity zones in the Tertiary Fort Union Formation with the abrupt bounds, accompanied by low density and low velocity readings. These are probably coaly intervals, as marked by extremely low gamma-ray counts (Figure 19).

Figure 20 is an expanded section of the Well-4 log data covering the uppermost Cretaceous section from 7,200 to 8,080 ft deep in the well. The greatest variability in velocity occurs at the base of the Lance Formation, an interval characterized by intercalated thin shales, mudstones, and sandstones. On the contrary, the Upper Almond sand bar (red star, Figure 20) is characterized by fairly uniform velocity values just above 13,000 ft/s (Figure 20). The presence of gas within the Upper Almond sand is confirmed by relatively high resistivity log readings (above 25 ohmm) and by density porosity uniformly meeting or exceeding neutron porosity.

Figure 21 shows the Well-4 rock velocity versus neutron-porosity crossplot. The measured depth interval, 5,000 to 8,080 feet, is the same as that of Figure 19, and covers the lowermost Tertiary–uppermost Cretaceous stratigraphic section. The color-coding scheme in Figure 21 is that of Figures 6 through 8 from Case Study 1, with the exception that the resistivity threshold is 25 ohmm in this case (red dots). The crossplot demonstrates a wide range of velocity values (~11,000 to ~16,000 ft/s) and a pronounced inverse trend in distribution that is characteristic of shaley lithologies (blue dots). Velocity clearly decreases with higher neutron-porosity readings.

A peculiarity of this case study is that the gas-producing interval is thoroughly defined in depth with low gamma-ray readings (Figure 20) and therefore can be identified and isolated on the velocity-porosity crossplots. The circled area in Figure 21 shows velocity/neutron-porosity measurements within this gas-charged interval. The concentrations of red and green dots within the circled area indicates mostly “sandy” lithology. The high resistivity-log profile over the gas-producing interval confirms the identification. It is clear on Figure 21 that velocities measured in the gas-saturated rocks (~13,400 ft/s) are slower than those measured outside the producing interval in the rocks with the same neutron porosity. However, P-wave velocities measured in this case in the gas-charged reservoir rocks are close in value to the mean velocity value (~13,500 ft/s) characteristic of the surrounding shales (Figure 20, smoothed velocity trend). This would make it difficult, if possible at all, to separate gas-charged intervals on this velocity-depth profile using velocity reversals only. Figure 21 proves that the slowest velocities correlate with non-reservoir “shaley” rocks in which high hydrogen content in clays results in high neutron porosity.

Figure 22 shows the Well-4 rock velocity versus density-porosity crossplot. Broad scatter and no clear correlation with porosity characterize the overall measured rock velocities. As on Figure 21, the circled area in Figure 22 shows measurements taken within the gas-charged interval only. A linear trend of velocity decrease with increasing porosity

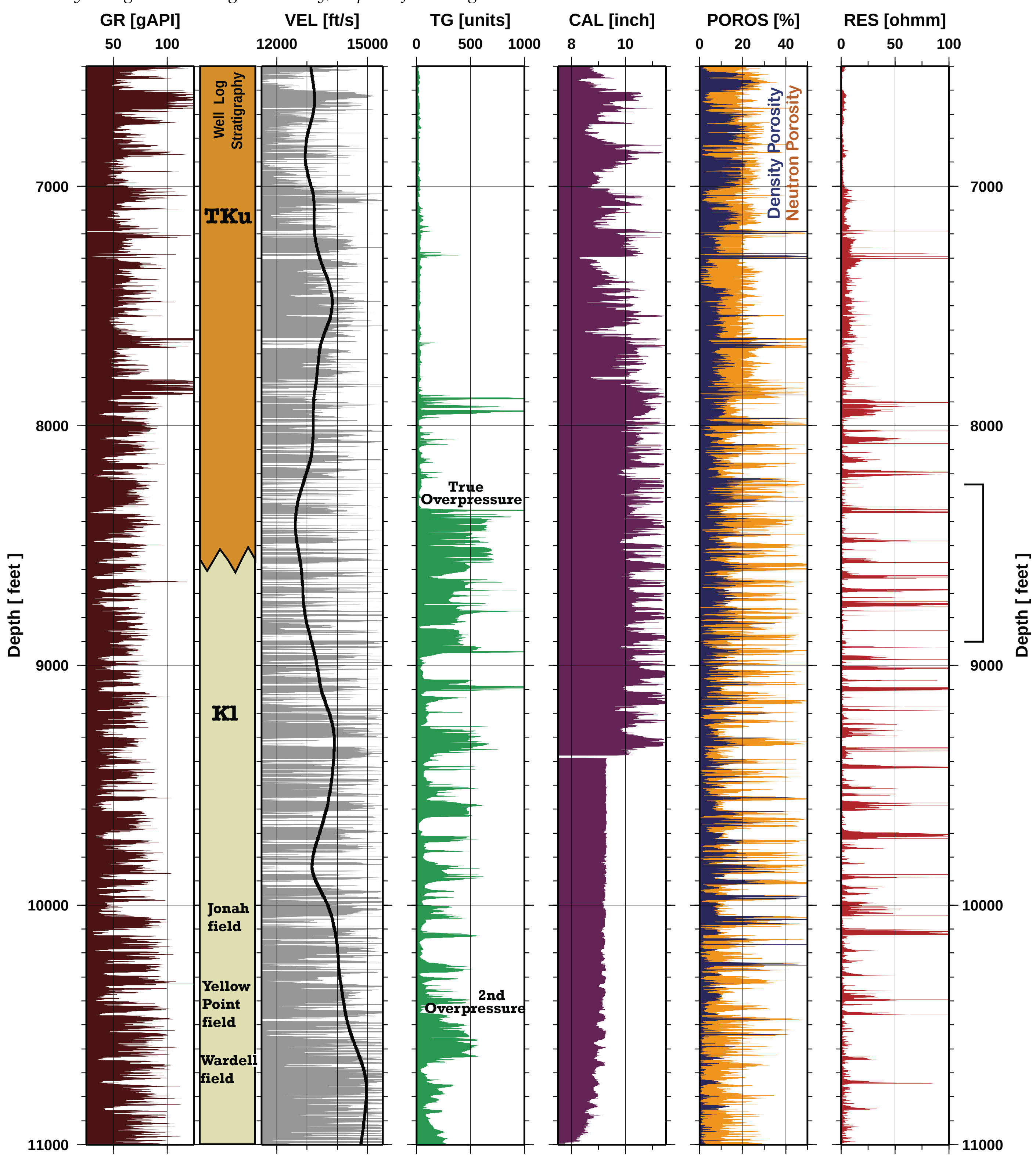

Figure 14. Well-3 composite wireline logs (Stud Horse 14–34 well, Jonah Field, Green River Basin): GR, gamma-ray; VEL, sonic P-wave velocity; TG, total gas (mud log); CAL, caliper; POROS, density (blue) and neutron (orange) porosity; RES, resistivity. Black solid line in velocity panel, velocity trend smoothed with 250-ft Gaussian operator. Stratigraphic interpretation based on WOGCC geologic markers and wireline log characteristics: Kl, Lance Fm; Kmv, Mesaverde Fm; Kc, Cody Sh; Kf, Fontier Fm; Kmr, Mowry Sh; Kmd, Muddy Ss; Kt, Thermopolis Sh. Production interval, 9,690–9,700 ft.

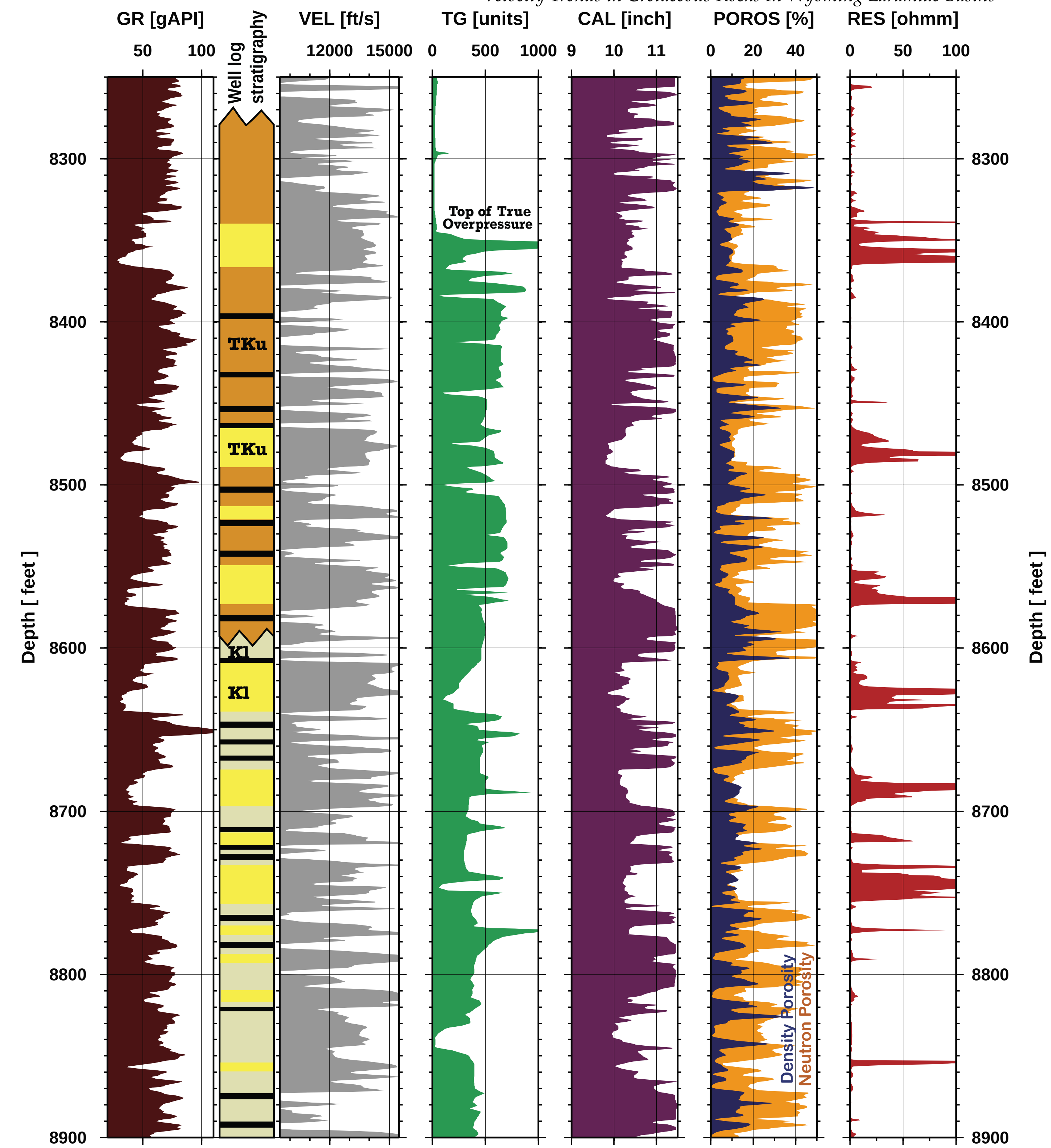

Figure 15. Expanded Well-3 composite wireline logs, depth interval 8,250–8,900 ft, and lithologic interpretation: GR, gamma-ray; VEL, sonic P-wave velocity; TG total gas (mud log); CAL, caliper; POROS, density (blue) and neutron (orange) porosity; RES, resistivity. Coaly (black bars) and sandy (yellow bars) intervals interpreted on basis of lithology log and wireline log data. Tku, Tertiary and Cretaceous rocks undivided; Kl, Lance Fm.

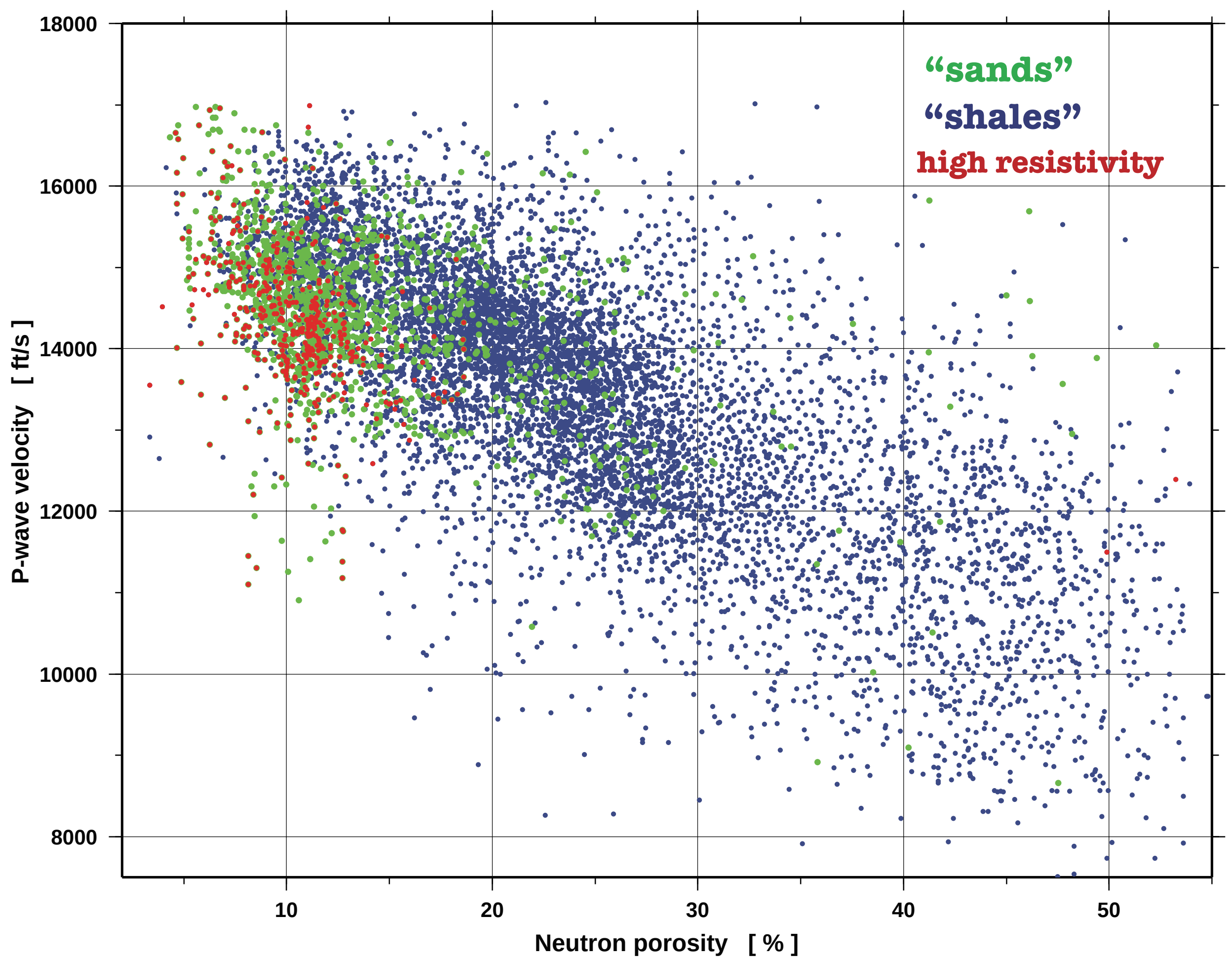

Figure 16. Well-3 velocity versus neutron-porosity crossplot, depth interval 6,500 to 11,00 ft (lower Tertiary–Upper Cretaceous). Green dots, "sands," rocks having natural gamma-ray intensity below 50 gAPI; blue dots, "shales," rocks having gamma-ray intensity above 50 gAPI; red dots, rocks showing resistivity above 50 ohmm. "Shales" show wide range in velocities and a pronounced inverse trend in distribution: velocity decreases with increasing neutron porosity. Presumed gas-saturated rocks with high resistivity values (red dots) are not characterized by extreme velocity values.

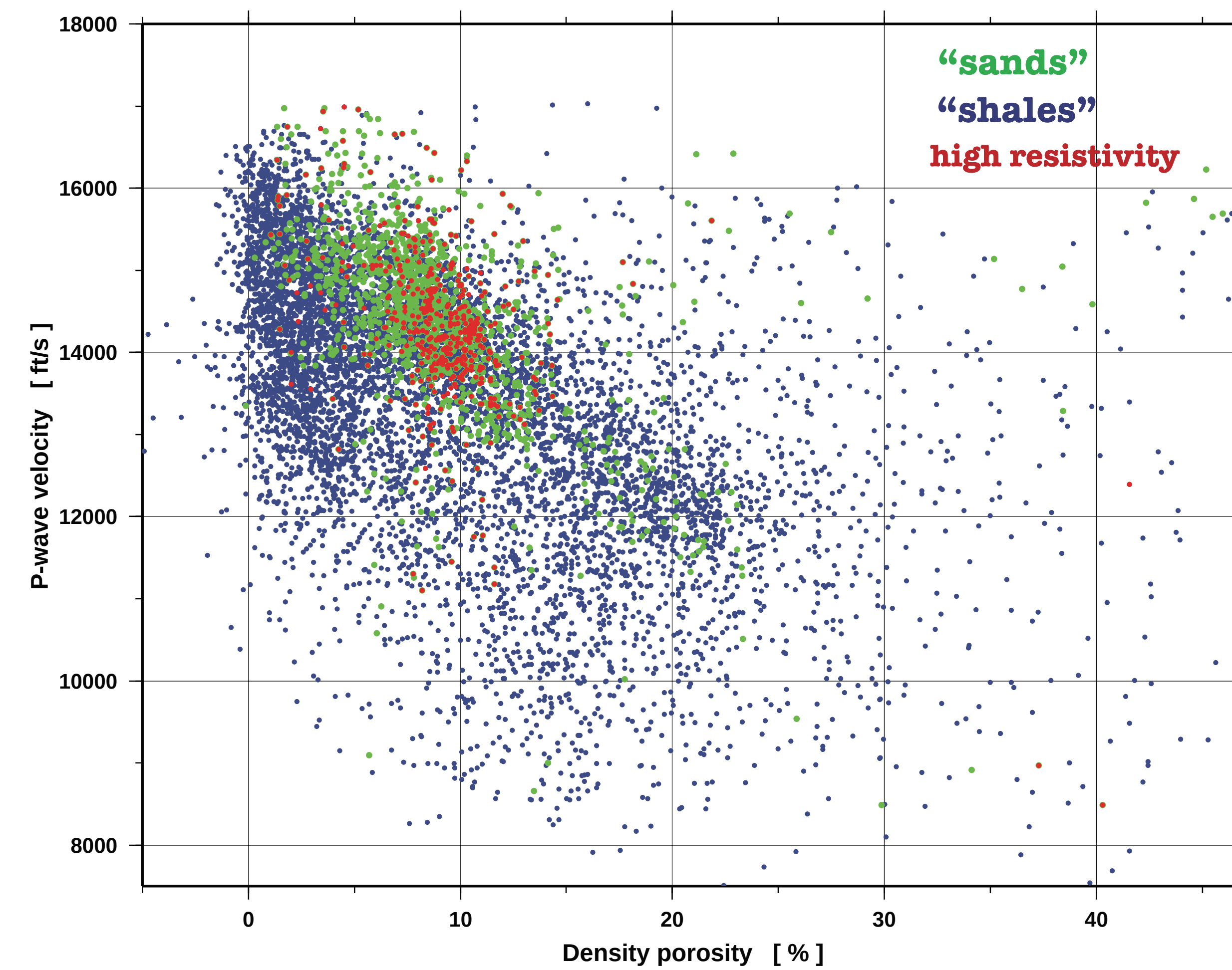

Figure 17. Well-3 velocity versus density-porosity crossplot, depth interval 6,500 to 11,000 ft (lower Tertiary–Upper Cretaceous). Green dots, "sands," rocks having natural gamma-ray intensity below 50 gAPI; blue dots, "shales," rocks having gamma-ray intensity above 50 gAPI; red dots, rocks showing resistivity above 50 ohmm. Note (1) the absence of overall correlation between velocity and porosity; (2) the wide range in measured P-wave velocities; and (3) the apparent presence of two groups of data ("sands" and "shales"). Presumed gas-saturated rocks with high resistivity values (red dots) are not characterized by extreme velocity values.

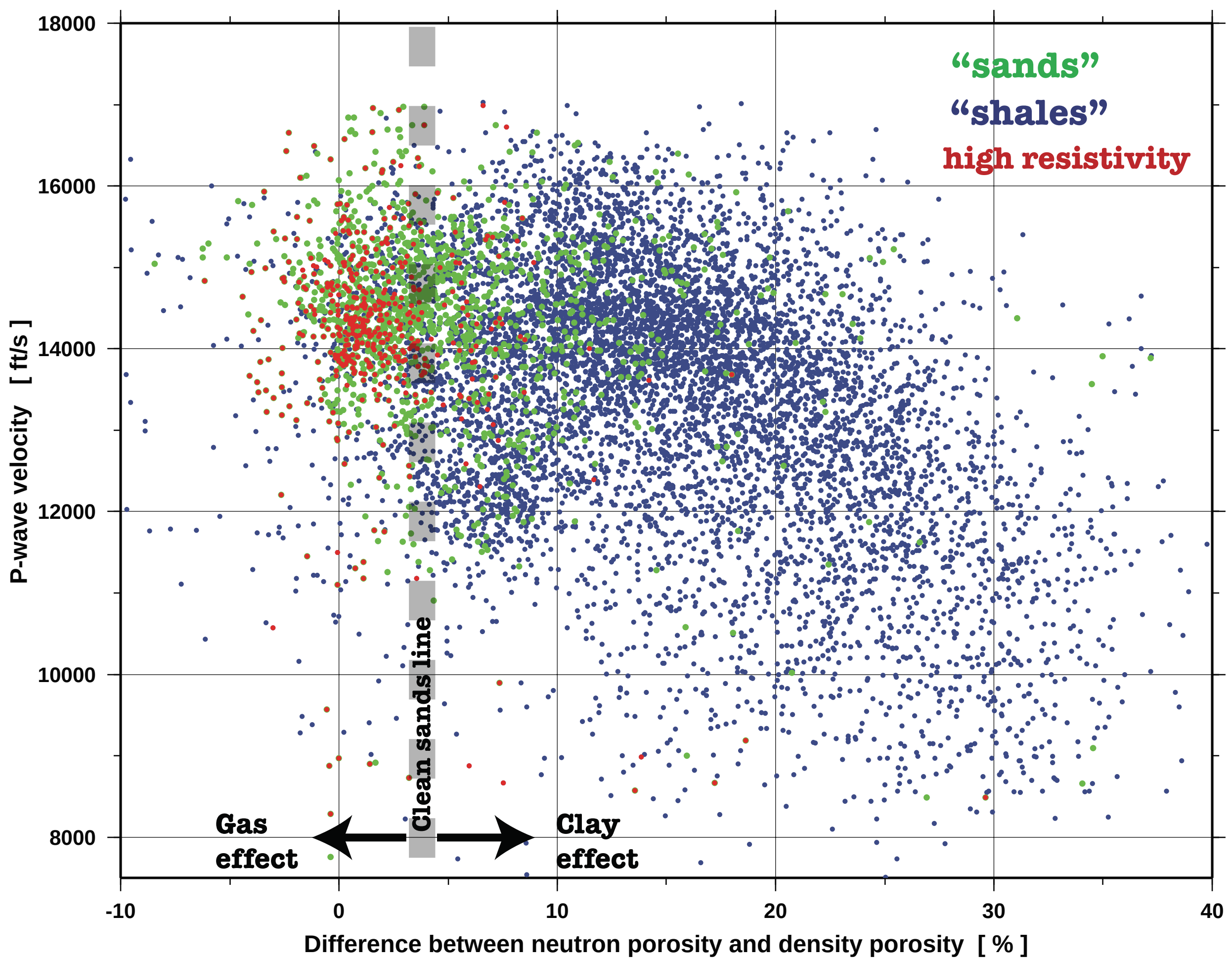

Figure 18. Well-3 velocity versus difference between neutron-porosity and density-porosity crossover with interpretive lithology estimation, depth interval 6,500 to 11,000 ft (lower Tertiary–Upper Createceous). Green dots, "sands," rocks having natural gamma-ray intensity below 50 gAPI; blue dots, "shales," rocks having gamma-ray intensity above 50 gAPI; red dots, rocks showing resistivity above 50 ohmm. Overall, measurements show little noticeable trend in distribution.

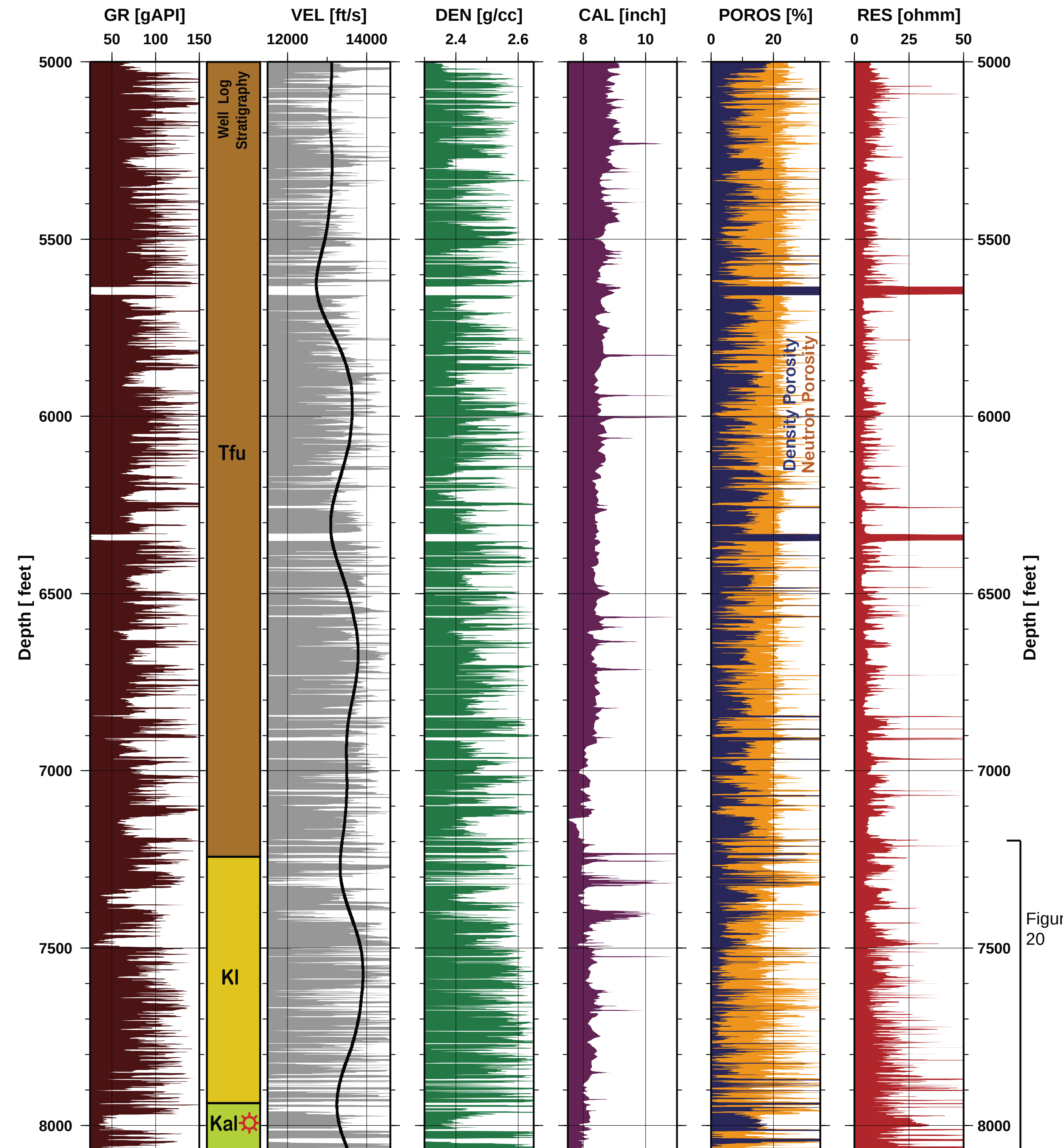

Figure 19. Well-4 composite wireline logs (Stagecoach Draw 16A well, Green River Basin): GR, gamma-ray; VEL, sonic P-wave velocity; DEN, bulk density; CAL, caliper; POROS density (blue) and neutron (orange) porosity; RES, resistivity. Black solid line in velocity panel, velocity smoothed with 250-ft Gaussian operator. Stratigraphic interpretation based on WOGCC geologic markers and wireline log characteristics: Tfu, Fort Union Fm; Kl, Lance Fm; Kal, Almond Fm. Lance may include thin Fox Hills and Lewis units indistinguishable at this location.

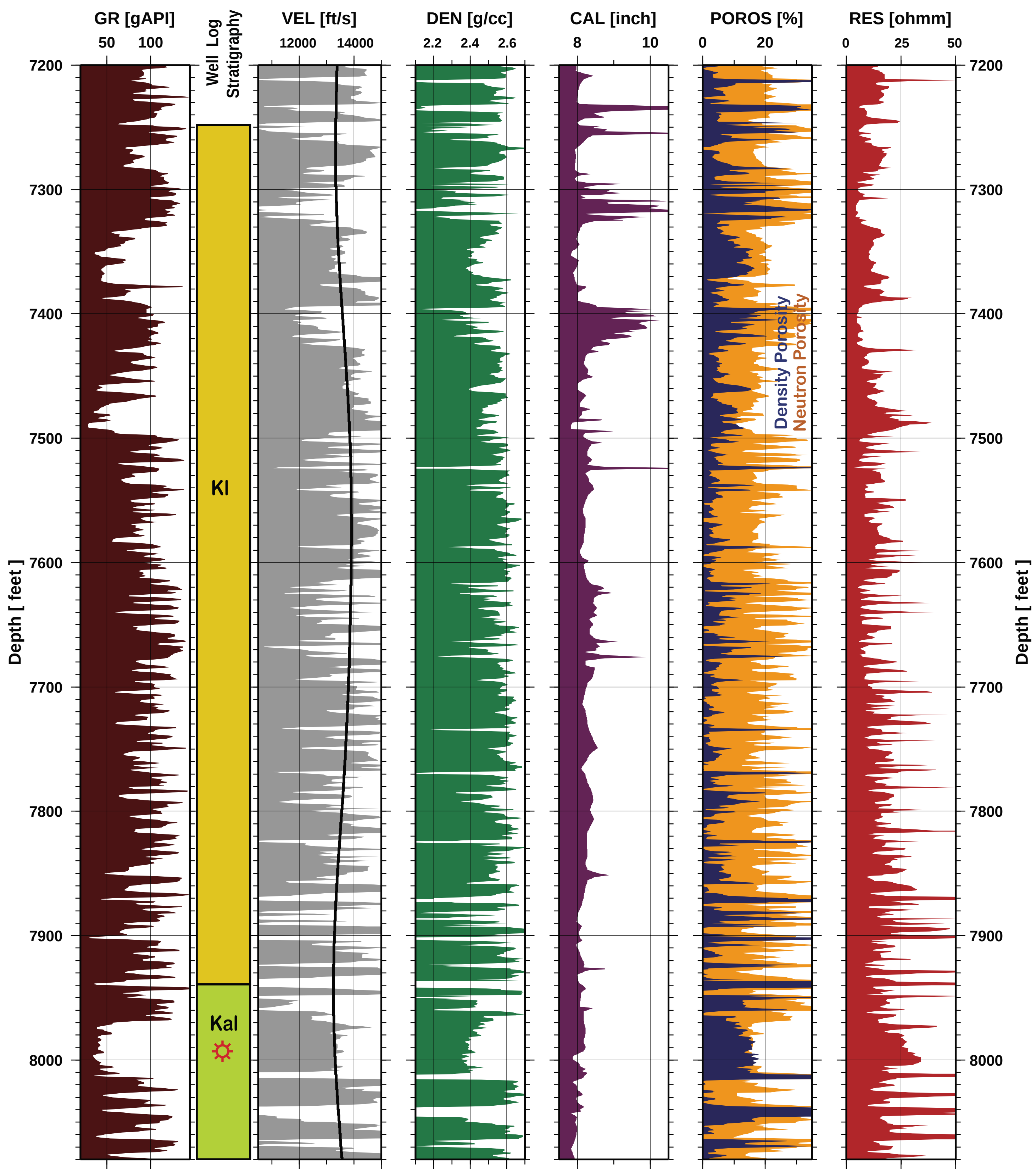

Figure 20, facing page. Expanded Well-4 composite wireline logs, depth interval 5,000–8,080 ft, including gas-producing interval, 7,980–8005 ft: GR, gamma-ray; VEL, sonic P-wave velocity; DEN, bulk density; CAL; caliper; POROS, density (blue) and neutron (orange) porosity; RES, resistivity. Black solid line in velocity panel, velocity smoothed with 250-ft Gaussian operator. Stratigraphic interpretation based on WOGCC geologic markers and wireline log characteristics: Kl, Lance Fm; Kal, Almond Fm. Lance may include thin Fox Hills and Lewis units indistinguishable at this location. Red star locates Upper Almond sand.

is clearly indicated for the gas-saturated rocks. As is expected, the greatest gas saturation (concentration of red dots) correlates with high porosity and low velocity. This observation is true for the upper Almond Sandstone only (circled area). However, in this case the Almond sandstone is characterized by relatively high density-porosity values, 12% to 18%, and therefore cannot strictly be called "tight gas sand."

Figure 23 shows the well-4 rock velocity versus difference between neutron porosity and density-porosity (ϕ_N-ϕ_D) crossplot. The "clean sands" line is slightly shifted from the zero value due to uncertainty in the matrix porosity estimates. Extreme scatter characterizes velocity measurements in the "shales," and they show no correlation with the (ϕ_N-ϕ_D) values. As is expected, well-log measurements within the highly gas-saturated rocks (red dots) cluster left of the "clean sands" line (negative difference between neutron porosity and density porosity). Interestingly, a definite trend line is observed for the measurements within the gas-production interval (Figure 23). An increased gas effect is manifested with decreased rock velocity values. This observation is in accord with theoretical predictions and laboratory measurements on sand samples. One might question if the velocity difference due the gas effect (about 500 ft/s in this case) would be a significant criterion for distinguishing "tight gas sand" using seismically derived velocities. There seems to be no definitive answer to that question at this time.

Case study 5: Fillmore Creek 9-1 well, Wamsutter arch, Greater Green River Basin

The Fillmore Creek 9-1 well (herein Well-5) is located in the eastern Greater Green River Basin on the Wumsutter arch (Figure 1). The well has produced gas from a sandy member of the Lewis Shale. The Lewis Shale in this area is composed mostly of shale, siltstone, and very-fine- to medium-grained sandstone. Figure 24 shows the gamma- ray, P-wave velocity, bulk density, total gas, density and neutron porosity (blue and orange, respectively), and resistivity logs for the 7,000-to-9,000-foot depth interval. This case study matches a conventional "tight gas sand" as defined by porosities in the pay zone not exceeding 10%.

The gas production interval (at about 8,400 feet depth – Figure 24) is marked by increased total gas, resistivity, density porosity, and velocity readings. A pronounced inverse trend in distribution is observed on the velocity versus neutron-porosity crossplot (Figure 25). Again, as in all the case studies above, we see a linear decrease in velocity with increasing neutron porosity. The rock velocity ranges between about 15,000 ft/s and 11,000 ft/s within the 2,000-foot depth interval depicted in Figure 24, but there is no correlation of velocity with depth. The velocity versus density-porosity crossplot shown in Figure 26 demonstrates again a wide range in measured P-wave velocity that does not correlate with density porosity. The "sand" (green dots) and gas reservoir rocks (red dots) correlate with relatively fast velocities, while "shales" measure at slower velocities. The velocity versus difference between neutron-porosity and density-porosity crossplot shown in Figure 27 separates gas-charged reservoir rocks both in color (red dots) and in space (below 10% porosity difference).

Case study 6: Echo Springs 17-5 well, Wamsutter arch, Greater Green River Basin

The Echo Springs 17-5 well (herein Well-6) is located in the eastern Greater Green River Basin on the Wumsutter arch (Figure 1). The well produces gas from an interval of low-permeability reservoirs at the top of the Almond Formation that directly underlies the Lewis Shale. The Almond Formation

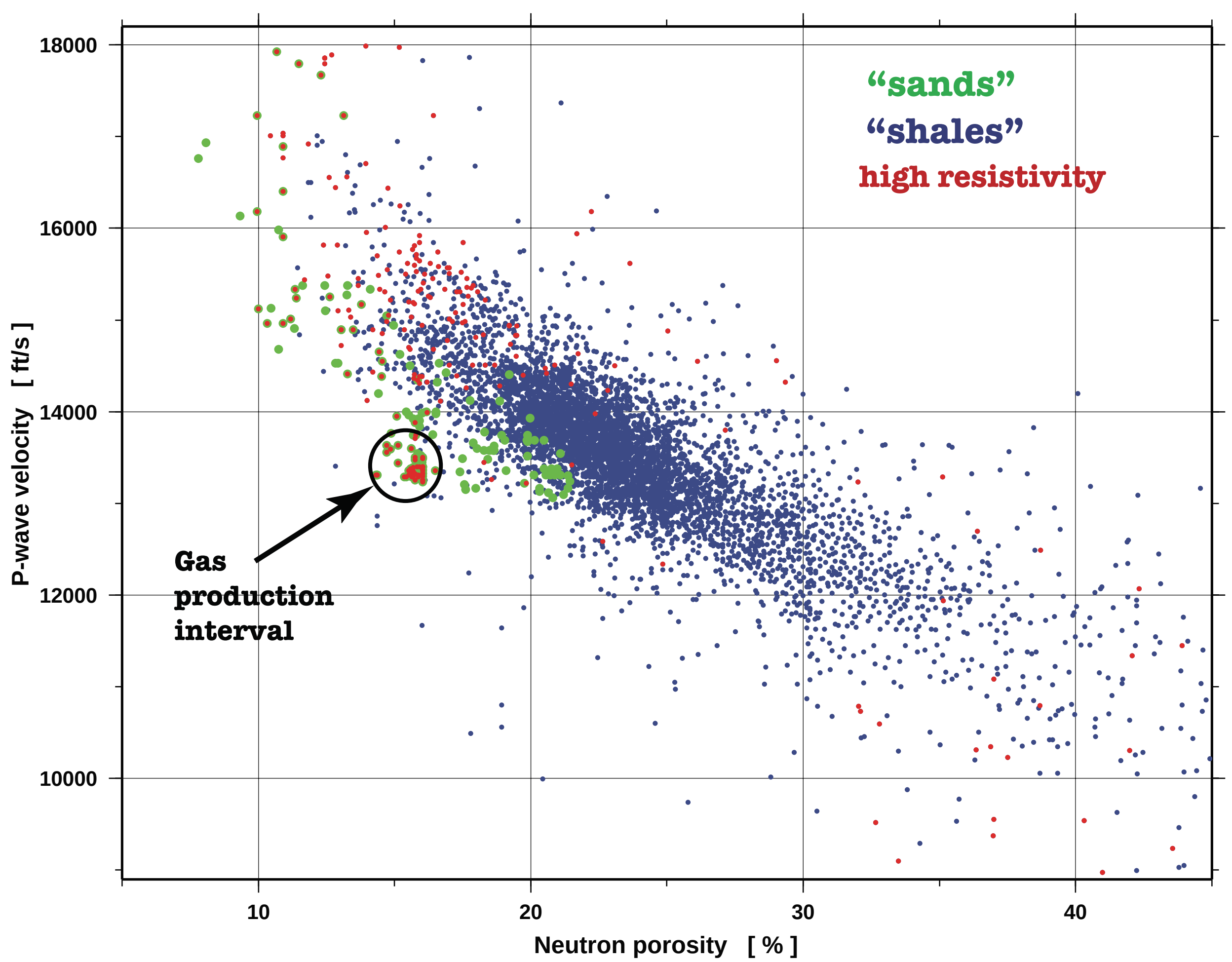

Figure 21. Well-4 velocity versus neutron-porosity crossplot, depth interval 5,000 to 8,080 ft (Fort Union through Almond Formations). Green dots, "sands," rocks having natural gamma-ray intensity below 50 gAPI; blue dots, "shales," rocks having gamma-ray intensity above 50 gAPI; red dots, rocks showing resistivity above 25 ohmm. Measurements within the "shales" show a pronounced inverse trend in distribution: velocity decrease with increasing neutron porosity. The circled area contains measurements only from the Almond gas-producing interval (7,980–8,005 ft).

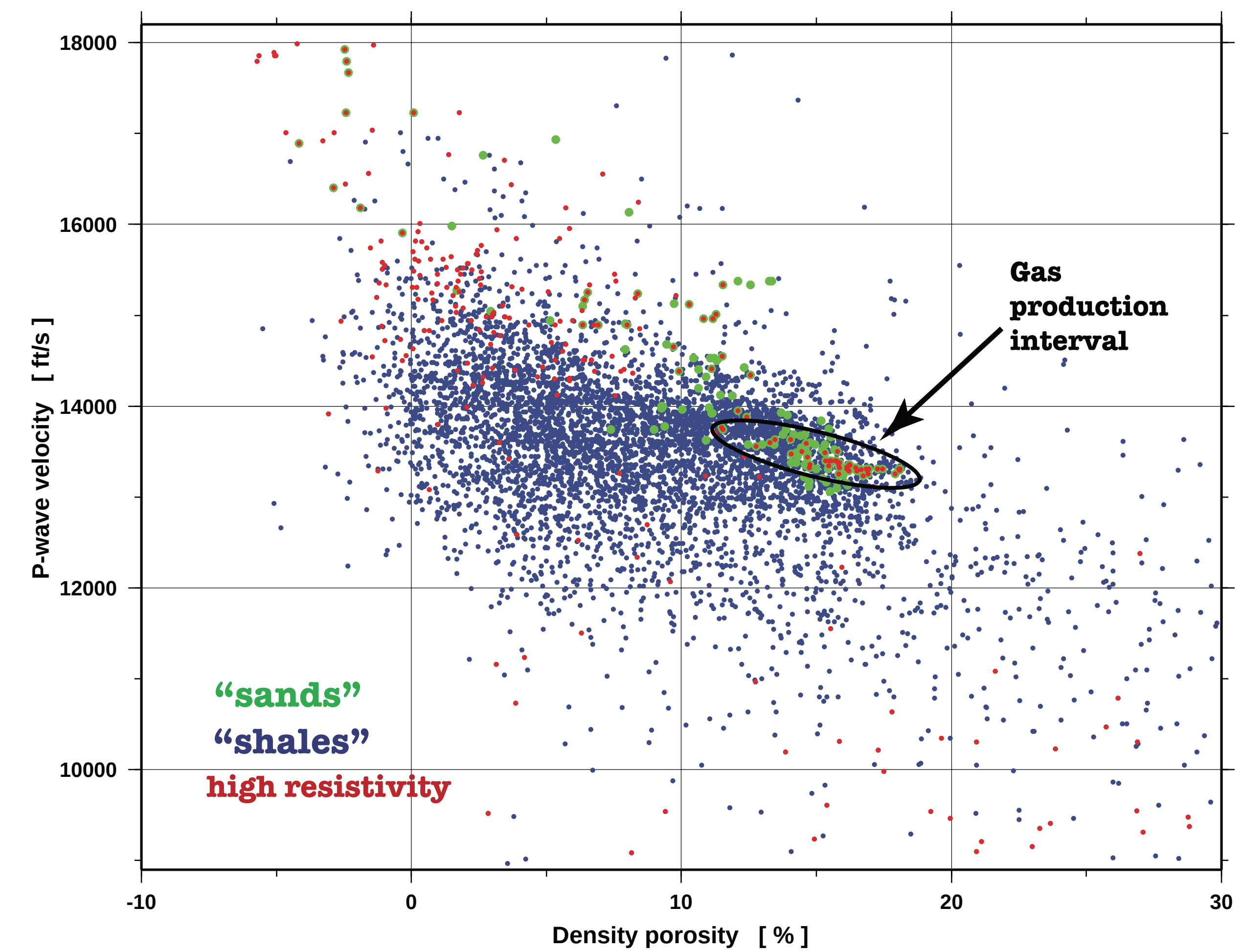

Figure 22. Well-4 velocity versus density-porosity crossplot, depth interval 5,000 to 8,080 ft (For Union through Almond Formations). Green dots, "sands," rocks having natural gamma-ray intensity below 50 gAPI; blue dots, "shales," rocks having gamma-ray intensity above 50 gAPI; red dots, rocks showing resistivity above 25 ohmm. Overall, measurements show noticeable trend in distribution. The circled area contains measurements only from the Almond gas-producing interval (7,980–8,005 ft).

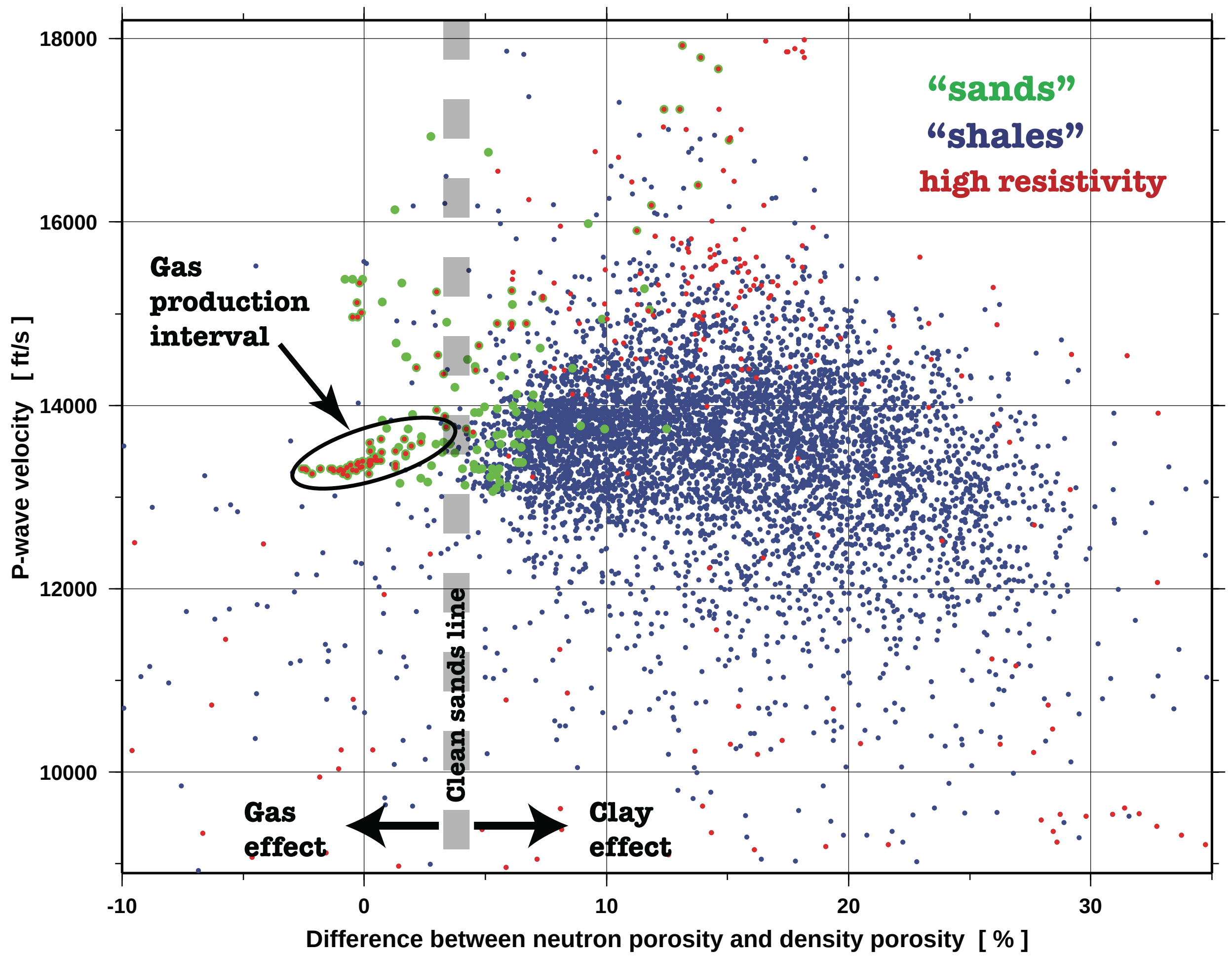

Figure 23. Well-4 velocity versus difference between neutron-porosity and density-porosity crossplot with interpretive lithology estimation, depth interval 5,000 to 8,080 ft (Fort Union through Almond Formations). Green dots, "sands," rocks having natural gamma-ray intensity below 50 gAPI; blue dots, "shales," rocks having gamma-ray intensity above 50 gAPI; red dots, rocks showing resistivity above 25 ohmm. Overall, measurements show no noticeable trend in distribution. The circled area contains measurements only from the Almond gas-producing interval (7,980–8,005 ft).

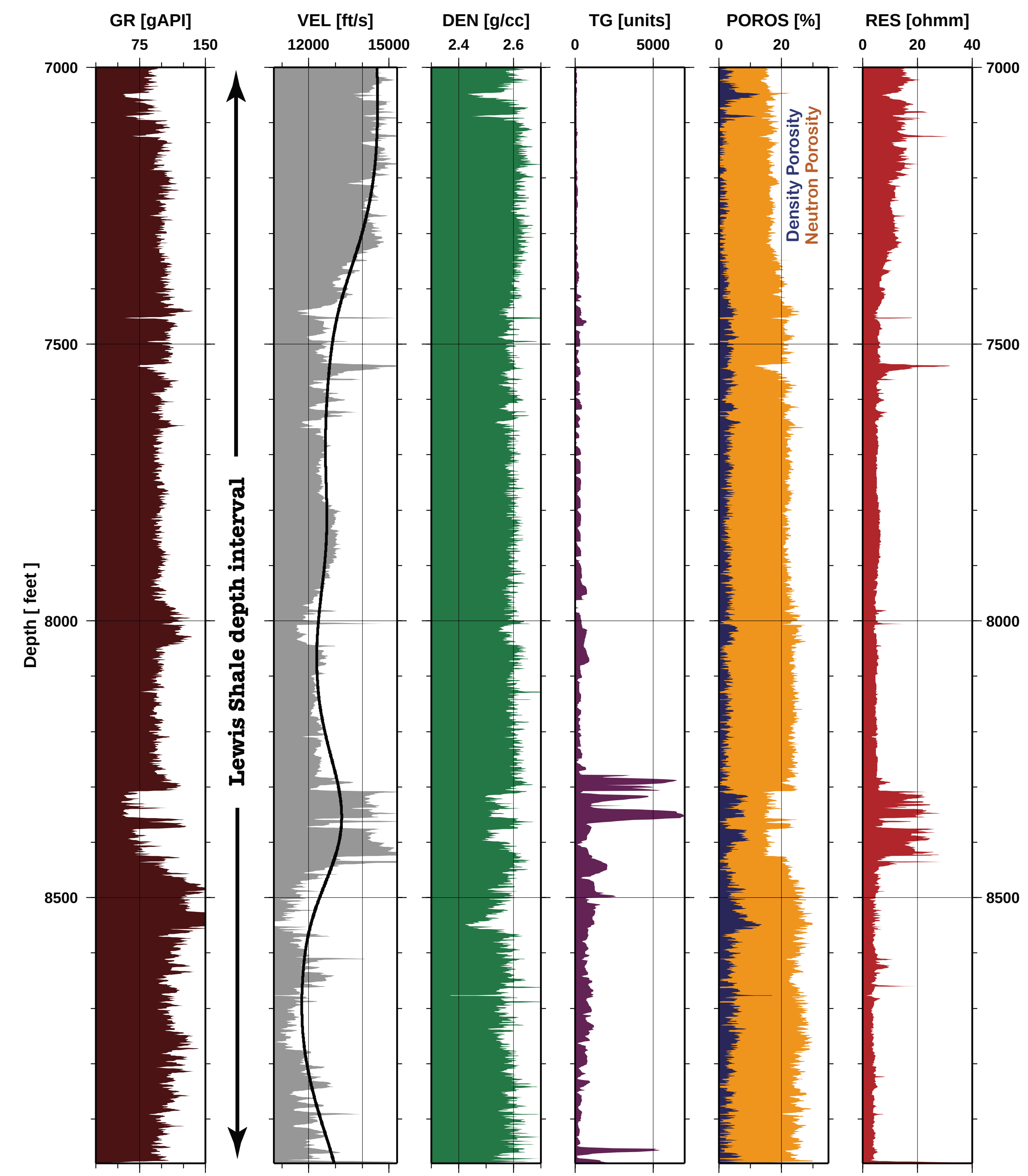

Figure 24. Well-5 wireline logs (Fillmore Creek 9-1 well, Greater Green River Basin): GR, gamma-ray; VEL, sonic P-wave velocity; DEN, bulk density; TG, total gas; POROS, density (blue) and neutron (orange) porosity; RES, resistivity. Black solid line in velocity panel, velocity smoothed with 250-ft Gaussian operator. Production interval starts at 8,383 ft depth, as indicated by an abrupt increase in gas shows.

is composed of discrete marine sandstone bodies intercalated with shales in the upper Almond and predominantly of nonmarine sediments in the lower part. Figure 28 shows the gamma-ray, P-wave velocity, bulk density, caliper, density and neutron porosity (blue and orange, respectively), and resistivity logs, for the 7,550-to-9,750-foot depth interval.

The gas production interval in the Almond Formation (perforated at 9,336–9,631 feet depth) is characterized by increased resistivity and density porosity readings. It is instructive that the overlying lower Lewis Shale (the sealing rock) registers much slower velocities than does the reservoir rock (smoothed velocity curve, Figure 28).

The familiar inverse trend in data distribution can be observed on the velocity versus neutron-porosity crossplot (Figure 29). Velocity varies greatly (~11,000 to ~16,000 ft/s) within a depth interval of only about 2,000 feet. Most of velocity scatter comes from "shale." "Sands" and "shales" are separated conventionally on the basis of gamma-ray intensity (60 gAPI threshold in this case study). In this velocity/neutron-porosity crossplot, the red dots designate measurements taken in the reservoir rocks of the gas producing interval. As can be seen on Figure 29, most velocity measurements within the gas-charged rocks cluster around 14000 ft/s, which is close to the mean velocity value for the whole measured depth interval. The slowest velocities (~11,000 ft/s) are associated with the rocks with the highest neutron porosity readings. However, the cluster of data-points characteristic of the gas-charged rocks seems to be shifted toward lower velocity values relative to the major trend line (Figure 29). The apparent velocity shift due to gas saturation (anomalous velocity) is about 2000 ft/s in this case study.

Case study 7: Tenneco-Federal 1-29 well, Bighorn Basin

The Tenneco-Federal 1-29 well (herein Well-7) is located in the southwestern Bighorn Basin (Figure 1). It was drilled in 1979 as an oil well, but was abandoned, and was plugged in 1980. The geological well log (WOGCC Web site) indicates multiple gas shows starting at the Cody Shale (~13,000 feet) and continuing down to the bottom of the well at ~16,450 feet. The stratigraphic succession logged over the Well-7 depth interval shown on Figure 30 is, youngest to oldest, the Upper Cretaceous Cody Shale, Frontier Formation, and Mowry Shale; Lower Cretaceous Muddy Sandstone, Thermopolis Shale, and Cloverly Formation; and Upper Jurassic Morison Formation. These units are interbedded fine- to medium-grained sandstones and variegated shales, siltstones, and mudstones of marine and nonmarine origin. Figure 30 shows the gamma-ray, P-wave velocity, bulk density, caliper, density and neutron porosity (blue and orange, respectively), and resistivity logs, as well as a corresponding stratigraphic column, for the 12,600-to-16,450-foot depth interval.

Elevated deep-resistivity values, above 50 ohmm, indicate possible gas saturation in parts of the Cody Shale (Figure 30). However, the greatest gas charge should be expected in the Frontier and Cloverly Formations where resistivity peaks above 100 ohmm are accompanied by density porosity surpassing neutron porosity.

Broad scatter characterizes the sonic rock velocities. No trend can be seen in the velocity-depth relationship (smoothed velocities, Figure 30). Several steep velocity reversals, of 1,500 to 2,500 ft/s, are indicated in the velocity panel of Figure 30. These velocity reversals correlate with increased caliper values, increased neutron-and density- porosity readings, and decreased resistivity (Figure 30).

Figure 31 shows the Well-7 rock velocity versus neutron-porosity crossplot. The depth interval, 12,500 to 16,400 feet, is the same as that of Figure 30, and corresponds to the lower part of the Cretaceous stratigraphic section. The crossplot in Figure 31 is color-coded as for Figures 6 through 8 for Case study 1, except that the resistivity threshold is 100 ohmm for these Well-7 plots. The very broad velocity scatter, values from ~12,000 ft/s to ~18,000 ft/s, on the crossplot reflects the poor correlation of velocity with depth apparent on Figure

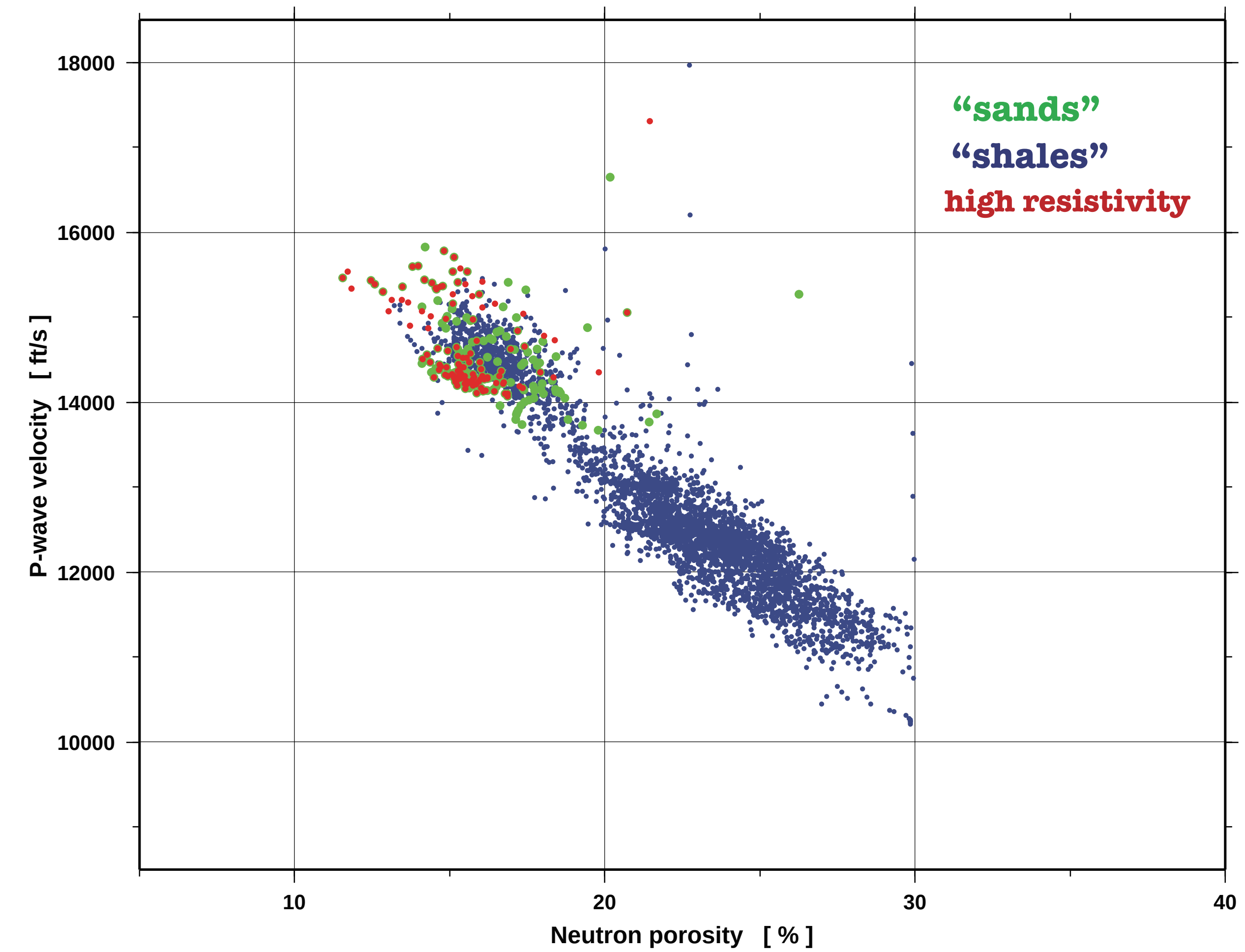

Figure 25. Well-5 composite velocity versus neutron-porosity crossplot, depth interval 7,000 to 8,980 ft (Lewis Shale). Green dots, "sands," rocks having natural gamma-ray intensity below 75 gAPI; blue dots, "shales," rocks having gamma-ray intensity above 75 gAPI; red dots, rocks showing resistivity above 20 ohmm. Overall, measurements show a pronounced inverse trend in distribution: velocity decreases with increasing neutron porosity.

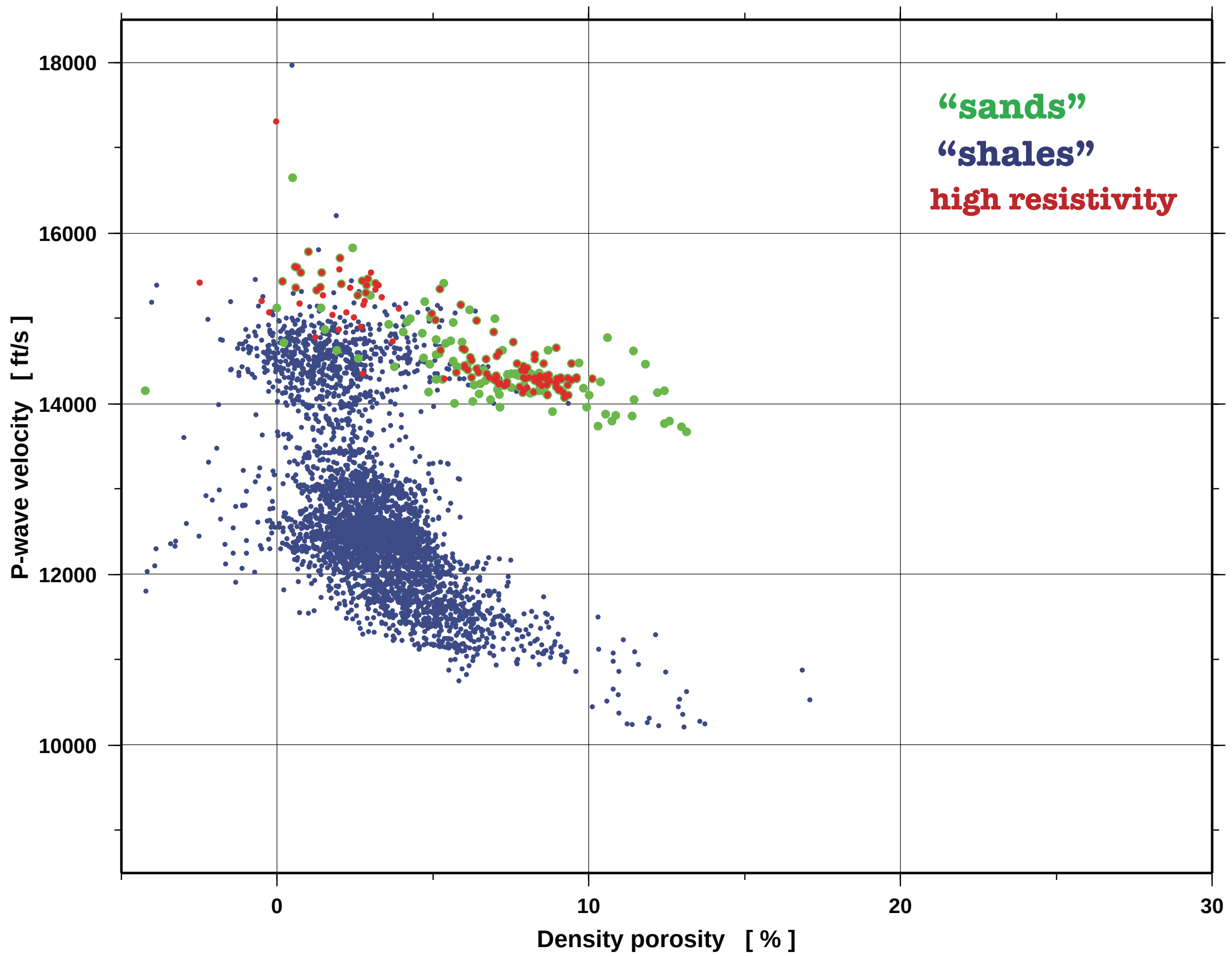

Figure 26. Well-5 velocity versus density-porosity crossplot, depth interval 7,000 to 8,980 ft (Lewis Shale). Green dots, "sands," rocks having natural gamma-ray intensity below 75 gAPI; blue dots, "shales," rocks having gamma-ray intensity above 75 gAPI; red dots, rocks showing resistivity above 20 ohmm. Rocks with lower shale content (green dots) tend to have relatively fast velocities, even those that are gas-saturated (red dots).

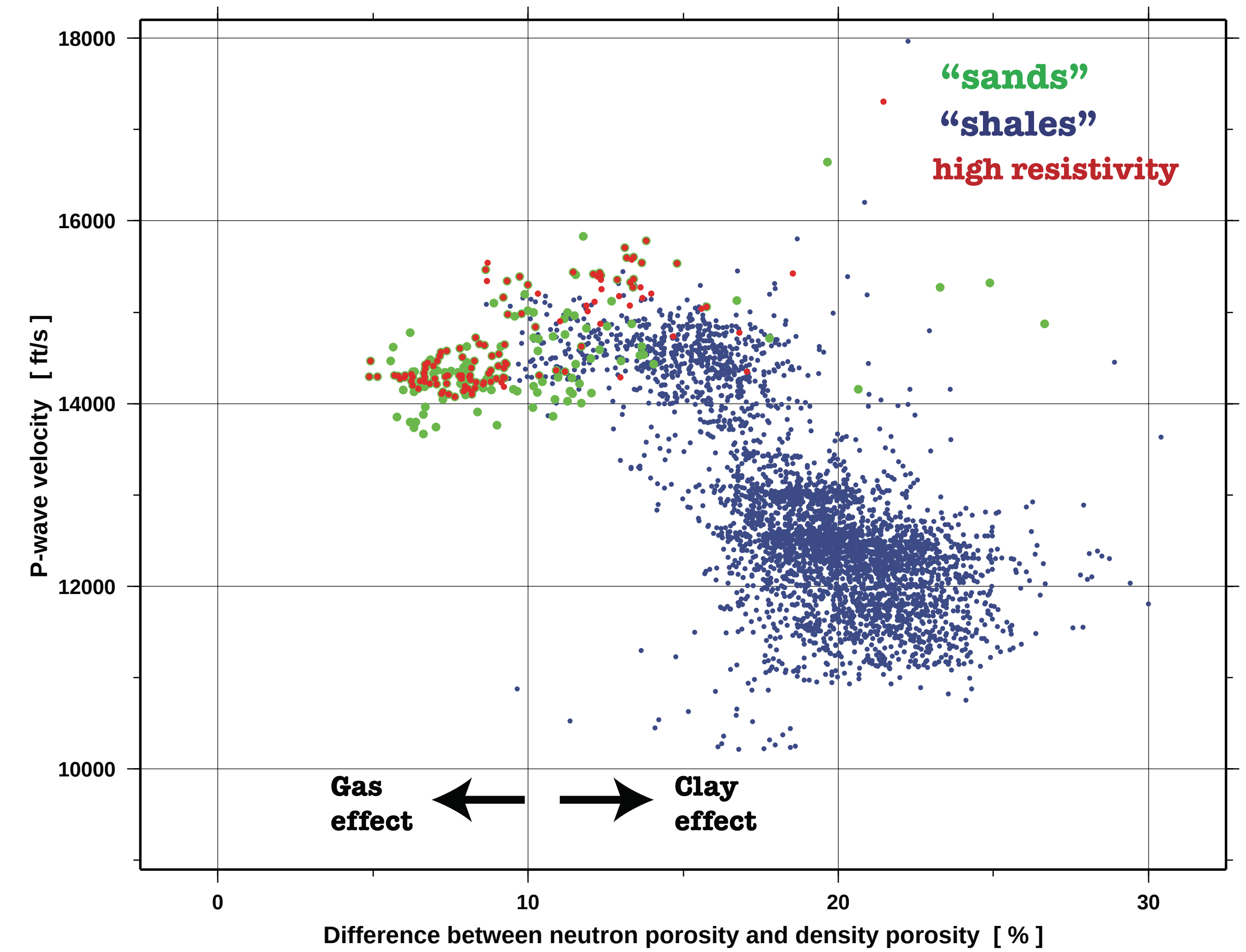

Figure 27. Well-5 velocity versus difference between neutron-porosity and density-porosity crossplot, depth interval 7,000 to 8,980 ft. Green dots, "sands," rocks having natural gamma-ray intensity below 50 gAPI; blue dots, "shales," rocks having gamma-ray intensity above 75 gAPI; red dots, rocks showing resistivity above 20 ohmm. Rocks with greater clay content ("shales") correlate with greater difference between neutron porosity and density porosity.

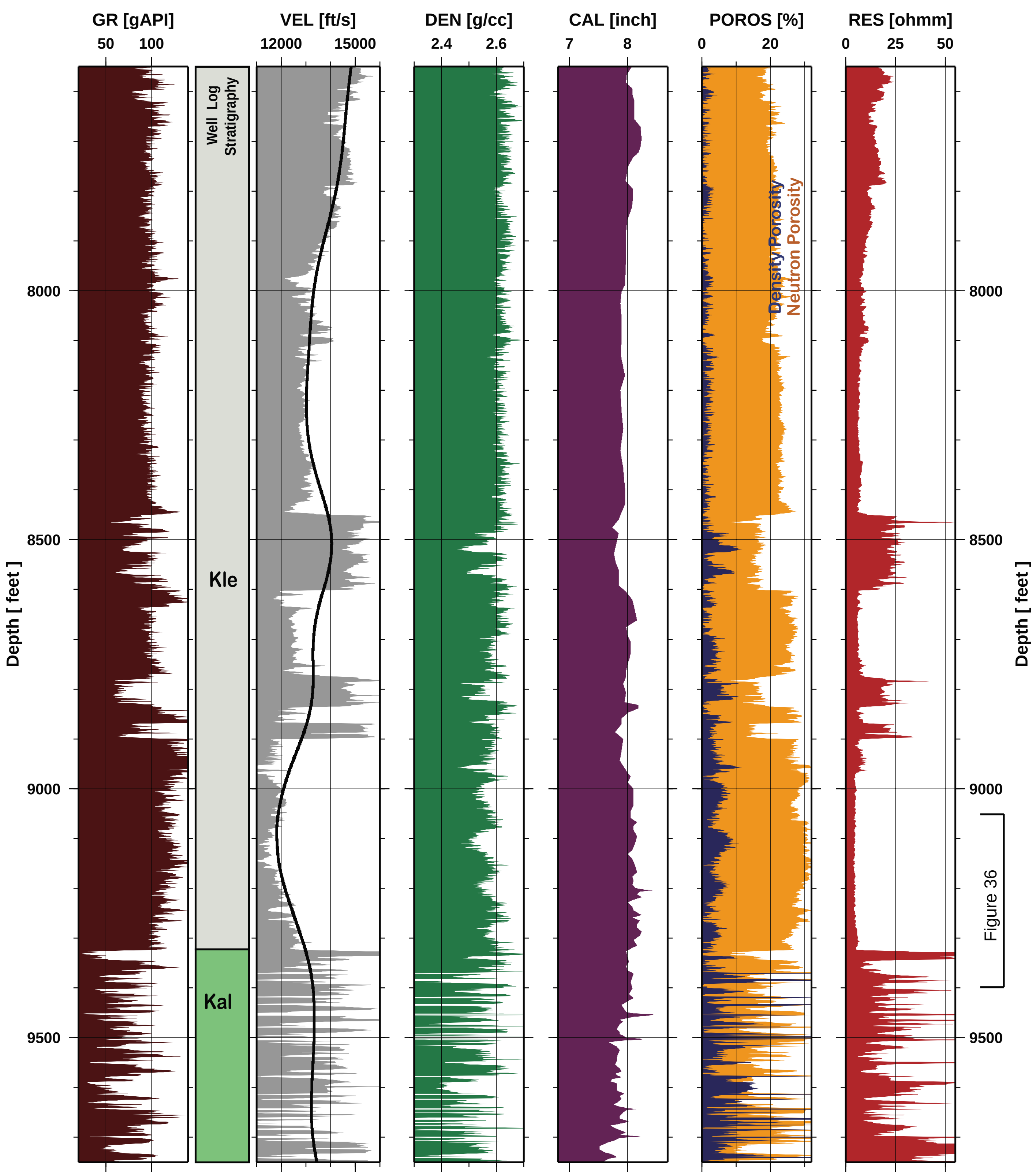

Figure 28. Well-6 composite wireline logs (Echo Springs 17-5 well, Wamsutter Arch): GR, gamma-ray; VEL, sonic P-wave velocity, DEN, bulk density; CAL, Caliper; POROS, density (blue) and neutron (orange) porosity; RES, resistivity. Black solid line in velocity panel, velocity smoothed with 250-ft Gaussian operator. Kle, Lewis Sh; Kal, Almond Fm.

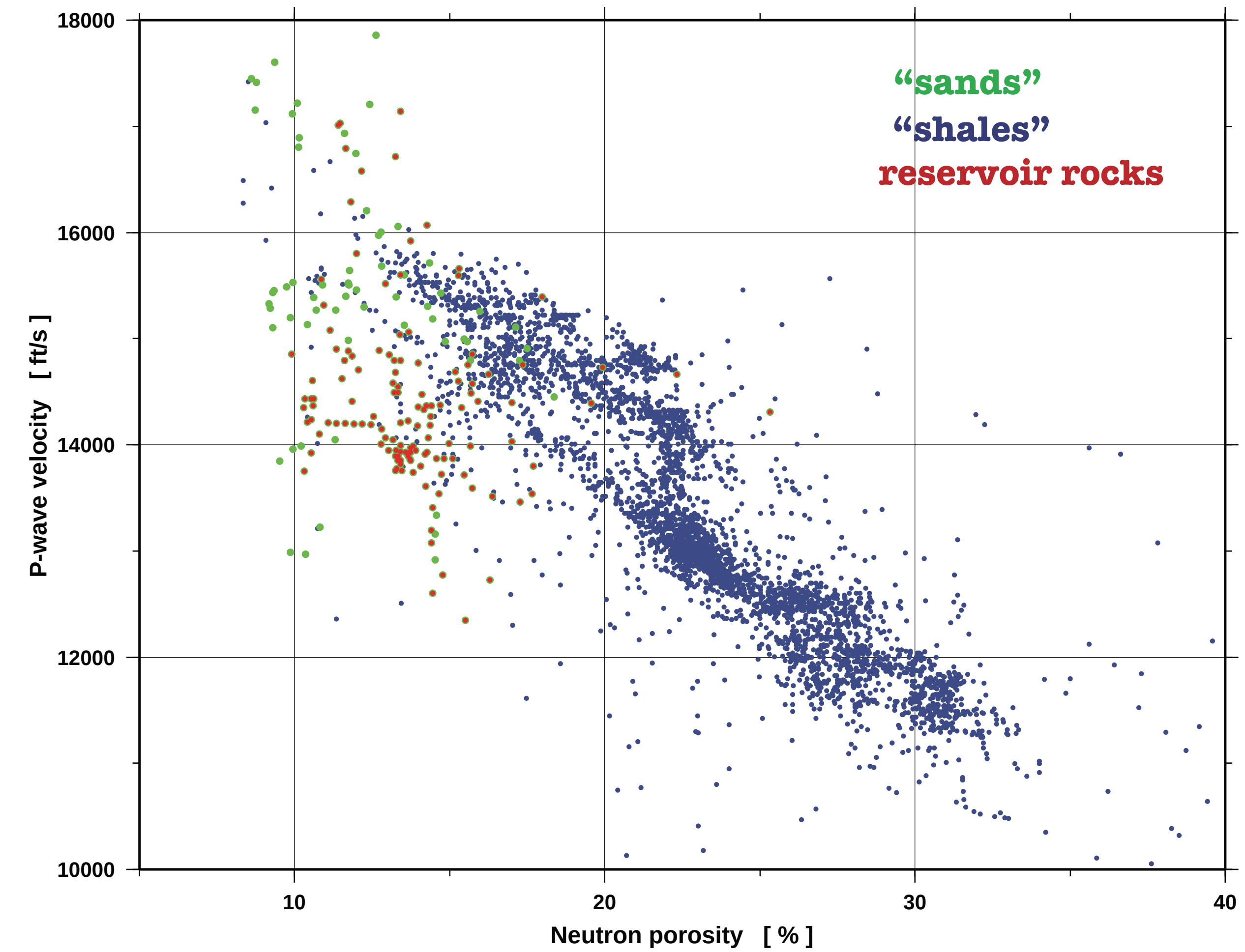

Figure 29. Well-6 velocity versus neutron-porosity crossplot, depth interval 7,550 to 9,750 ft (Upper Cretaceous formations). Green dots, "sands," rocks having natural gamma-ray intensity below 50 gAPI; blue dots, "shales," rocks having gamma-ray intensity above 60 gAPI; red dots, measurements within the reservoir rocks of producing interval (9,336 to 9,631 ft). "Shales" show a pronounced inverse trend in distribution: velocity decreases with increasing neutron porosity. Most measurements within the gas-saturated rocks cluster about a velocity of 14,000 ft/s.

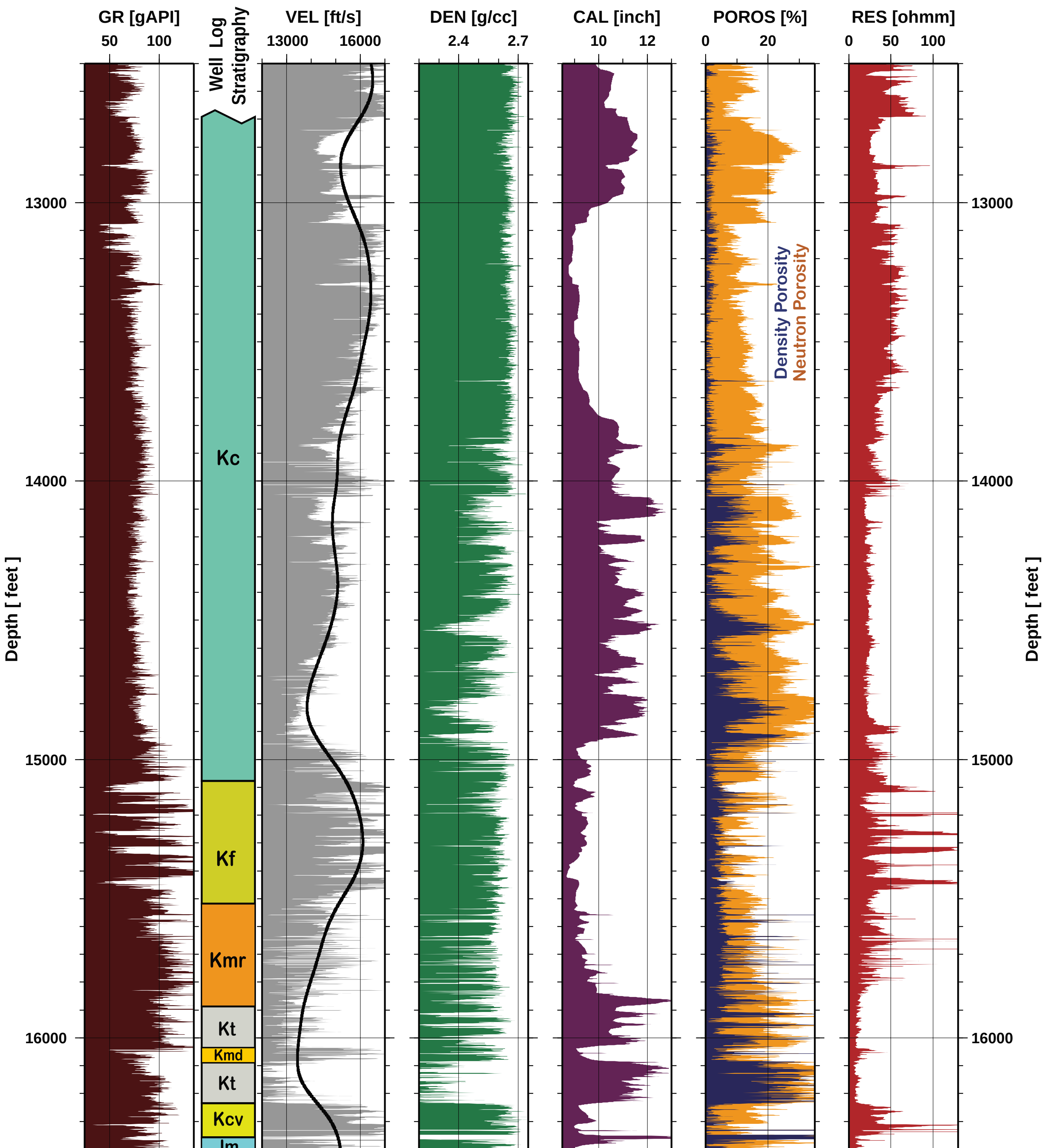

Figure 30, facing page. Well-7 composite wireline logs (Tenneco-Federal 1-29 well, southwestern Bighorn Basin): GR, gamma-ray; VEL, sonic P-wave velocity; DEN, bulk density; CAL, caliper; POROS, density (blue) and neutron (orange) porosity; RES, resistivity. Black solid line in velocity panel, velocity smoothed with 250-ft Gaussian operator. Stratigraphic interpretation based on the WOGCC geological markers and wireline log characteristics: Kc, Cody Sh; Kf, Frontier Fm; Kmr, Mowry Sh; Kmd, Muddy Ss; Kt, Thermopolis Sh; Kcv, Cloverly FM; Jm, Morrison Fm.

30. On the other hand, the velocity/neutron-porosity crossplot shows a very well defined trend: rock velocity decreases linearly with increasing neutron porosity. Correspondingly, the "sands" defined by low gamma-ray readings generally have the fastest velocities (Figure 31).

Figure 32 shows the Well-7 rock velocity versus density-porosity crossplot. This velocity display again demonstrates broad scatter in velocity measurements and no discernable linear trend. There is only vague correlation between rock velocity and porosity in this study. Density porosity calculated within "sands" does not exceed 10%; thus the Well-7 measurements indicate a typical "tight gas sand."

Figure 33 shows the Well-7 rock velocity versus difference between neutron porosity and density-porosity crossplot. The crossplot allows separation of measurements in the gas-saturated rocks (left of the clean sands line) from those in the "shales." Due to uncertainty in matrix porosity assumptions, the "clean sands line" does not match the zero value on the horizontal axis. The measurements in "sands" are characterized by lower GR readings and small differences between neutron porosity and density porosity. "Sands," including those with high resistivity readings, cluster in an area with high velocity values (Figure 33). "Shales," unlike "sands," do tend to decrease in velocity with increasing clay effect (increased difference between neutron porosity and density porosity). Broad data scatter in the low-velocity area on all velocity-density crossplots is due to the unreliability of measurements in the washed-out zones.

Case study 8: Echeta Federal 11-13 well, Powder River Basin

The Echeta Federal 11-13 well (herein Well-8) is located in the Amos Draw Field in the central Powder River Basin (Figure 1). It was drilled and logged in 2002 and currently produces oil and gas from the Muddy Sandstone. The perforated interval is 9,292 to 9,360 feet. The Cretaceous rocks penetrated by the well within the depth interval from 5,300 to 9,650 feet are mostly marine shales with some thin intercalated sandstone and siltstone beds. The major units penetrated by the well, top to bottom, are the Upper Cretaceous Lewis Shale, Steel Shale, Niobrara Formation, and Mowry Shale (with interbedded Muddy Sandstone), and Lower Cretaceous Scull Creek Shale. Figure 34 shows the gamma-ray, P-wave velocity, bulk density, caliper, density and neutron porosity (blue and orange, respectively), and resistivity logs, as well as a corresponding stratigraphic column, for the 5,300-to-9,650-foot depth interval.

As shown on Figure 34, the sonic-log velocities neither increase nor decrease regularly with depth but fluctuate significantly about a mean value (~12,200 ft/s). Multiple velocity reversals of more than 1,000 ft/s can be observed on the smoothed velocity curve. These velocity reversals correlate inversely with neutron-porosity fluctuations (Figure 34).

The velocity versus neutron-porosity crossplot shows a clear inverse linear correlation (Figure 35). The measured depth interval, 5,300 to 9,650 feet, is the same as that of Figure 34. This crossplot is color-coded as in Figures 6–8 for Case Study 1 with the exception that the red dots designate measurements within the perforated, oil-gas-prolific zone in the Muddy Sandstone (9,292-9,360 feet depth). Unlike the velocity-depth relationship (velocity panel in Figure 34), the velocity/neutron-porosity relationship shows a very well defined trend: rock velocity decreases linearly with increasing neutron porosity. Overall scatter of velocity values between 10,000 and 16,000 ft/sec is far greater than the scatter of velocities about an inferred

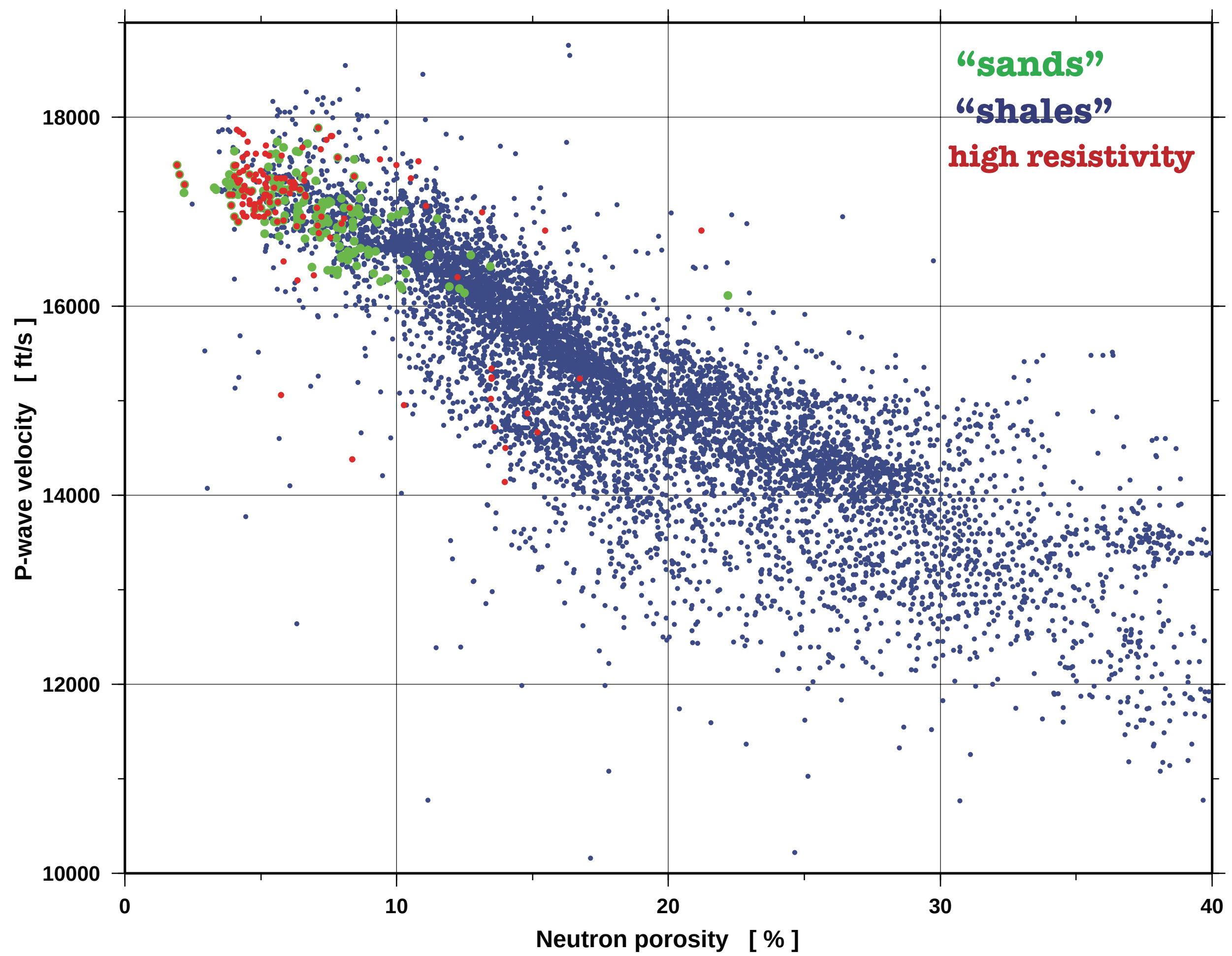

Figure 31. Well-7 velocity versus neutron-porosity crossplot, depth interval 12,500 to 16,400 ft (Cretaceous stratigraphic section from Cody Shale to Cloverly Formation, and into Upper Jurassic Morrison Formation). Green dots, "sands," rocks having natural gamma-ray intensity below 50 gAPI; blue dots, "shales," rocks having gamma-ray intensity above 50 gAPI; red dots, rocks showing resistivity above 100 ohmm. "Shales" show a pronounced inverse trend in distribution: velocity decreases with increasing neutron porosity. Presumed gas-saturated "sands," reservoir rocks with high resistivity values (red dots), are characterized by relatively fast velocity.

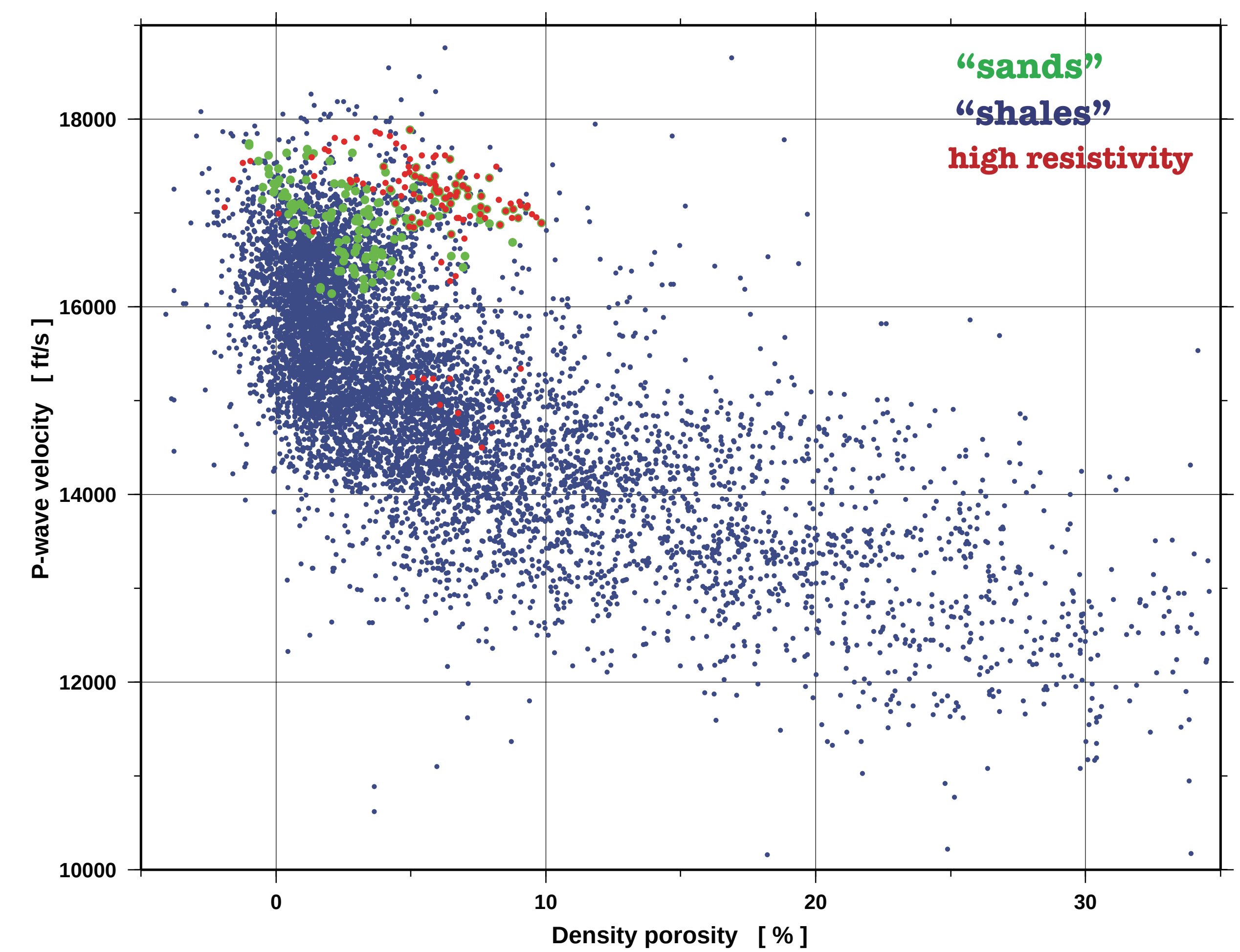

Figure 32. Well-7 velocity versus density-porosity crossplot, depth interval 12,500 to 16,400 ft (Cretaceous Stratigraphic section from Cody Shale to Cloverly Formation and into Upper Jurassic Morrison Formation). Green dots, "sands," rocks having natural gamma-ray intensity below 50 gAPI; blue dots, "shales," rocks having gamma-ray intensity above 50 gAPI; red dots, rocks showing resistivity above 100 ohmm. Overall, measurements show no noticeable trend in distribution. Presumed gas-saturated "sands," reservoir rocks with high resistivity values (red dots), are characterized by relatively fast velocity.

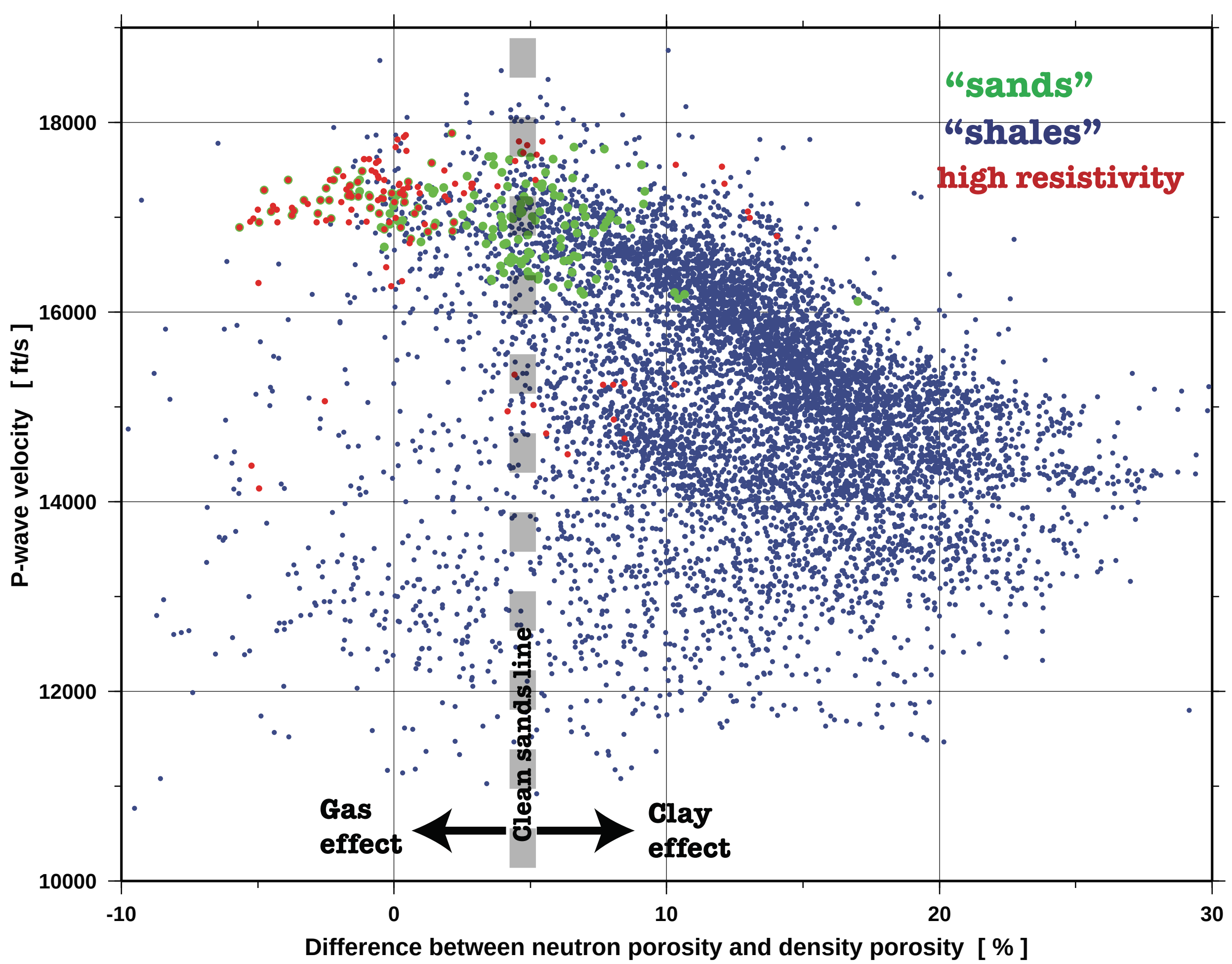

Figure 33. Well-7 velocity versus difference between neutron-porosity and density-porosity crossplot, with interpretive lithology estimation, depth interval 12,500 to 16,400 ft (Cretaceous stratigraphic section from Cody Shale to Cloverly Formation and into Upper Jurassic Morrison Formation). Green dots, "sands," rocks having natural gamma-ray intensity below 50 gAPI; blue dots, "shales," rocks having gamma-ray intensity above 50 gAPI; red dots, rocks showing resistivity above 100 ohmm. "Shales" show an inverse trend in distribution: velocity decreases with increasing difference between neutron and density porosity. Presumed gas-saturated "sands," rocks with high resistivity values (red dots), are characterized by relatively fast velocity.

regression line of rock velocity on neutron porosity. Sparse inclusions of "sands," as defined by low gamma-ray readings, appear to have the fastest velocities (Figure 35). Measurements within the reservoir rocks (red dots) have relatively low neutron-porosity values and scattered over a broad range in velocity about a relatively high mean value (~14,000 ft/s).

DISCUSSION OF CASE STUDIES 1–8

The tightly compacted, Cretaceous-age rocks documented in case studies 1–8 are characterized by wide range in measured P-wave velocity. For the eight data sets, velocities are nearly independent of density porosity and show a pronounced inverse dependence on neutron porosity (hydrogen content). Analysis of velocity/porosity crossplots suggests that the data can be divided into two groups, "sands," (shaley sand) and "shales" (sandy shale), according to the sand-shale transition model of Marion et al. (1992). Data points grouped as "sands" show weak correlation with porosity, while velocity/density relationships for "shales" cannot be easily established from a crossplot.

The correlation coefficient was used in this report to quantify the relationship of rock velocity to other physical rock parameters recorded on the wireline logs. In statistical analysis the correlation coefficient indicates the strength and sign of a linear relationship between two sets of variables. More strictly, the correlation coefficient is a measure of the correlation of two variables, x and y, measured on the same object. The correlation coefficient ranges from -1.0 to 1.0; both -1.0 and 1.0 indicate perfect linear correction. A value of 1.0 means that all data points lie directly on a regression line with positive (upward) slope, y varying directly with x (y increasing with increasing x). A value of -1.0 means that all data points lie on a regression line with negative (downward) slope, y varying inversely with x (y decreasing with increasing x). Decimal values between -1.0 and 1.0 mean that the data points are scattered about a regression line, indicates lesser degrees of correlation of y with x. The Well-8 crossplot of rock velocity (y) vs. neutron porosity (x) (Figure 35) has a correlation coefficient of -0.80, a fairly high value. A value of 0.0 means that there is no linear relationship between the variables. Table 2 shows correlation coefficients calculated for sonic-velocity logs against other geophysical logs described in Case Studies 1–8. In all cases, the depth interval for correlation coefficient calculation is the same as for crossplotting and spans several thousand feet.

The figures in Table 2 indicate that velocity neither increases nor decreases regularly with depth over these depth intervals (note different signs) and that the overall (average) correlation of velocity with depth is very poor (low absolute value). Velocity correlation with GR is always negative, which means that increase in gamma-ray intensity is generally associated with velocity decrease. However, correlation is relatively strong in only one case, Well-5. In all other cases the correlation of GR with sonic log data is poor or negligible. Well-5 is also an example of strong correlation between velocity and deep-resistivity measurements. In this case, increased resistivity is associated with increased velocity; the other case studies do not support this velocity-resistivity relationship.

There is consistent negative correlation between rock velocity and density porosity: increase in porosity is generally associated with velocity decrease. However, the velocity/density-porosity relationship is nonlinear, as follows from its low average correlation coefficient (-0.43).

The velocity/neutron-porosity correlation is the strongest one among those computed, for all case studies. The sign and magnitude (-0.80) of the average correlation coefficient of velocity against neutron porosity indicate strong inverse linear interdependence. We suggest that the greater concentration of hydroxyls associated with higher clay content causes increased neutron-porosity readings and decreased sonic-velocity readings.

The evidence above suggests that it is

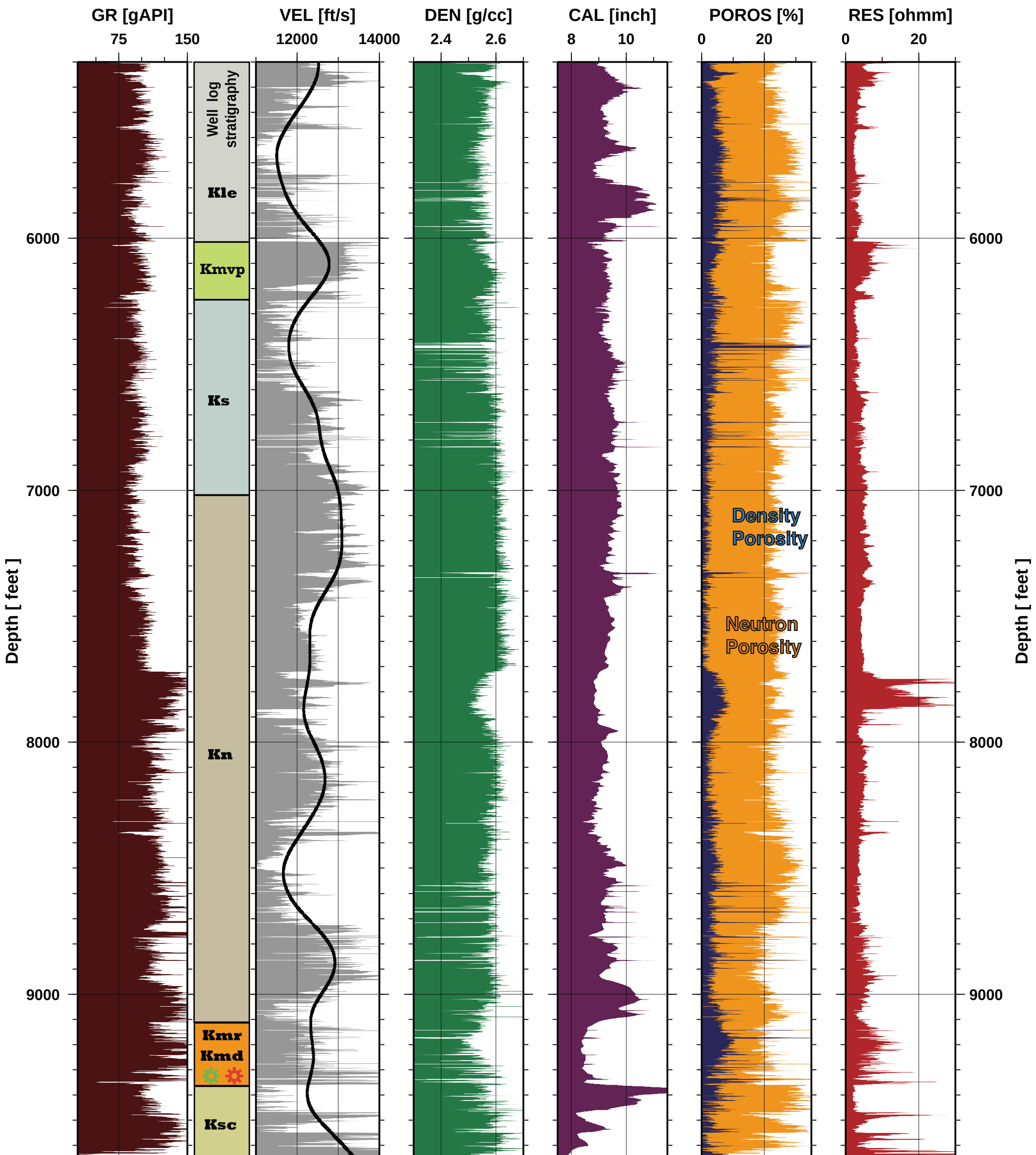

Figure 34. Well-8 composite wireline logs (Echeta Federal 11–13, Amos Draw field, Powder River Basin): GR, gamma-ray; VEL, sonic P-wave velocity; DEN, bulk density; CAL, caliper; POROS, density (blue) and neutron (orange) porosity; RES, resistivity. Black solid line in velocity panel, velocity smoothed with 250-ft Gaussian operator. Stratigraphic interpretations based on WOGCC geological markers, lithological log, and wireline log characteristics: Kle, Lewis Sh; Kmvp, Parkman Ss Mbr, Mesaverde Fm; Ks, a mbr of the Cody Sh (?); Kn, Niobrara Fm; Kmr, Mowry Sh; Kmd, Muddy Ss; Ksc, Skull Creek Sh.

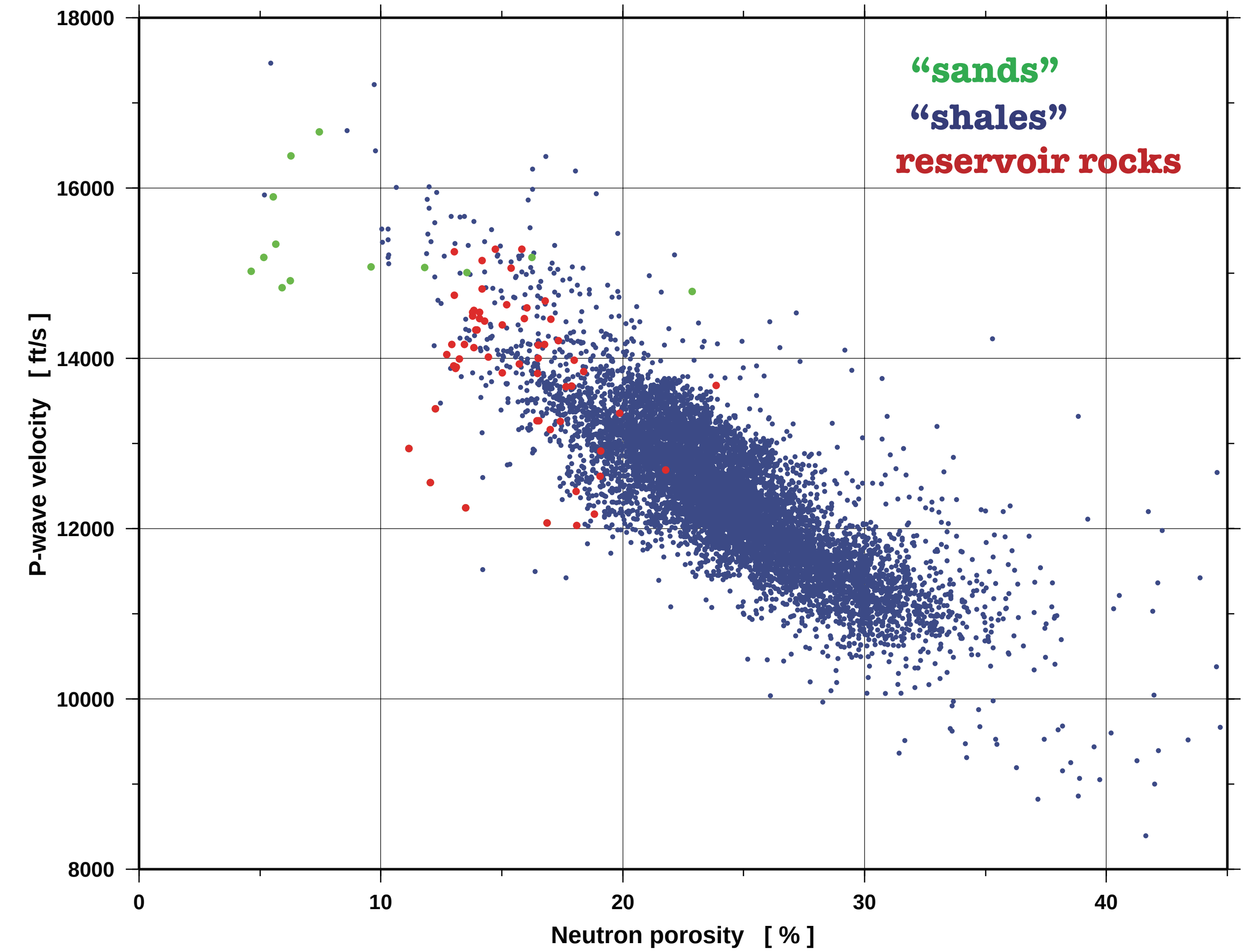

Figure 35. Well-8, velocity versus neutron-porosity crossplot, depth interval 5,300 ft to 9,600 ft (Cretaceous Lewis Shale to Scull Creek Shale). Note the broad range in P-wave velocity, ~10,000 ft/s to ~16,000 ft/s. There is a definite inverse dependence of rock velocity on neutron porosity: velocity decreases with increasing neutron porosity. Red dots indicate measurements made within the oil-and-gas-prolific zone (perforated interval from 9,300 to 9,360 ft). Data from reservoir rocks (red dots) cluster within a low-neutron and high-velocity domain.

clay content that introduces scatter into the velocity-porosity relationship. The inclusion of clay minerals in the rock matrix affects the bulk elastic properties. However, it does not seem possible to explain the observed velocity variations solely by mineralogical differences.

The great observed scatter of velocities is anomalous for low-porosity rocks with relatively uniform composition (sand-shale mixtures). The caliper and GR logs show that clay-rich shales are softer and more fissile than the mechanically stronger and harder sandstones and siliceous shales. Difference in pore geometry within the rocks must be considered in this case because pores with large aspect ratios are much stiffer than those with small ones. This is the basis for proposing that it is the pore aspect ratio that most influences the velocity/porosity relationship. The preferred orientation of clay particles results in compliant pores with small aspect ratios. Only such crack-like pores can produce discernable velocity variation with very small porosity change.

Velocity measurements within gas-saturated rocks do not differ much from the mean velocity values. Natural gas present in pores does not seem to slow rock velocity as much as does high clay content and associated microcracks. Therefore, since rock velocity

Table 2. Correlation coefficients, velocity vs. other log variables

[GR, gamma-ray intensity (gAPI); NP, neutron porosity (%); DP, density porosity (%); RES, resistivity (ohmm)]

Case Study	Correlation coeffiecient, rock velocity vs.				
Well	Depth	GR	NP	DP	RES
Well-1	0.06	-0.19	-0.55	-0.31	0.12
Well-2	0.52	-0.35	-0.84	-0.23	-0.04
Well-3	0.25	-0.28	-0.73	-0.51	0.06
Well-4	0.12	-0.10	-0.85	-0.71	-0.41
Well-5	-0.63	-0.62	0.93	-0.36	0.86
Well-6	-0.33	-0.50	-0.84	-0.32	0.40
Well-7	-0.45	-0.42	-0.83	-0.65	0.50
Well-8	0.14	-0.26	-0.80	-0.40	0.44
Average	-0.04	-0.34	-0.80	-0.43	0.24

plotted versus depth (vertical velocity profile) cannot be used as a diagnostic tool for gas exploration in the low-porosity Cretaceous-age rocks described in these case studies, the author poses two questions: (1) Can the velocity variation due to variable clay content be isolated from the velocity decrease due to gas saturation? (2) Is the velocity decrease due to gas saturation significant enough (adequately separable from the effect of clay content) in the "tight gas sands" to be measured seismically? The following case study, based on multiple sonic velocity measurements in the Upper Almond sandstone bar in three-dimensional array, addresses these questions.

Case study 9: Multiple wells, Wamsutter field area, Greater Green River Basin

The Wamsutter field area is an 18-by-11-mile area on the Wamsutter arch, a northwest-southeast trending feature that separates the Washakie and Great Divide subbasins of the Greater Green River Basin (Figure 1). The Echo Springs and Standard Draw gas fields produce from low-permeability reservoirs in the Almond Formation in the Wamsutter field area. The greatest production is from a marine shore-face sandstone unit, informally known as the Upper Almond bar; it is the uppermost unit of the Mesaverde group and is directly overlain by the basal Lewis shale unit. Figure 36 shows the interpreted well-log stratigraphy and associated set of logs for a 350-foot section of the Echo Springs 17-5 well discussed above in Case Study 6 (Figures 28 and 29). The Upper Almond bar is about 20 feet thick in the study area and can be clearly identified on the well logs by abruptly decreased gamma-ray and increased resistivity log values. On Figure 36 the Upper Almond bar is also characterized by a significant increase in P-wave velocity (with several values more than 16,000 ft/s) and decrease in neutron porosity. Just above the Almond bar in the basal Lewis shale unit the average velocity is about 12,500 ft/s in this well (Figure 36).

This case study compares rock velocity variation over the Upper Almond bar with the surface distribution of gas-producing wells within the Wamsutter field area. GR and sonic logs from 52 wells were processed to calculate the mean velocity values within a 350-foot section containing the lowermost Lewis Shale (275 ft), the Upper Almond Bar (20 ft), and 55 ft of the Almond Formation below the Upper Almond Bar. The velocities were smoothed spatially with a 1-mile-radius Gaussian operator, separately for the set of Upper Almond velocities and the basal Lewis velocities. Figure 37 shows the resultant color-coded average velocity maps for the basal Lewis shale interval (**a**) and the Upper Almond bar (**b**). The color-code scale ranges in velocity from 11,000 ft/s (blue) to 17,000 ft/s (red). Both velocity maps in Figure 37 are overlaid with an Upper Almond bar structure contour map given in feet below sea level. The Upper Almond bar velocity map also shows the surface locations of gas-producing wells (red "starry" circles). Both maps also show the locations of the 52 wells used for velocity and structural mapping (black circles).

A broad range of average velocity values characterizes the Upper Almond bar (Figure 37**b**). The velocity varies by as much as ~2,000 ft/s within this lithologically uniform sandstone unit. Although variations in thickness that result in unequal and sometimes insufficient numbers of velocity samples are partly responsible for the observed fluctuations, there is a definite trend in the smoothed velocity field that cannot be produced by random velocity fluctuations. Figure 37**b** shows pronounced decrease in Upper Almond bar average rock velocity in the eastern half of the study area. This area of relatively slow Upper Almond bar velocity appears to have pronounced structural control (the most uplifted, southeastern corner shows the slowest velocities). A high concentration of gas-producing wells, corresponding to the Echo Springs and Standard Draw gas fields, trends roughly north-south in the central study area (R.93W., Figure 37). Average rock velocities within the Upper Almond bar slow from about 15,500 ft/s to about 14,000 ft/s from the westernmost area with relatively low gas-well concentration to the central, gas-prolific area. Of course, more sonic data from a denser well distribution is required for confident statements, but still it is clear that there is correlation between rock velocity and gas producibility in the Upper Almond bar within the Wamsutter field area.

The basal Lewis shale does not show the broad range of average velocities that the Upper Almond bar shows (Figure 37**a**). The depth averaged, spatially smoothed velocities for the lowermost Lewis Shale occur in quite uniform distribution across the study area. The mean velocity value is ~12,000 ft/s, much slower than any Upper Almond bar velocity. The velocity within the Lewis does not fluctuate within the study area (note the almost unchanging color in Figure 37**a**). There is no correlation between the gas-producing well distribution and almost uniform rock velocity in the basal Lewis Shale. This may indicate the overall good sealing capacity of the lowermost Lewis Shale unit.

This case study indicates that the lower Lewis Shale is not only a regional seal but is also a regional velocity inversion surface with rock velocities that are consistently much slower than those within the underlying, gas-saturated Upper Almond bar. Any attempt to interpret this regional low velocity slowdown as a result of gas saturation will be misleading. However, the gas effect is clearly manifested within the reservoir rocks of the Upper Almond Bar. To map velocity variation laterally along a lithologically uniform horizon seems to be a viable way to separate the "anomalous velocity" due to gas saturation from that produced by variable clay content. The horizon-based sonic-velocity analysis performed on the "tight gas sand" reservoir in this case study reveals velocity reversals as great as 500 ft/s that correlate with gas production. Theoretically, velocity variations with this order of magnitude should be detectable with a horizon-based seismic velocity analysis based on a 3-D reflection survey. But the resolution of any seismic-based analysis will depend on the horizon thickness relative to the dominant seismic wavelength.

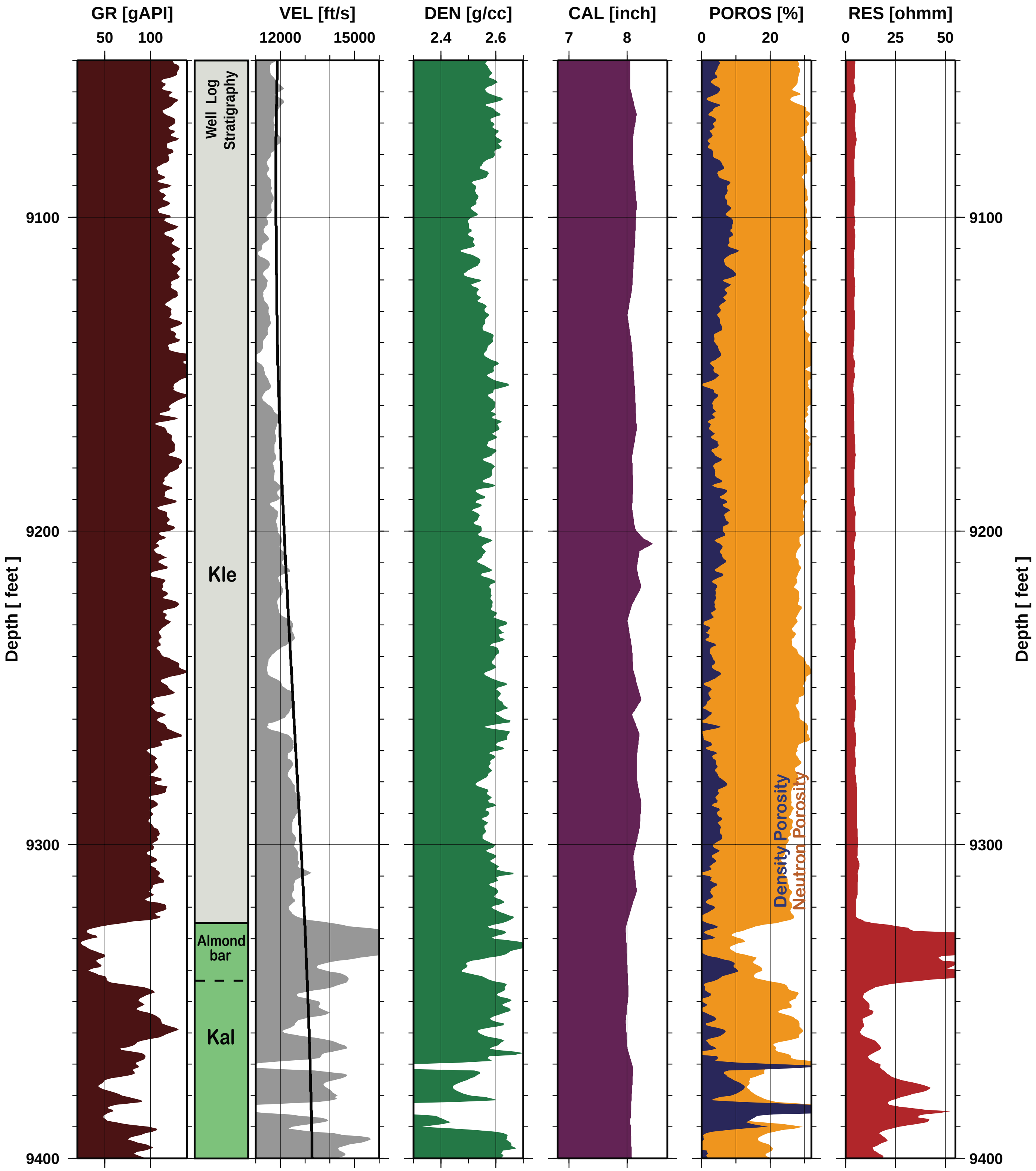

Figure 36, facing page. Well-6 composite wireline logs, (Figure 28) expanded about the Upper Almond bar, depth interval 9,050– 9,400 ft: GR, gamma-ray; VEL, sonic P-wave velocity; DEN, bulk density; CAL, caliper; POROS, density (blue) and neutron (orange) porosity; RES, resistivity. Black solid line in velocity panel velocity smoothed with 250-ft Gaussian operator. Upper Almond bar location interpreted on basis of GR and resistivity characteristic features and confirmed by WOGCC geologic markers. Well-6 stratigraphy typifies that of the Wamsutter field area (Figures 1 and 37). Kle, Lewis; Kal, Almond Fm.

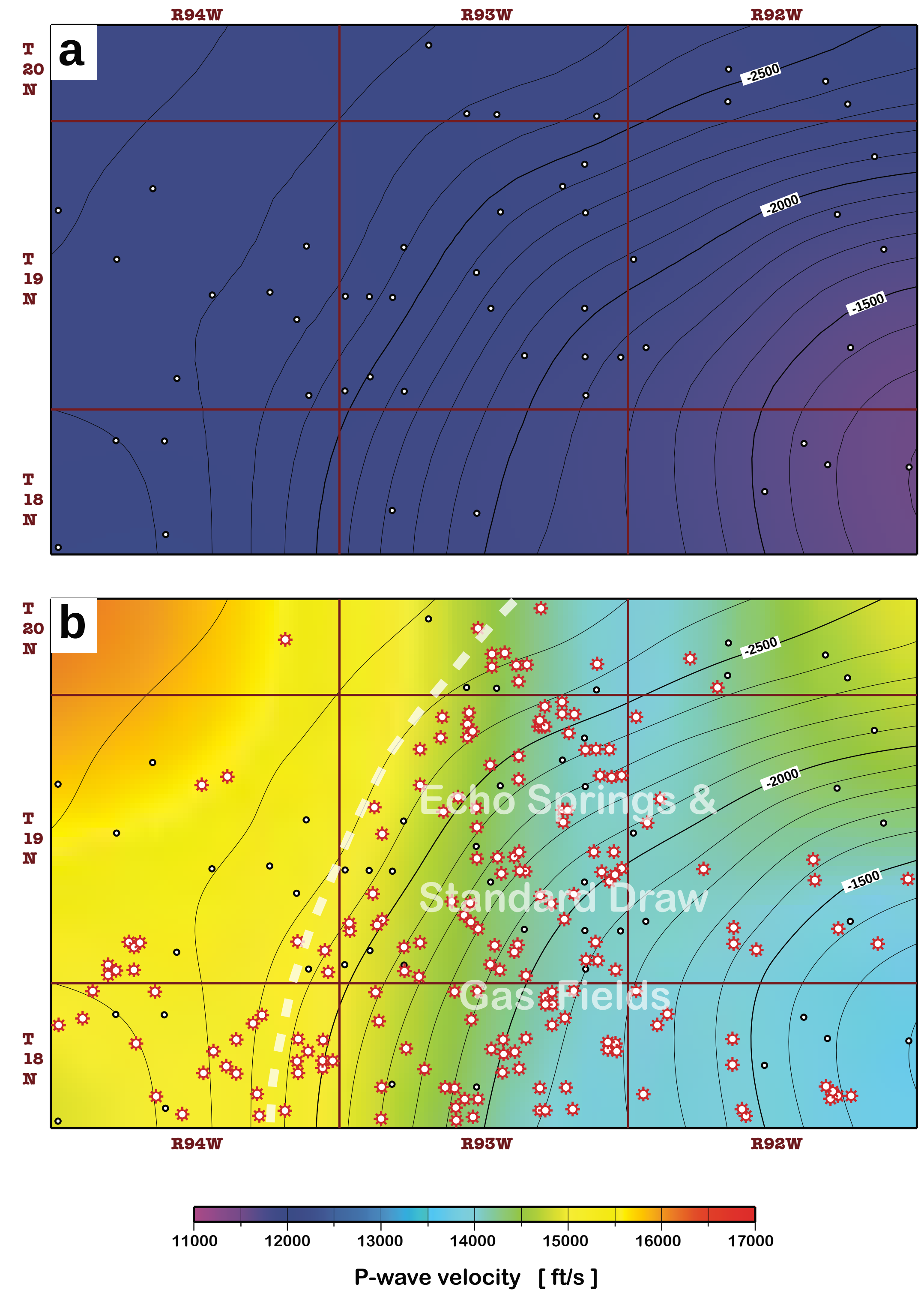

Figure 37. Color-coded average velocity maps of the (**a**) basal Lewis Shale and (**b**) underlying Upper Almond bar, Wamsutter field area (Figure 1). Color-coded velocity scale for both maps. Both maps overlaid with Upper Almond bar structure contours in feet of elevation with respect to sea level, contour interval 100 ft. Black circles, 52 wells with sonic log data used for mapping velocity; red circles, wells with gas production from the Almond Formation (WOGCC Web site, 2007 data).

CONCLUSIONS

Rock velocity variation with depth represents a complicated function of multiple parameters; important among them are mineralogical composition, porosity, pore type, and pore-fluid composition. That is why any kind of velocity trend estimation as a function of depth alone is associated with great uncertainty. This study investigates correlating velocity with physical rock properties rather than with depth. The crossplotting technique applied in this study to geophysical log data may exemplify a key to more revealing seismic data interpretations than current methods allow, particularly as applied in sedimentary basins with clay-dominated siliciclastic rock units.

The wide range in P-wave velocity observed in all the case studies, along with the very poor correlation with porosity, is interpreted to result from the variable concentration of clay minerals in the Cretaceous-age rocks under investigation. Some of these clay minerals are associated with crack-like pores, even a small volume of microcracks within the rock matrix may contribute to large variation in velocity. In low-porosity rocks, such as those in Wyoming sedimentary basins, pore microstructure may be more important than other factors affecting velocity such as rock composition, porosity, and pore-fluid composition. Clearly this may constrain our ability to use sonic or seismic velocities as a measure of gas content in low-porosity reservoirs. The well-log database compiled in this study for the Cretaceous strata in Wyoming sedimentary basins combined with velocity/porosity crossplot analyses demonstrates that widespread velocity reversals occur within these clay-rich non-reservoir rocks.

Results of this study suggest that the following points be considered when evaluating velocities within the tightly compacted rocks of Wyoming sedimentary basins:

1) Multiple velocity reversals within those Cretaceous rocks cannot be explained without considering crack-like pores in the rock matrix.
2) The presence of compliant crack-like pores in the rock matrix may significantly weaken the *measured* rock volume, which will result in lower measured velocities.
3) The wide range of rock velocities observed in sonic log data in this study and the poor correlation between velocity and density porosity indicate variable concentration of high- and-low-aspect-ratio pores.
4) No simple functional relationship of rock velocity with depth can be derived from sonic measurements in the case of nonlinear velocity/porosity relationships. This makes calculation of any kind of "ideal velocity-depth trend" inappropriate for the Cretaceous-age rocks of Wyoming sedimentary basins.
5) Gas-charged compartments within "tight gas sand" reservoirs should be delineated on the basis of horizon-based analysis in map view.

REFERENCES

Al-Chalabi, M., 1997, Parameter nonuniqueness in velocity versus depth functions: Geophysics, v. 62, p. 970–979.

Athy, L.F., 1930, Density, porosity, and compaction of sedimentary rocks: American Association of Petroleum Geologists Bulletin, v. 14, p. 1–24.

Asquith, G., and Krygowski, D., 2004, Basic well log analysis (2d ed.): American Association of Petroleum Geologists Methods in Exploration Series no.16, 244 p.

Bell, D.W., 2002, Velocity estimation for pore pressure prediction, *in* Huffman, A.R., and Bowers, G.L., editors, Pressure regimes in sedimentary basins and their prediction: American Association of Petroleum Geologists Memoir 76, p. 217–233.

Dewan, J.T., 1983, Essentials of modern open-hole log interpretation: Tulsa, Okla., Penwell Publishing, 361 p.

Ellis, D.V., and Singer, J.M., 2007, Well logging for earth scientists" (2d ed.): Netherlands, Springer, 548 p.

Han, D.H., Nur, A., and Morgan, D., 1986, Effects of porosity and clay content on wave velocities in sandstones: Geophysics, v. 51, p. 2093–2107.

Issler, D.R., 1992, A new approach to shale compaction and stratigraphic restoration – Beaufort-McKenzie Basin and McKenzie corridor, North Canada: American Association of Petroleum Geologists Bulletin, v. 76, p. 1170–1189.

Jiao, Z.S., and Surdam, R.C., 1997, Characteristics of anomalously pressured cretaceous shales in the Laramide basins of Wyoming, *in* Surdam, R.C., editor, Seals, traps, and the petroleum system: American Association of Petroleum Geologists Memoir 67, p. 245–253.

Katahara, K., 2008, What is shale to a petrophysicist?: The Leading Edge, June, p. 738–741.

Keys, R.G., and Xu, S., 2002, An approximation for the Xu-White velocity model: Geophysics, v. 67, p. 1406–1414.

Magara, K., 1976, Thickness of removed sedimentary rocks, paleopore pressure, and paleotemperature, southwestern part of Western Canada Basin: American Association of Petroleum Geologists Bulletin, v. 60, p. 554–566.

Marion, D., Nur, A., Yin, H., and Han, D., 1992, Compressional velocity and porosity in sand-clay mixtures: Geophysics, v. 57, p. 554–563.

Raymer, D.S., Hunt, E.R., and Gardner, J.S., 1980, An improved sonic transit time-to-porosity transform: Society of Professional Well-log Analysts, 21st Annual Logging Symposium, Transaction P, paginated by transaction, 13 p.

Surdam, R.C., Jiao, Z.S., and Ganshin, Yuri, 2005, A new approach to exploring for anomalously pressured gas accumulations: Wyoming State Geological Survey Exploration Memoir No. 1, 96 p.

Surdam, R.C., Jiao, Z.S., and Heasler, H.P., 1997, Anomalously pressured gas compartments in Cretaceous rocks of the Laramide basins of Wyoming – A new class of hydrocarbon accumulation *in* Surdam, R.C., editor, Seals, traps, and the petroleum system: American Association of Petroleum Geologists Memoir 67, p. 199–222.

Surdam, R.C., Robinson, John, Jiao, Z.S., and Boyd, N.K., III, 2001, Delineation of Jonah Field using seismic and sonic velocity interpretations, *in* Anderson, D.S., et al., editors, Gas in the Rockies: Denver, Rocky Mountain Association of Geologists, p. 189–208.

Whittaker, A., 1991, Mud Logging Handbook: Englewood Cliffs, N.J., Prentice Hall, 531 p.

Wyllie, M.R. J., Gregory, A.R., and Gardner, L.W., 1956, Elastic wave velocities in heterogeneous and porous media: Geophysics, v. 21, p. 41–70.

Xu, S., and White, R.E., 1995, A new velocity model for clay-sand mixtures: Geophysical Prospecting, v. 43, p. 91–118.

WOGCC [Wyoming Oil and Gas Conservation Commission] Web site: http://wogcc.state.wy.us